ISSN 2413-5577

№ 4 Октябрь – Декабрь 2022

Экологическая безопасность прибрежной и шельфовой зон моря

Ecological Safety of Coastal and Shelf Zones of Sea

No. 4 October – December 2022

ecological-safety.ru

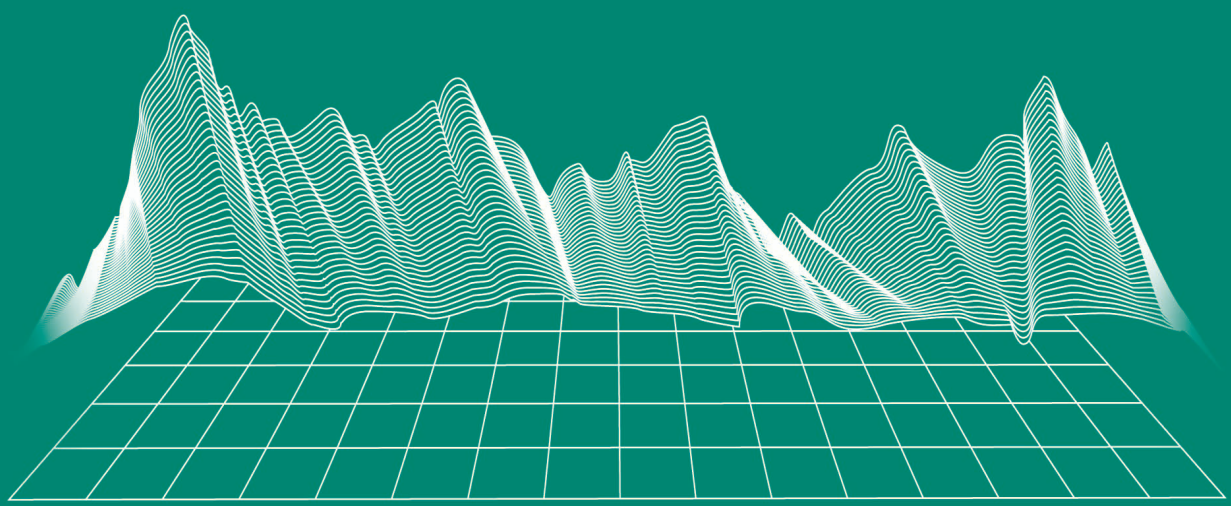

ISSN 2413-5577
No. 4, 2022
October – December

Publication frequency:
Quarterly
16+

ECOLOGICAL SAFETY OF COASTAL AND SHELF ZONES OF SEA

Scientific and theoretical peer reviewed journal

FOUNDER AND PUBLISHER:
Federal State Budget Scientific Institution
Federal Research Centre
“Marine Hydrophysical Institute of RAS”

The Journal publishes original research results, review articles (at the editorial board's request) and brief reports.

The Journal aims at publication of results of original scientific research concerning the state and interaction of geospheres (atmosphere, lithosphere, hydrosphere, and biosphere) within coastal and shelf areas of seas and oceans, methods and means of study thereof, ecological state of these areas under anthropogenic load as well as environmental protection issues.

The Journal's editorial board sees its mission as scientific, educational and regulatory work to preserve the ecological balance and restore the resource potential of coastal and shelf areas believing that despite the geographical limitations of the areas under study, the processes taking place within them have a significant impact on the waters of the seas and oceans and economic activity.

The Journal publishes original research materials, results of research performed by national and foreign scientific institutions in the coastal and shelf zones of seas and oceans, review articles (at the editorial board's request) and brief reports on the following major topics:
- Scientific basis for complex use of shelf natural resources
- Marine environment state and variability
- Coastal area state and variability; coast protection structures
- Monitoring and estimates of possible effects of anthropogenic activities
- Development and implementation of new marine environment control and monitoring technologies

The outcome of the research is information on the status, variability and possible effects of anthropogenic activities in the coastal and shelf marine areas, as well as the means to perform calculations and to provide information for making decisions on the implementation of activities in the coastal zone.

e-mail: ecology-safety@mhi-ras.ru

website: http://ecological-safety.ru

Founder, Publisher and Editorial Office address:
2, Kapitanskaya St.,
Sevastopol, 299011, Russia

Phone, fax: + 7 (8692) 54-57-16

EDITORIAL BOARD

РЕДАКЦИОННАЯ КОЛЛЕГИЯ

CONTENTS

№ 4. 2022 October – December, 2022

СОДЕРЖАНИЕ

№ 4. 2022 Октябрь – Декабрь, 2022

DOI: 10.22449/2413-5577-2022-4-6-24

Hydrological Water Structure and Distribution of Total Suspended Matter off the Coast of Crimea in Spring 2021

Yu. V. Artamonov, E. A. Skripaleva *, A. A. Latushkin, A. V. Fedirko, D. A. Ryabokon

Marine Hydrophysical Institute of RAS, Sevastopol, Russia
* *e-mail: sea-ant@yandex.ru*

Abstract

The paper analyzes features of the hydrological structure of waters and the distribution of total suspended matter off the coast of Crimea within the economic zone of Russia between the Heraclea Peninsula and Cape Opuk in April-May 2021 according to field measurements carried out during the 116th cruise of the R/V *Professor Vodyanitsky*. It is shown that the Rim Current formed anticyclonic eddies to the south of the Heraclea and Kerch Peninsulas, to the east and south of Cape Meganom. Cyclonic eddies and meanders were observed near the southwestern and southeast boundaries of the polygon. A decrease in sea surface temperature east of Cape Meganom and in Feodosiya Bay associated with coastal upwelling was revealed. It is shown that intense freshening of surface waters was observed in the coastal northeastern part of the polygon. The mixing of the Azov Sea waters propagating from the Kerch Strait and the waters of Feodosiya Bay led to the formation of a tongue of freshened waters spreading to the south of the Kerch Peninsula. It is shown that water freshening in the northeast part of the polygon was not accompanied by an increase in the total suspended matter concentration, and its minimum was revealed in Feodosiya Bay. The transport of these transparent waters along the periphery of the anticyclonic eddy led to the formation of a tongue of waters of increased transparency south of the Kerch Peninsula, which coincides in position with the tongues of waters of low temperature and salinity. Waters of maximum turbidity were traced on the shelf between Cape Ayu-Dag and Cape Sarych and to the west of the Heraclea Peninsula. It is shown that the highest content of suspended matter was observed either within the upper quasi-homogeneous layer or in the layer of the lower seasonal thermocline and pycnocline. The turbidity deeper than the seasonal thermocline, halocline and pycnocline, was lower than that in the surface layer. A low level of consistency was revealed between the horizontal fields of the total suspended matter concentration and thermohaline parameters in the upper 30–40-meter layer. Deeper, the consistency level increased to a significant level, and colder, saltier, and denser waters were characterized by increased transparency.

Keywords: Black Sea, water circulation, Rim Current, temperature, salinity, density, upper quasi-homogeneous layer, cold intermediate layer, thermocline, pycnocline, halocline, total suspended matter

Acknowledgements: the work was carried out under FSBSI FRC MHI State Order no. 0555-2021-0003 “Development of operational oceanology methods based on interdisciplinary research of processes of the marine environment formation and evolution and on mathematical modeling using data of remote and contact measurements” (“Operational oceanology” code) and no. 0555-2021-0004 “Fundamental studies of oceanological processes which determine the state and evolution of the marine environment influenced by natural and anthropogenic factors, based on observation and modeling methods**”** (“Oceanological processes” code). The authors are grateful to members of the hydrology and currents detachment S.A. Shutov, D.V. Deryushkin and R.O. Shapovalov for carrying out hydrological measurements during cruise 116 of the R/V *Professor Vodyanitsky*.

For citation: Artamonov, Yu.V., Skripaleva, E.A., Latushkin, A.A., Fedirko, A.V. and Ryabokon, D.A., 2022. Hydrological Water Structure and Distribution of Total Suspended Matter off the Coast of Crimea in Spring 2021. *Ecological Safety of Coastal and Shelf Zones of Sea*, (4), pp. 6–24. doi:10.22449/2413-5577-2022-4-6-24

Гидрологическая структура вод и распределение общего взвешенного вещества у берегов Крыма весной 2021 года

Ю. В. Артамонов, Е. А. Скрипалева *, А. А. Латушкин, А. В. Федирко, Д. А. Рябоконь

Морской гидрофизический институт РАН, Севастополь, Россия
***** *e-mail: sea-ant@yandex.ru*

Аннотация

Целью данной работы является анализ гидрологической структуры вод у берегов Крыма весной 2021 г. и оценка ее связи с распределением взвешенного вещества по данным комплексных гидролого-гидрооптических измерений, выполненных в рамках программы экспедиционных исследований МГИ РАН в ходе 116-го рейса НИС «Профессор Водяницкий». Работы проводились в пределах экономической зоны России между Гераклейским п-овом и м. Опук. Показано, что к югу от Гераклейского и Керченского п-овов, к востоку и югу от м. Меганом Основное Черноморское течение формировало антициклонические круговороты. У юго-западной и юго-восточной границ полигона наблюдались циклонические круговороты и меандры. Выявлено понижение температуры поверхности моря к востоку от м. Меганом и в Феодосийском заливе, связанное с прибрежным апвеллингом. Показано, что в прибрежной северо-восточной части полигона наблюдалось интенсивное распреснение поверхностных вод. Смешение азовоморских вод, поступающих из Керченского пролива, и вод Феодосийского залива привело к формированию языка распресненных вод, распространяющегося на юг от Керченского п-ова. Показано, что распреснение вод в северо-восточной части полигона не сопровождалось повышением концентрации общего взвешенного вещества, в Феодосийском заливе был выявлен ее минимум. Перенос этих прозрачных вод вдоль периферии антициклонического круговорота привел к формированию южнее Керченского п-ова языка вод повышенной прозрачности, совпадающего по положению с языками вод пониженной температуры и солености. Воды максимальной мутности прослеживались на шельфе между м. Аю-Даг и м. Сарыч и к западу от Гераклейского п-ова. Показано, что наибольшее содержание взвешенных веществ наблюдалось либо в пределах верхнего квазиоднородного слоя, либо в слое нижнего сезонного термоклина и пикноклина. Мутность вод глубже

сезонных термоклина, галоклина и пикноклина была ниже, чем в поверхностном слое. Выявлен низкий уровень согласованности горизонтальных полей концентрации общего взвешенного вещества и термохалинных параметров в верхнем 30–40-метровом слое. Глубже уровень согласованности повышался до значимого и более холодные, соленые и плотные воды характеризовались повышенной прозрачностью.

Ключевые слова: Черное море, циркуляция вод, Основное Черноморское течение, температура, соленость, плотность, верхний квазиоднородный слой, холодный промежуточный слой, термоклин, пикноклин, галоклин, общее взвешенное вещество

Благодарности: работа выполнена в рамках государственного задания ФГБУН ФИЦ МГИ по темам № 0555-2021-0003 «Развитие методов оперативной океанологии на основе междисциплинарных исследований процессов формирования и эволюции морской среды и математического моделирования с привлечением данных дистанционных и контактных измерений» (шифр «Оперативная океанология») и № 0555-2021-0004 «Фундаментальные исследования океанологических процессов, определяющих состояние и эволюцию морской среды под влиянием естественных и антропогенных факторов, на основе методов наблюдения и моделирования» (шифр «Океанологические процессы»). Авторы выражают благодарность членам отряда гидрологии и течений С. А. Шутову, Д. В. Дерюшкину и Р. О. Шаповалову за проведение гидрологических измерений в ходе 116-го рейса НИС «Профессор Водяницкий».

Для цитирования: Гидрологическая структура вод и распределение общего взвешенного вещества у берегов Крыма весной 2021 года / Ю. В. Артамонов [и др.] // Экологическая безопасность прибрежной и шельфовой зон моря. 2022. № 4. С. 6–24. doi:10.22449/2413-5577-2022-4-6-24

Introduction

Under the conditions of ongoing climate change and increasing anthropogenic impact on the water area of the Black Sea, monitoring the state of the marine ecosystem and studying the processes that determine its evolution at various spatio-temporal scales are becoming increasingly important [1, 2]. Hydrological processes in the upper layer of the Black Sea are the main factors influencing ecosystem changes and determining the development of water bioproductivity. The most important ecosystem component, reflecting the state of the aquatic environment, is the total suspended matter (TSM). The light beam attenuation coefficient (BAC) serves as an indicator of the content of TSM [1)] [3–6]. The study of the content variability of suspended particles and its relationship with the features of the hydrological structure of waters is an important element of environmental monitoring. The development of remote sensing methods made it possible to obtain new data on the variability of hydrological and hydrooptical structure of waters on the sea surface [7–14]. At the same time, only contact methods can provide information about the structure of waters in the deep layers of the sea, therefore, the Marine Hydrophysical Institute (MHI) RAS regularly conducts expeditionary studies in the Black Sea [15–17]. Carrying out instrumental measurements of currents

[1)] Mankovsky, V.I., Solov'iev, M.V. and Mankovskaya, E.V., 2009. [*Hydrooptical Properties of the Black Sea*]. A reference book. Sevastopol: MGI NAN Ukrainy, pp. 20–21.

that are quasi-synchronous with hydrological and hydrooptical observations significantly expands the possibilities for interpreting the features of the thermohaline and hydrooptical structure of waters [18–22].

The purpose of this work is to analyse the hydrological structure of waters off the coast of Crimea in the spring of 2021 and evaluate its relationship with the distribution of suspended matter according to the complex hydrological and hydrooptical measurements carried out as part of the MHI RAS expeditionary research program during the 116th cruise of the R/V *Professor Vodyanitsky*.

Materials and methods

The work used data from hydrological and hydrooptical measurements at 99 stations performed off the coast of Crimea in the period from 22.04.2021 to 8.05.2021 (Fig. 1). At each station, temperature, electrical conductivity, and hydrostatic pressure were measured in the depth range from the surface to 500 m using the IDRONAUT OCEAN SEVEN 320PlusM sounding CTD complex, and the speed and direction of currents in the upper 200-meter layer were determined using the WORKHORSE ADCP acoustic doppler profiler 300 kHz.

Simultaneously with hydrological measurements at each station, measurements of the directional light beam attenuation coefficient were carried out, for which the SIPO4 probing spectral meter of BAC, developed in the Department of Optics and Biophysics of the Sea of MGI RAS, was used [2)]. BAC measurements

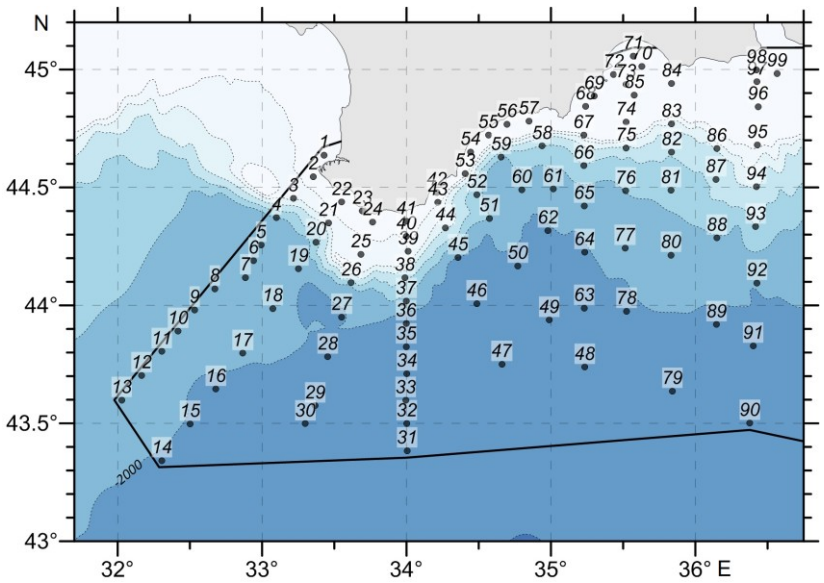

Fig. 1. Layout of stations measured near Crimean coasts during the 116th cruise of the R/V *Professor Vodyanitsky*

[2)] Latushkin, A.A. and Martynov, O.V., 2016. [*Method for in situ Determination of Spectral Index of Spotlight Attenuation in Sea Water*]. Russia. No. 2605640.

were carried out in the red region of the spectrum at a wavelength of 625 nm with a vertical resolution of 0.1 m from the surface to the limiting depth, which, depending on the time allotted for hydrooptical measurements and weather conditions, varied from 50 to 130 m. Based on the BAC measurements, the concentration of the total suspended matter (C_{TSM}) was calculated based on the empirical ratio $C_{TSM} = 1.514 \cdot BAC(625) - 0.23$. This ratio was obtained earlier for the northern part of the Black Sea based on the measurement data of BAC and the determination of TSM concentration by the gravimetric method from water samples, which were additionally taken at the stations together with the BAC measurements [23]. The concentration of total suspended matter was understood as the concentration of all suspended particles that remained on the filter.

For a quantitative assessment of the consistency of the spatial distributions of C_{TSM} and thermohaline parameters at each horizon with a discreteness of 1 m up to the limiting depth of hydrooptical measurements, series of C_{TSM} values, temperature, salinity, and density were formed for the totality of all stations, between which the linear correlation coefficients R were calculated.

Main results

Water circulation. The distributions of dynamic heights (Fig. 2, *a*), geostrophic vectors (Fig. 2, *b*) and instrumentally measured currents (Fig. 2, *c – f*) show that during the measurement period western flows corresponding to the Rim Current (RC) prevailed on the polygon.

The maximum RC velocities reached 50–55 cm/s according to geostrophic calculations (Fig. 2, *b*) and 40–45 cm/s according to instrumental measurements (Fig. 2, *c – f*). The results obtained by the dynamic method differ somewhat from the results of direct current measurements. According to geostrophic calculations, one can note a weakening of the RC velocity (up to 25–35 cm/s) over the continental slope between Cape Sarych and Cape Ai-Todor (Fig. 2, *b*). According to instrumental measurements, the RC velocity in the surface layer in this region was higher and reached 35–45 cm/s (Fig. 2, *c*).

The time of the survey (end of April – beginning of May) fell on the beginning of the weakening of the RC velocity in the climatic seasonal cycle [24, 25]. According to [19, 25–27], the RC meandering intensifies during this period and synoptic eddies are formed (cyclonic to the left of the RC core and anticyclonic to the right). According to geostrophic calculations based on the survey data, a cyclonic meander was observed near the southwestern boundary of the polygon, and the southern periphery of the anticyclonic meander was traced above the continental slope in the northwestern part of the polygon (Fig. 2, *b*). Geostrophic calculations do not make it possible to assess the features of circulation in shallow shelf areas, therefore a more complete picture of the meanders and eddies formed by the RC is provided by the data of instrumental measurements of currents. Thus, anticyclonic eddies were traced over the coastal shelf south of the Heraclea Peninsula in the upper 50-m layer (Fig. 2, *c*, *d*) and east of Cape Meganom at depths of 10–25 m (Fig. 2, *c*). Two more eddies were recorded above the continental slope in the entire measurement layer south of Cape Meganom and south

of the Kerch Peninsula (Fig. 2, *c* – *f*). In the field of dynamic heights, these eddies manifested themselves only in the form of an anticyclonic bend in isodynams (Fig. 2, *a*).

At the southwestern boundary of the polygon, a cyclonic eddy was traced throughout the measurement layer, most clearly expressed at the horizons of 75–125 m (Fig. 2, *e*, *f*). At the southeastern boundary of the survey, an intense cyclonic meander was traced, which at depths of 25–50 m was transformed into an eddy (Fig. 2, *d*).

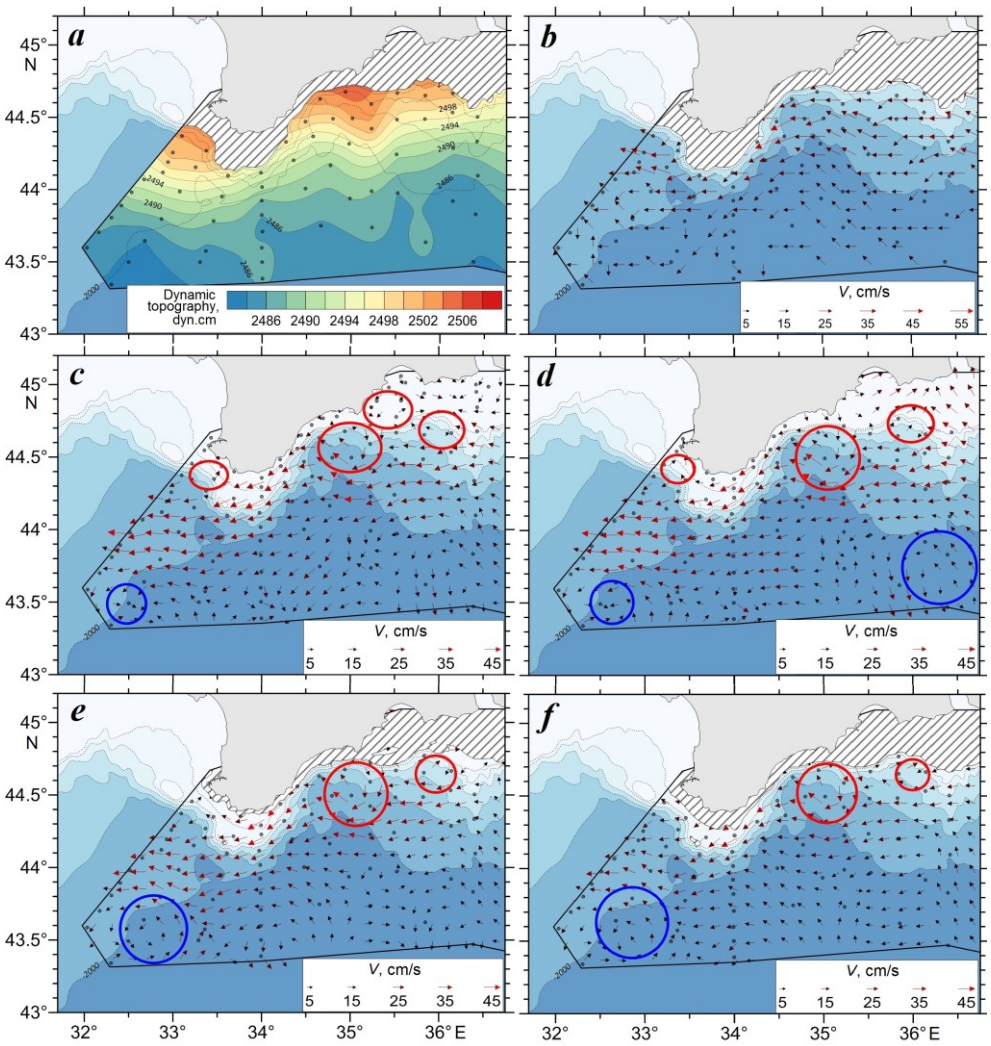

Fig. 2. Dynamic topography relative to reference level 300 dbar (*a*), geostrophic current vectors at 2 m horizon (*b*), vectors of instrumentally measured currents at 10 m (*c*), 50 m (*d*), 75 m (*e*), 100 m (*f*) horizons. Ellipses show anticyclonic (red) and cyclonic (blue) eddies

Thermohaline structure of waters. The sea surface temperature distribution (SST) was formed as a result of intensive spring warming of surface waters and water circulation features. The temperature minimum (10–10.5 °C) was observed near the southwestern boundary of the polygon in the area of a cyclonic eddy, which is associated with the rise of colder subsurface waters (Fig. 3, *a*). In general, the water temperature in the surface layer in the eastern part of the polygon (approximately east of 34.5° E) was higher (13–15 °C) than in the western part (10–12 °C) (Fig. 3, *a*). On the one hand, higher temperatures in the east of the polygon can be explained by the peculiarities of water circulation – advection of the RC warm waters along the Caucasian and Crimean coasts. This advection is also observed on the climatic scale according to satellite SST measurements [24]. On the other hand, an increase in SST values in the eastern part of the polygon may be associated with a longer period of spring warming of surface waters in this area, since the measurements were carried out as the vessel moved from west to east. The difference between the time of measurements at the western and eastern boundaries of the polygon was almost half a month. During the survey period, warmer waters penetrated into the western part of the water area in the zone of the RC main jet, reaching 34° E according to the position of the 12 °C isotherm. Despite higher temperature in the eastern part of the polygon, near the coast east of Cape Meganom and in Feodosiya Bay, the SST values decreased to 12–12.5 °C (Fig. 3, *a*), a possible reason for which was coastal upwelling caused by the southwest wind. At the same time, the tongue of waters of low temperature (up to 13 °C) spread to the south from Cape Chauda to about 44.5° N (Fig. 3, *a*). According to the distribution of current vectors, the reason for the appearance of such a tongue is the transfer of colder waters from Feodosiya Bay by the alongshore flow, first eastward and then southward along the periphery of the anticyclonic eddy (Fig. 2, *c*).

The distribution of the sea surface salinity (SSS) showed that along the entire Crimean coast above the shelf and the slope of the depths there were freshened waters with a salinity below 18.4‰ (Fig. 3, *b*). The minimum salinity (18.1–18.2 ‰) was observed off the coast of the Kerch Peninsula and in the eastern part of Feodosiya Bay. The tongue of freshened waters along the isohaline of 18.25 ‰

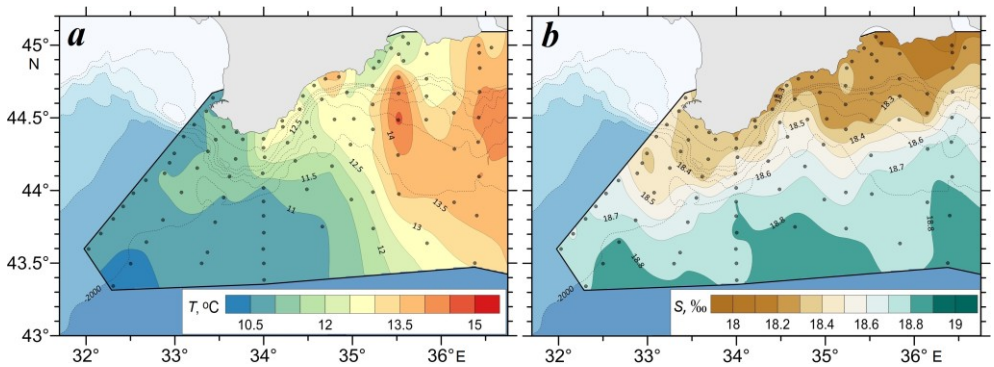

F i g . 3 . Distribution of temperature (*a*) and salinity (*b*) in the surface layer

spread to the south from the Kerch Peninsula, reaching almost 44.5° N. This tongue was formed as a result of the mixing of the Sea of Azov waters coming from the Kerch Strait and the waters of Feodosiya Gulf, transported eastward and then southward along the periphery of the anticyclonic eddy (Fig. 2, *c*). Further above the slope of the depths, these low-salinity waters were captured by the RC flow, and as they were transferred to the west, their salinity gradually increased. Nevertheless, judging by the configuration of the 18.5 ‰ isohaline, the Kerch–Feodosiya freshening reached the western boundary of the polygon. An increase in salinity (up to 18.7 ‰) was observed in the southern part of the polygon, where the cyclonic direction of flows prevailed. As a result of the rise of more saline deep waters to the surface, the salinity reached its maximum values (18.8–18.85 ‰) in the zones of cyclonic meanders and eddies (Fig. 3, *b*).

Typical distributions of thermohaline characteristics on vertical profiles are shown in Fig. 4, *a*. At most stations, an upper thin layer of relatively warm waters, i.e., an upper quasi-homogeneous layer (UQHL), was observed. The formation of this layer was associated with spring warming. The UQHL thickness in the water area was 2–17 m in the western part of the polygon and 2–10 m in the eastern part (Fig. 5, *a*).

Under the upper UQHL-1, in the temperature field, the second lower UQHL-2 remained, which formed in the previous winter period (Fig. 4, *a*). The depth of the lower boundary of UQHL-2 varied from 18 to 45 m in the western part of the polygon and from 10 to 30 m in the eastern part.

In the conditional density field, as well as in the temperature field, UQHL at most stations was characterized by a stepped structure (stations 19, 61, and 63 in Fig. 4, *a*), while the depths of the lower boundaries of UQHL-1 and UQHL-2 in the density field almost coincided with the depths of the lower boundaries of UQHL-1 and UQHL-2 in the temperature field.

In the salinity field, in contrast to the fields of temperature and density, predominantly one UQHL was traced, a two-step structure was observed only at some stations (station 61 in Fig. 4, *a*). The vertical thickness of UQHL was 10–25 m in the western part of the polygon (stations 15 and 19 in Fig. 4, *a*), in the eastern part of the polygon it decreased to 5–17 m (stations 61 and 63 on Fig. 4, *a*).

Under UQHL, there was a layer of maximum vertical gradients of temperature (VGT), salinity (VGS), and conditional density ($VG\sigma_t$) – seasonal thermocline, halocline, and pycnocline (Fig. 4, *b*). The two-layer UQHL structure in the fields of temperature and density caused the formation of two maxima (in absolute value) of the VGT and $VG\sigma_t$, which were recorded at most stations (Fig. 4, *b*). The upper maximum of the VGT and $VG\sigma_t$ was located in the depth range of 5–20 m (Fig. 4, *b*). The spatial distribution of the depth of the lower maximum of VGT showed that in the western part of the polygon it was 21–47 m, and in the eastern part it noticeably decreased and amounted to 13–35 m (Fig. 5, *b*). In the salinity field, predominantly one VGS maximum was observed, located in the depth range of 10–30 m (Fig. 4, *b*).

Deeper than the seasonal thermocline, pycnocline, and halocline, the cold intermediate layer (CIL), the main pycnocline, and halocline were well traced on the VGT, VGS, and $VG\sigma_t$ profiles. The position of the CIL core is characterized

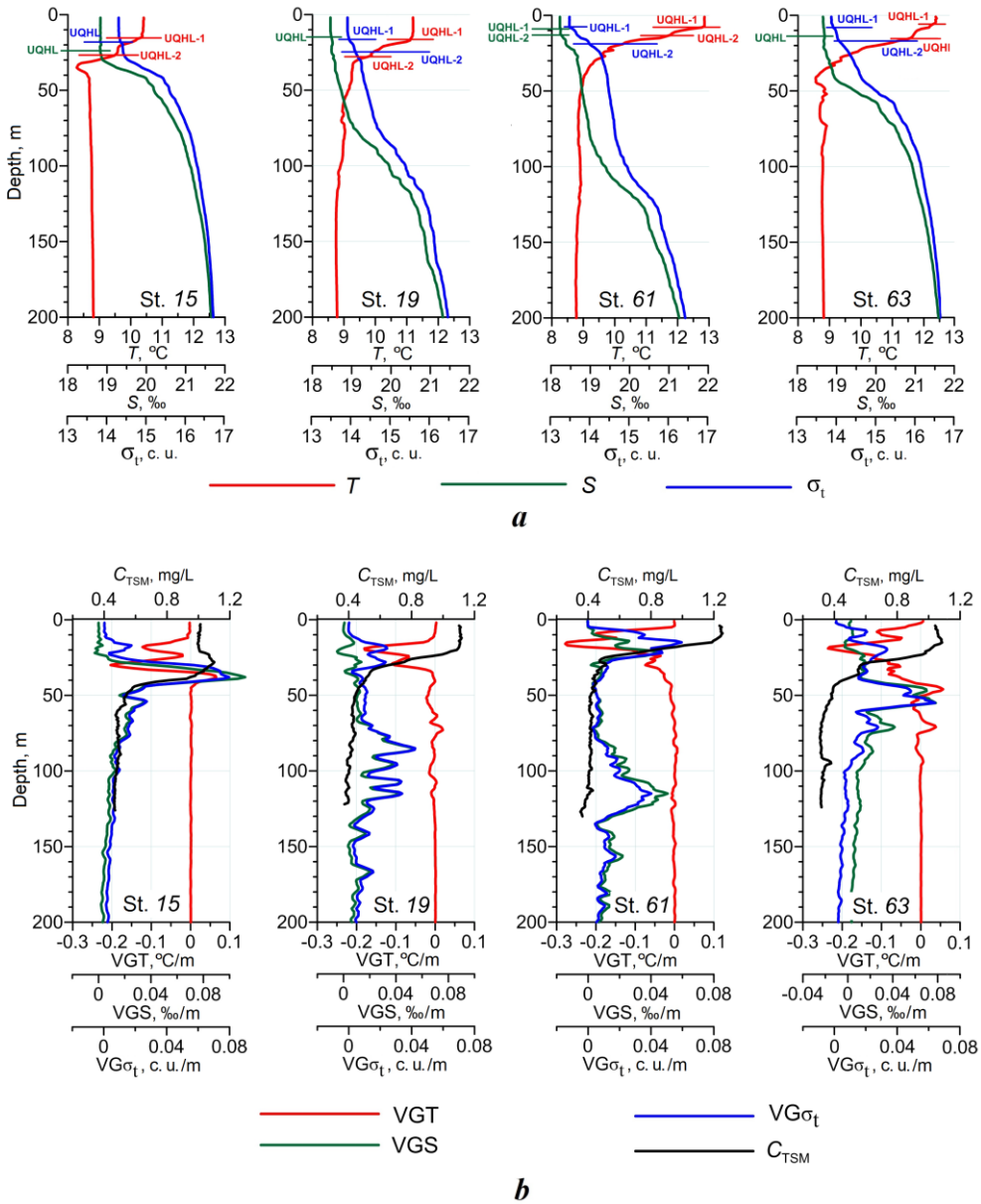

Fig. 4. Vertical distributions of temperature (T), salinity (S), conditional density (σ_t) (*a*), their vertical gradients and TSM concentration (*b*) at individual stations. Lower boundaries of the upper quasi-homogeneous layer (UQHL) steps are shown in the fields of temperature (red line segments), salinity (green line segments), density (blue line segments)

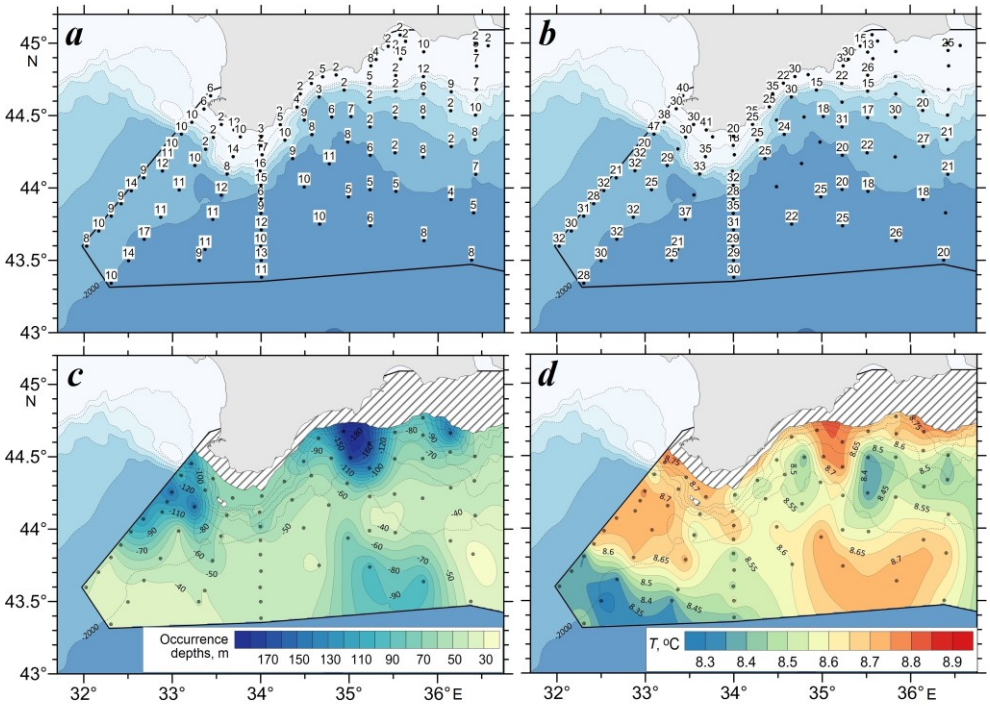

F i g . 5 . Distributions of occurrence depths (m) of the lower boundary of the upper UQHL-1 in the temperature field (*a*), lower maximum of the vertical gradient of temperature (VGT) (*b*), core of the cold intermediate layer (CIL) (*c*), and temperature distribution in the CIL core (*d*)

by a change in the sign of the VGT values. The main pycnocline and halocline are traced on the profiles by the maximum positive values of VGS and VGσ_t. It should be noted that in the spring of 2021, the distribution of the depths of the main pycnocline, halocline, and CIL core clearly showed the features of water circulation and synoptic eddy formations. Thus, the depth of the main pycnocline and halocline decreased noticeably (to 45–55 m) in the southern deep-water part of the polygon (station 63 in Fig. 4, *b*) and was minimal (40–45 m) in the southwest of the polygon in the area of cyclonic eddy (station 15 in Fig. 4, *b*). Closer to the continental slope and in the zones of anticyclonic meanders and eddies, it noticeably increased (up to 90–125 m) (stations 19 and 61 in Fig. 4, *b*). The depth of occurrence of the CIL core (Fig. 5, *c*) was also minimal (35–40 m) in the area of cyclonic eddy in the southwest of the polygon and increased to 100–130 m in the zones of anticyclonic formations located south of the Heraclea and Kerch Peninsulas. The maximum deepening of the CIL core (up to 150–180 m) was traced in the area of the anticyclonic eddy south of Cape Meganom. The temperature in the CIL core (Fig. 5, *d*) varied from 8.3–8.4 °C in the zone of cyclonic eddy in the southwest of the polygon to 8.7–8.8 °C in the areas of anticyclonic formations near the continental slope.

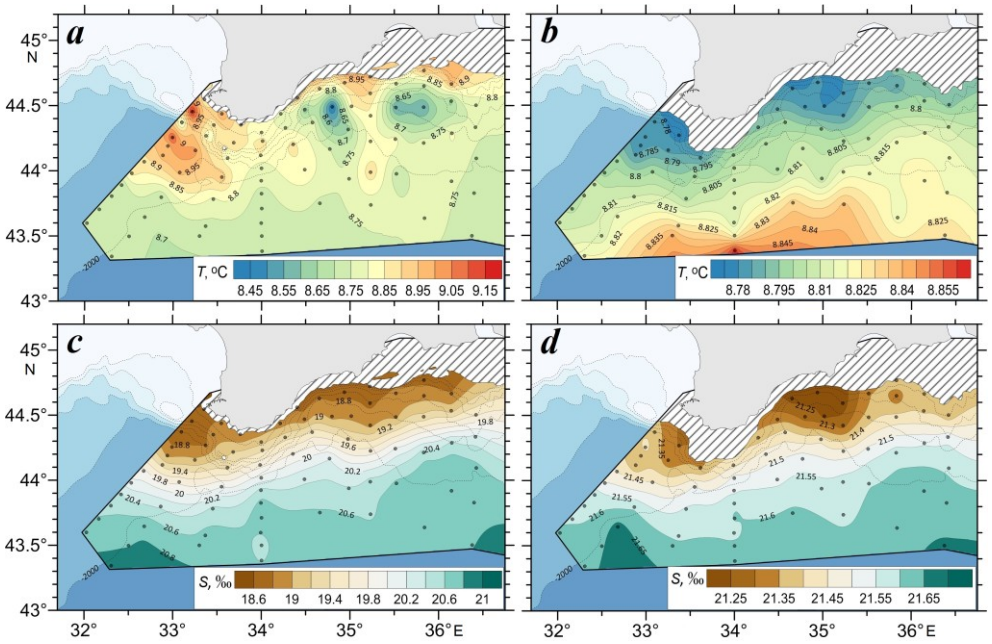

Fig. 6. Distributions of temperature (*a*, *b*) and salinity (*c*, *d*) at 75 m (*a*, *c*) and 200 m (*b*, *d*) horizons

In general, synoptic eddies in the horizontal temperature distributions above and below the CIL manifested themselves differently (Fig. 6). At depths above the CIL, in the zones of anticyclonic meanders and eddies in the north of the polygon, elevated temperatures were noted due to the subsidence of warmer surface waters (Fig. 6, *a*). At depths below the CIL, due to the subsidence of its waters, the temperature in the zones of these eddies was lower than that of the surrounding waters (Fig. 6, *b*). In the areas of cyclonic eddies and meanders in the southern part of the polygon, due to the rise of water, a decrease in temperature above the CIL (Fig. 6, *a*) and its increase below the CIL (Fig. 6, *b*) were observed. In the field of salinity in the entire measurement layer, a decrease was noted in anticyclonic formations, and an increase in salinity – in cyclonic formations (Fig. 6, *c*, *d*). These features of manifestation of eddy formations in thermohaline fields, depending on the depth, are fairly stable patterns and were observed from the results of hydrological measurements performed earlier [19].

Distribution of total suspended matter concentration. A feature of the TSM concentration distribution on the surface in the spring of 2021 was that in the northeastern part of the polygon, intense water freshening was not accompanied by an increase in turbidity, in contrast to other surveys [21, 23] and satellite observations [11]. Along the coast, from Cape Meganom to the Kerch Strait, the TSM concentration did not exceed 1.1 mg/L, and its minimum (0.55–0.9 mg/L) was detected in the Feodosiya Bay (Fig. 7, *a*). This C_{TSM} minimum, as well as the decrease in temperature in this region, is associated with the rise of colder

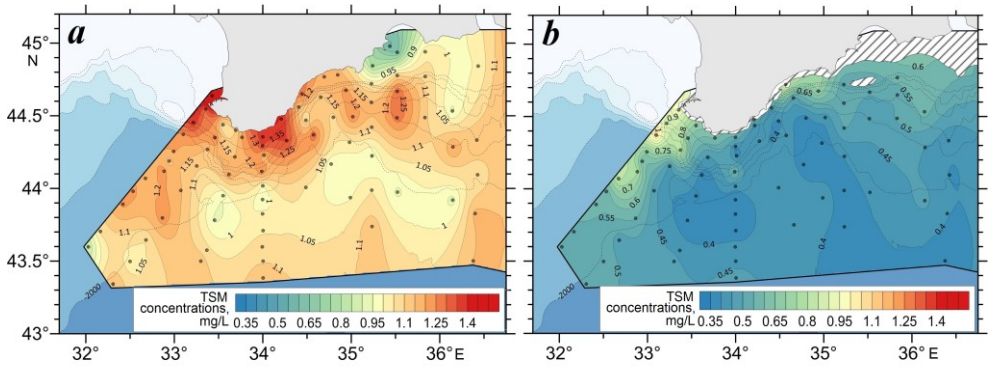

Fig. 7. Distributions of TSM concentrations in the surface layer (*a*) and at 50 m horizon (*b*)

and clearer waters in the upwelling zone. The transport of clear waters by the alongshore flow, first in an eastward and then in the southward direction along the periphery of the anticyclonic eddy (Fig. 2, *c*), led to the appearance of waters of increased transparency south of the Kerch Peninsula tongue. The C_{TSM} values in it did not exceed 1 mg/L (Fig. 7, *a*). The position of this tongue coincided with the position of the tongues of low temperature waters (Fig. 3, *a*) and low salinity waters (Fig. 3, *b*).

An increase in TSM concentration (up to 1.2–1.3 mg/L) was observed in the form of individual spots that were traced in the Rim Current zone, above the continental slope and on the shelf. TSM concentration maxima (1.35–1.4 mg/L) were traced in the shelf zone between Cape Ayu-Dag and Cape Sarych and to the west of the Heraclea Peninsula (Fig. 7, *a*).

The vertical structure of the TSM concentration field, in contrast to the structure of the temperature and density fields, was characterized by the presence of one upper quasi-homogeneous layer ($UQHL_{TSM}$). The thickness of $UQHL_{TSM}$ exceeded the thickness of the upper UQHL-1 in the fields of temperature and density and approximately coincided with the thickness of the UQHL in the salinity field. The lower boundary of the $UQHL_{TSM}$ was located in the layer of the upper seasonal thermocline and pycnocline and varied on the polygon in the depth range of 7–25 m (Fig. 4, *b*). A more developed $UQHL_{TSM}$ can be associated with different adaptation times for the temperature and density fields and the TSM concentration field to changes in synoptic conditions during the period of intense spring warming. The same reason can explain noticeable differences in the depth of the maximum TSM concentration at different stations. At some stations, the maximum concentration of TSM was observed below the $UQHL_{TSM}$ in the layer of the lower seasonal thermocline and pycnocline (stations 15 and 63 in Fig. 4, *b*). At other stations, on the contrary, there was no subsurface maximum of TSM concentration, and the highest content of suspended matter was observed within the $UQHL_{TSM}$, deeper than which, in the layer of the lower seasonal thermocline and pycnocline, there was a sharp decrease in the TSM concentration (stations 19 and 61 in Fig. 4, *b*).

In general, at all stations deeper than the seasonal thermocline, halocline, and pycnocline, the TSM concentration markedly decreased compared to its values in the surface layer. Thus, already at the 50-m horizon (Fig. 7, *b*), in most of the polygon, the values of C_{TSM} did not exceed 0.35–0.55 mg/L. At the same time, due to the subsidence of more turbid waters from the overlying layers of the sea in the areas of anticyclonic eddies to the south of Cape Meganom and the Kerch Peninsula, the C_{TSM} values increased to 0.6–0.7 mg/L, and to the southwest of the Heraclea Peninsula, to 0.9–1 mg/L (Fig. 7, *b*).

It should be noted that, in the depth range of 85–115 m, one more relatively weak maximum of TSM concentration (0.33–0.89 mg/L) was observed at a number of stations (stations 61, 63 in Fig. 4, *b*). A similar TSM maximum was revealed according to the data of the spring survey in 2019, in which the depth of hydrooptical measurements reached 200 m, i.e., the depth of the hydrogen sulphide zone [22]. In the spring of 2019, this C_{TSM} maximum was located under the main pycnocline and halocline in the depth range of 80–170 m, which corresponded to a layer of occurrence of isopycnal surfaces of 15.9–16.3 c. u. According to [28], this layer covers the lower boundary of the suboxygen redox zone and the upper layer of the hydrogen sulfide zone, the upper boundary of which is conventionally determined by the position of the isopycna 16.2 c. u. Unfortunately, in the analyzed survey, the depth of hydrooptical soundings did not exceed 130 m, therefore, at many stations, the maximum TSM concentration in the suboxygen and hydrogen sulfide layers could not be recorded. In general, an increase in the TSM content in the boundary layer of the transition of the oxygen zone into the hydrogen sulfide zone, observed according to the survey data of 2019 and 2021, was also noted earlier in the work [1)]. According to the authors of this work, the main reason for such an increase in turbidity is oxidation of manganese and iron entering the suboxygen zone and formation of a suspension of their oxides.

An analysis of the linear relationship between the series of C_{TSM} values, temperature, salinity, and density for the totality of all stations at each horizon with a discreteness of 1 m showed that the level of consistency between horizontal distributions of C_{TSM} and thermohaline parameters noticeably changes with depth (Fig. 8, *a* – *c*). In the upper 30–40 m layer, which covers the UQHL in the fields of temperature, salinity, and density and the layer of seasonal thermocline, halocline, and pycnocline, an insignificant level of linear correlation was revealed (Fig. 8). The low agreement between the horizontal fields of C_{TSM} and the thermohaline parameters in the upper layer is associated with different rates of adaptation of these fields to changes in synoptic conditions. As a result, at a number of stations in the layer of the lower seasonal thermocline and pycnocline, the TSM maximum was observed, and at other stations, a sharp decrease in the content of suspended matter occurred in this layer.

Deeper than the seasonal thermocline, halocline, and pycnocline, the connection level increased and the values of the linear correlation coefficients R were 0.5–0.6; at the same time, a positive correlation was revealed between the values of C_{TSM} and temperature (Fig. 8, *a*), and a negative correlation between the values of C_{TSM} and salinity and density (Fig. 8, *b*, *c*). The maximum level of linear correlation with R values reaching 0.67 in absolute value was found between the distributions of C_{TSM} and temperature at the 48 m horizon (Fig. 8, *d*), between the distributions of C_{TSM} and salinity and density at the 120 m horizon (Fig. 8, *e*, *f*).

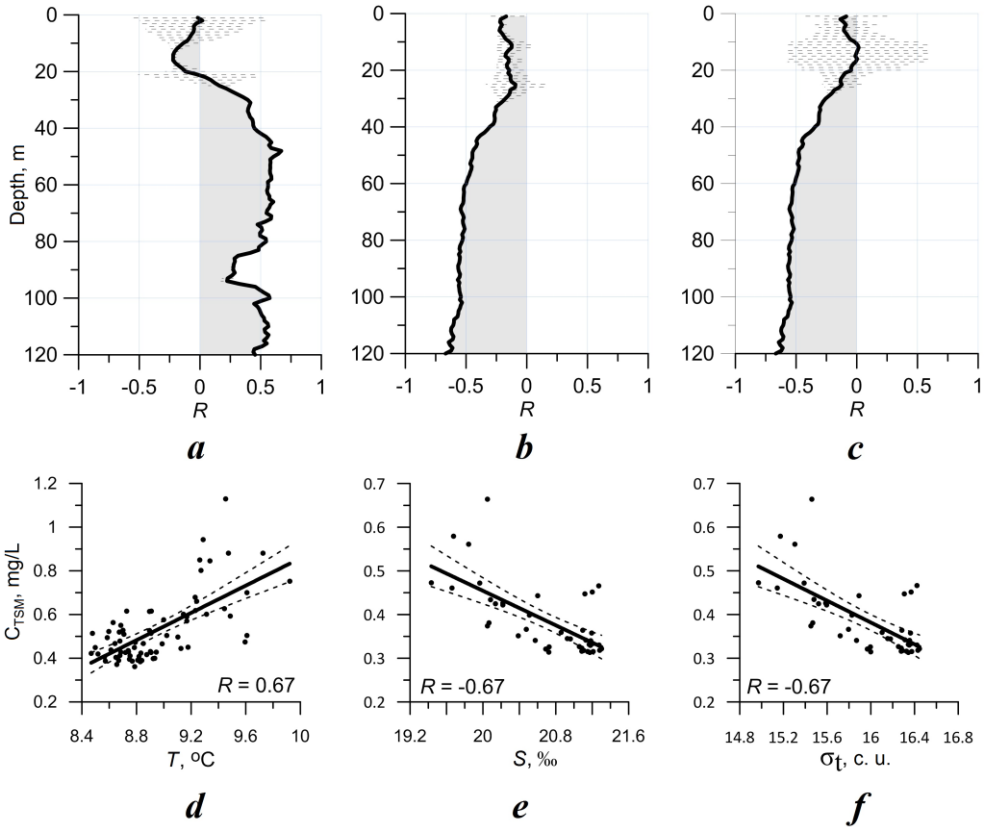

Fig. 8. Vertical distributions of linear correlation coefficients R between C_{TSM} values and values of temperature (*a*), salinity (*b*) and density (*c*) on totality of all stations with a depth increment of 1 m (*d*); charts of linear correlation between C_{TSM} and salinity (*e*), between C_{TSM} and density (*f*) at 120 m horizon. Dashed lines show 95 % confidential intervals

A higher than in the upper 40-m layer, the level of agreement between the horizontal distributions of TSM and thermohaline parameters below the seasonal thermocline, halocline, and pycnocline is due to a decrease with depth in the level of synoptic variability in thermohaline fields [25]. In general, a significant level of agreement between the horizontal distributions of TSM and thermohaline parameters indicates that at these depths, colder, saline, and denser waters were characterized by increased transparency, and the rise and fall of certain isosurfaces in thermohaline fields were accompanied by a similar behaviour of isosurfaces in the field of C_{TSM} concentration.

Conclusions

According to the data of hydrological and hydrooptical measurements performed during the 116th cruise of the R/V *Professor Vodyanitsky* in April–May 2021, it was shown that the Rim Current formed anticyclonic eddies located above the coastal shelf to the south of the Heraclea Peninsula in the upper 50 m layer, to the east of Cape Meganom at depths of 10–25 m, above the continental slope in the entire measurement layer south of Cape Meganom and south of the Kerch Peninsula. At the southwestern boundary of the polygon, a cyclonic eddy was traced throughout the measurement layer, most clearly expressed at the horizons of 75–125 m. At the southeastern boundary, an intense cyclonic meander was observed, which manifested itself as a closed eddy at depths of 25–50 m.

It was revealed that the water temperature in the surface layer in the eastern part of the polygon (to the east of 34.5° E) was higher (13–15 °C) than in the western part (10–12 °C), which is due, on the one hand, with the Rim Current advection of warm waters along the Caucasian and Crimean coasts, on the other hand, with longer spring warming of surface waters in this area. A decrease in SST (to 12–12.5 °C), associated with coastal upwelling, was noted near the coast east of Cape Meganom and in Feodosiya Bay. The temperature minimum (10–10.5 °C), caused by the rise of colder deep waters, was observed in the area of the cyclonic eddy near the southwestern boundary of the polygon.

It is shown that the minimum salinity (18.1–18.2 ‰) was observed off the coast of the Kerch Peninsula and in the eastern part of Feodosiya Bay, while the tongue of desalinated waters along the isohaline of 18.25 ‰ extended to the south from the Kerch Peninsula. This tongue was formed as a result of mixing of freshened Azov-sea waters coming from the Kerch Strait and the waters of Feodosiya Bay, carried along the periphery of the anticyclonic eddy. The maximum salinity values (18.8–18.85 ‰) due to the rise of more saline deep waters to the surface were noted in the zones of cyclonic meanders and eddies.

It was revealed that in the spring of 2021, UQHL of relatively warm waters was observed at most stations, due to spring heating, under which the second lower quasi-homogeneous layer, which formed in the previous winter period, remained. In the conditional density field, the UQHL at most stations was also characterized by a two-step structure. In the field of salinity, in contrast to the fields of temperature and density, one UQHL was predominantly traced. The two-layer UQHL structure caused the formation of two maxima (in absolute value) of the vertical temperature and density gradients.

It was shown that the features of water circulation were well manifested in the distribution of the depths of occurrence of the main pycnocline, halocline, and CIL core. The depth of the main pycnocline and halocline decreased markedly (to 45–55 m) in the southern deep part of the polygon and was minimal (40–45 m) in the southwest of the polygon in the area of the cyclonic eddy. Closer to the slope of the depths and in the zones of anticyclonic meanders and eddies, it noticeably increased (up to 90–125 m). The depth of the CIL core occurrence was also minimal (35–40 m) in the area of cyclonic eddy in the southwest of the polygon and increased to 100–130 m in the zones of anticyclonic formations

south of the Heraclea and Kerch Peninsulas. The maximum deepening of the CIL core (up to 150–180 m) was traced in the area of the anticyclonic eddy south of Cape Meganom.

It is shown that in the spring of 2021, intense water freshening in the northeastern part of the polygon was not accompanied, as usual, by an increase in TSM concentration. In Feodosiya Bay, a minimum TSM concentration (0.55–0.9 mg/L) was revealed, and to the south of the Kerch Peninsula, a tongue of waters of increased transparency, coinciding in position with the tongues of waters of low temperature and salinity was revealed. An increase in TSM concentration (up to 1.2–1.3 mg/L) was observed in the form of individual spots in the Rim Current zone, above the continental slope and on the shelf, and its maxima (1.35–1.4 mg/L) were traced on the shelf between Cape Ayu-Dag and Cape Sarych and to the west of the Heraclea Peninsula.

The vertical structure of the TSM field was characterized by the presence of one UQHL, the lower boundary of which was located in the layer of the upper seasonal thermocline and pycnocline. The highest content of suspended matter was observed either in the upper layer, coinciding in thickness with the UQHL in thermohaline fields, or in the layer of the lower seasonal thermocline and pycnocline. In general, deeper than the seasonal thermocline, halocline, and pycnocline, the TSM concentration markedly decreased compared to its values in the surface layer. In the areas of anticyclonic eddies at these depths, an increase in TSM concentration was observed due to the subsidence of more turbid waters from the overlying layers of the sea.

It was found that the level of consistency between the horizontal distributions of TSM concentration and thermohaline parameters changed markedly with depth. In the upper 30–40 m layer, a low agreement between the horizontal fields of C_{TSM} and the thermohaline parameters was revealed. Deeper than the seasonal thermocline, halocline, and pycnocline, the level of correlation between C_{TSM} and thermohaline parameters increased to a significant level. The values of the linear correlation coefficients R were 0.5–0.6, while a positive correlation was revealed between the values of C_{TSM} and temperature, and a negative correlation between the values of C_{TSM} and salinity and density, i.e., colder, saline and denser waters were characterized by increased transparency.

REFERENCES

1. Bondur, V.G., Ivanov, V.A., Vorobiev, V.E., Dulov, V.A., Dolotov, V.V., Zamshin, V.V., Kondratiev, S.I., Lee, M.E. and Malinovsky, V.V., 2020. Ground-to-Space Monitoring of Anthropogenic Impacts on the Coastal Zone of the Crimean Peninsula. *Physical Oceanography*, 27(1), pp. 95–107. doi:10.22449/1573-160X-2020-1-95-107
2. Izrael, Yu. A. and Tsyban, A.V., 2009. *Anthropogenic Ecology of Ocean*. Moscow: Flinta; Nauka, 529 p. (in Russian).
3. Eisma, D., 1993. *Suspended Matter in the Aquatic Environment*. Berlin, Heidelberg: Springer-Verlag, 315 p. doi:10.1007/978-3-642-77722-6
4. Man'kovskii, V.I. and Solov'ev, M.V., 2003. Relationship between the Beam Attenuation Coefficient and the Concentration of Suspended Matter in Black-Sea Waters. *Physical Oceanography*, 13(2), pp. 123–128. https://doi.org/10.1023/A:1023752514790
5. Kukushikin, A.S., Agafonov, E.A. and Prokhorenko, Yu.A., 2006. Distribution of the Beam Attenuation Coefficient in the Black Sea Surface Coastal Waters. *Morskoy Gidrofizicheskiy Zhurnal*, (5), pp. 30–43 (in Russian).

6. Kukushkin, A.S., 2017. Spatial and Temporal Variability of the Water Transparency Distribution in the North-Western Black Sea. *Optika Atmosfery i Okeana*, 30(9), pp. 750–762. doi:10.15372/AOO20170904 (in Russian).
7. Ginzburg, A.I., Kostianoy, A.G. and Sheremet, N.A., 2004. Seasonal and Interannual Variability of the Black Sea Surface Temperature as Revealed from Satellite Data (1982–2000). *Journal of Marine Systems*, 52(1–4), pp. 33–50. doi:10.1016/j.jmarsys.2004.05.002
8. Volpe, V., Silvestri, S. and Marani, M., 2011. Remote Sensing Retrieval of Suspended Sediment Concentration in Shallow Waters. *Remote Sensing of Environment*, 115(1), pp. 44–54. doi:10.1016/j.rse.2010.07.013
9. Kremenchutskiy, D.A., Kubryakov, A.A., Zav'yalov, P.O., Konovalov, B.V., Stanichniy, S.V. and Aleskerova, A.A., 2014. Determination of the Suspended Matter Concentration in the Black Sea Using to the Satellite MODIS Data. In: MHI, 2014. *Ekologicheskaya Bezopasnost' Pribrezhnoy i Shel'fovoy Zon i Kompleksnoe Ispol'zovanie Resursov Shel'fa* [Ecological Safety of Coastal and Shelf Zones and Comprehensive Use of Shelf Resources]. Sevastopol: ECOSI-Gidrofizika. Iss. 29, pp. 5–9 (in Russian).
10. Kubryakov, A.A. and Stanichny, S.V., 2015. Mesoscale Eddies in the Black Sea from Satellite Altimetry Data. *Oceanology*, 55(1), pp. 56–67. https://doi.org/10.1134/S0001437015010105
11. Aleskerova, A.A., Kubryakov, A.A., Goryachkin, Yu.N. and Stanichny, S.V., 2017. Propagation of Waters from the Kerch Strait in the Black Sea. *Physical Oceanography*, (6), pp. 47–57. https://doi.org/10.22449/1573-160X-2017-6-47-57
12. Artamonov, Yu.V., Skripaleva, E.A., Latushkin, A.A. and Fedirko, A.V., 2019. Multi-Year Average Intra-Annual Cycle of Hydrooptical Characteristics, Chlorophyll a and Surface Temperature of the Black Sea from Satellite Data. *Sovremennye Problemy Distantsionnogo Zondirovaniya Zemli iz Kosmosa = Current Problems in Remote Sensing of the Earth from Space*, 16(1), pp. 171–180. doi:10.21046/2070-7401-2019-16-1-171-180
13. Yu, X., Lee, Z., Shen, F., Wang, M., Wei, J., Jiang, L. and Shang, Z., 2019. An Empirical Algorithm to Seamlessly Retrieve the Concentration of Suspended Particulate Matter from Water Color across Ocean to Turbid River Mouths. *Remote Sensing of Environment*, 235, 111491. doi:10.1016/j.rse.2019.111491
14. Zamshin, V.V., Matrosova, E.R., Khodaeva, V.N. and Chvertkova, O.I., 2021. Quantitative Approach to Studying Film Pollution of the Sea Surface Using Satellite Imagery. *Physical Oceanography*, 28(5), pp. 567–578. doi:10.22449/1573-160X-2021-5-567-578
15. Fedirko, A.V., Artamonov, Yu.V., Skripaleva, E.A., Deryushkin, D.V., Kolmak, R.V., Zavialov, D.D., Shapovalov, R.O., Shapovalov, Yu.I. and Shcherbachenko, S.V., 2019. [Manifestation of Seasonal and Synoptic Variability in the Hydrological Structure of the Waters of the Northern Black Sea]. In: IMBR, 2019. [*Results of Expedition Research in 2018 in the World Ocean, Internal Waters and the Svalbard Archipelago: Conference Proceedings*]. Sevastopol: IMBR, pp. 174–175. doi:10.21072/978-5-6042938-1-2 (in Russian).
16. Fedirko, A.V., Artamonov, Yu.V., Deryushkin, D.V., Nikolsky, N.V., Ozerov, S.A., Skripaleva, E.A., Shutov, S.A., Shapovalov, R.O., Shapovalov, Yu.I. and Shcherbachenko, S.V., 2020. [Circulation and Thermohaline Structure of Waters in the Northern Part of the Black Sea according to Hydrological Measurements in 2019 (Cruises 106, 108, 110, 111 of the R/V Professor Vodyanitsky)]. In: IBSS, 2020. [*Results of Expedition Research in 2019 in the World Ocean, Internal Waters and the Svalbard Archipelago: Conference Proceedings*]. Sevastopol: IBSS, pp. 206–212. doi:10.21072/978-5-6044865-0-4 (in Russian).

17. Konovalov, S.K., Artamonov, Yu.V., Garmashov, A.V., Orekhova, N.A. and Latushkin, A.A., 2021. [Experimental Studies of Variability of Oceanological Fields in the Black Sea and the Sea of Azov in 2020]. In: T. V. Dabizha, ed., 2021. *Results of Field Research in the World Ocean and Internal Waters in 2020. Conference Proceedings*. *Moscow, 24–26 February 2021.* Sevastopol, pp. 131–133 (in Russian).
18. Morozov, A.N. and Mankovskaya, E.V., 2020. Cold Intermediate Layer of the Black Sea according to the Data of the Expedition Field Research in 2016–2019. *Ecological Safety of Coastal and Shelf Zones of Sea*, (2), pp. 5–16. doi:10.22449/2413-5577-2020-2-5-16 (in Russian).
19. Artamonov, Yu.V., Skripaleva, E.A., Fedirko, A.V., Shutov, S.A., Derjushkin, D.V., Shapovalov, R.O., Shapovalov, Yu. I. and Shcherbachenko, S.V., 2020. Waters Circulation in the Northern Part of the Black Sea in Summer – Winter of 2018. *Ecological Safety of Coastal and Shelf Zones of Sea*, (1), pp. 69–90. doi:10.22449/2413-5577-2020-1-69-90 (in Russian)
20. Morozov, A.N. and Mankovskaya, E.V., 2021. Spatial Characteristics of the Black Sea Cold Intermediate Layer in Summer, 2017. *Physical Oceanography*, 28(4), pp. 404–413. doi:10.22449/1573-160X-2021-4-404-413
21. Latushkin, A.A., Artamonov, Yu.V., Skripaleva, E.A., Fedirko, A.V. and Kudinov, O.B., 2020. Spatial Features of the Hydro-Optical Waters Structure in the Northern Part of the Black Sea in Spring 2019 according to Contact Measurements on R/V Professor Vodyanitsky. In: G. G. Matvienko and O. A. Romanovskii, eds., 2020. *Proceedings of SPIE*. Bellingham: SPIE. Vol. 11560: 27th International Symposium on Atmospheric and Ocean Optics: Atmospheric Physics, 115602R. doi:10.1117/12.2574281
22. Latushkin, A.A., Artamonov, Yu.V., Skripaleva, E.A., Fedirko, A.V. and Kudinov, O.B., 2021. Features of Relationship between the Biooptical Parameters' Distributions and Hydrological Water Structure in the Northern Black Sea in Winter 2020. In: G. G. Matvienko and O. A. Romanovskii, eds., 2021. *Proceedings of SPIE*. Bellingham: SPIE. Vol. 11916: 27th International Symposium on Atmospheric and Ocean Optics: Atmospheric Physics, 119163J. doi:10.1117/12.2603317
23. Klyuvitkin, A.A., Garmashov, A.V., Latushkin, A.A., Orekhova, N.A., Kochenkova, A.I. and Malafeev, G.V., 2019. Comprehensive Studies of the Black Sea during the Cruise 101 of the R/V Professor Vodyanitskiy. *Oceanology*, 59(2), pp. 287–289. doi:10.1134/S0001437019020097
24. Artamonov, Yu.V., Latushkin, A.A., Skripaleva, E.A. and Fedirko, A.V., 2019. Rim Current Manifestation in the Climatic Fields of Hydro-Optical and Hydrological Characteristics at the Coast of Crimea. In: SPIE, 2019. *Proceedings of SPIE.* Bellingham: SPIE. Vol. 11208: 25th International Symposium on Atmospheric and Ocean Optics: Atmospheric Physics, 112084X. doi:10.1117/12.2540803
25. Ivanov, V.A. and Belokopytov, V.N., 2013. *Oceanography of the Black Sea*. Sevastopol: EKOSI-Gidrofizika, 210 p.
26. Staneva, J.V., Dietrich, D.E., Stanev, E.V. and Bowman, M.J., 2001. Rim Current and Coastal Eddy Mechanisms in an Eddy-Resolving Black Sea General Circulation Model. *Journal of Marine Systems*, 31(1–3), pp. 137–157. doi:10.1016/S0924-7963(01)00050-1
27. Kubryakov, A.A., Mizyuk, A.I., Puzina, O.S. and Senderov, M.V., 2018. Three-Dimensional Identification of the Black Sea Mesoscale Eddies according to NEMO Numerical Model Calculations. *Physical Oceanography*, 25(1), pp. 18–26. doi:10.22449/1573-160X-2018-1-18-26

28. Yakushev, E.V., Chasovnikov, V.K., Murray, J.W., Pakhomova, S.V, Podymov, O.I. and Stunzhas, P.A., 2007. Vertical Hydrochemical Structure of the Black Sea. In: A. G. Kostianoy and A. N. Kosarev, eds., 2007. *The Black Sea Environment*. The Handbook of Environmental Chemistry, vol. 5Q. Berlin, Heidelberg: Springer, pp. 277–307. doi:10.1007/698_5_088

Submitted 26.05.2022; accepted after review 5.06.2022;
revised 02.11.2022; published 23.12.2022

About the authors:

Yuri V. Artamonov, Leading Research Associate, Marine Hydrophysical Institute of RAS (2 Kapitanskaya St., Sevastopol, 299011, Russian Federation), Dr.Sci. (Geogr.), **ResearcherID: AAC-6651-2020**, *artam-ant@yandex.ru*

Elena A. Skripaleva, Senior Research Associate, Marine Hydrophysical Institute of RAS (2 Kapitanskaya St., Sevastopol, 299011, Russian Federation), Ph.D. (Geogr.), **ResearcherID: AAC-6648-2020**, *sea-ant@yandex.ru*

Aleksandr A. Latushkin, Junior Research Associate, Marine Hydrophysical Institute of RAS (2 Kapitanskaya St., Sevastopol, 299011, Russian Federation), **ORCID ID: 0000-0002-3412-7339**, *sevsalat@gmail.com*

Aleksandr V. Fedirko, Junior Research Associate, Marine Hydrophysical Institute of RAS (2 Kapitanskaya St., Sevastopol, 299011, Russian Federation), **ResearcherID: AAC-6629-2020**, *vault102@gmail.com*

Danil A. Ryabokon, Leading Research Engineer, Marine Hydrophysical Institute of RAS (2 Kapitanskaya St., Sevastopol, 299011, Russian Federation), **SPIN-code: 3729-4228**, *akronis_white@mail.ru*

Contribution of the authors:

Yuri V. Artamonov – general scientific supervision of the study, setting of study aims and objectives, development of methods and performance of experiments, qualitative analysis of the results and interpretation thereof, discussion of the study results, drawing conclusions

Elena A. Skripaleva – review of literature on the study topic, qualitative analysis of the results and interpretation thereof, processing and description of the study results, discussion of the study results, drawing conclusions, article text preparation and refinement

Aleksandr A. Latushkin – development of methods and conducting experimental studies, qualitative analysis of the results and interpretation thereof, discussion of the study results

Aleksandr V. Fedirko – development and debugging of software for experiment data secondary processing, computer implementation of algorithms, chart and diagram construction, participation in discussion of the article

Danil A. Ryabokon – development of methods and conducting experimental studies, discussion of the study results

All the authors have read and approved the final manuscript.

DOI: 10.22449/2413-5577-2022-4-25-38

Vertical Mixing in the Black Sea Active Layer from Small-Scale Measurement Data

A. N. Morozov *, E. V. Mankovskaya

Marine Hydrophysical Institute of RAS, Sevastopol, Russia
**e-mail: anmorozov@mhi-ras.ru*

Abstract

The paper considers the methodological issues of using the G03 parameterization to estimate the vertical turbulent diffusion coefficient from current velocity and density stratification data collected with a depth increment of 4 m. Based on the expedition materials obtained during the 87th cruise of the R/V *Professor Vodyanitsky* (30 June to 18 July 2016) in the central sector of the northern Black Sea, this coefficient was estimated at the upper boundary of the cold intermediate layer and the depth layer of 350–390 m. The results of measurements in the acoustic Doppler current profiler exposure mode near the sea surface and at the lower sounding point were used as input data on the current velocity. In the upper sea layer at a potential density of 14.2 kg/m^3, the coefficient value was $7.26 \cdot 10^{-6}$ m^2/s, which is close to its value of $6 \cdot 10^{-6}$ m^2/s in the core of the cold intermediate layer estimated from the thermal conductivity equation from the 2017 expedition measurements. The corresponding heat flux into the cold intermediate layer is 1.79 W/m^2. An indirect estimate of the coefficient in the seasonal thermocline was $2.26 \cdot 10^{-7}$ m^2/s. This value is comparable to the molecular heat diffusion coefficient. Salt flux at a potential density value of 14.2 kg/m^3 is 2,977 g/(m^2·year), the corresponding salt transport through the isopycnal surface is $1.1 \cdot 10^{15}$ g/year, or about 22 % of the mass of salt brought into the Black Sea by the lower Bosphorus current per year. In the layer of 350–390 m depth at a potential density value of about 16.9 kg/m^3, the estimated vertical turbulent diffusion coefficient was $2.66 \cdot 10^{-6}$ m^2/s. The corresponding heat flux was $3.9 \cdot 10^{-3}$ W/m^2, or about 10 % of the geothermal flux. Salt flux of 4.110^{-6} g/(m^2/s) corresponds to its transport of $3.9 \cdot 10^{13}$ g/year through the isopycnal surface and represents 0.75 % of the mass of salt brought by the lower Bosphorus current per year. The ratio of the kinetic energy of small-scale processes to their potential energy was found to be 1.53 for the near-surface layer and 11 for the lower sounding point. This variability determines an almost threefold enhancement of vertical mixing at the upper measurement point according to the G03 parameterization

Keywords: Black Sea, vertical mixing, shear, strain, current velocity, heat flux, salt flux

Acknowledgements: the work was performed under state assignment no. 0555-2021-0003 on topics “Operational oceanology”, no. 0555-2021-0005 “Coastal studies”.

For citation: Morozov, A.N. and Mankovskaya, E.V., 2022. Vertical Mixing in the Black Sea Active Layer from Small-Scale Measurement Data. *Ecological Safety of Coastal and Shelf Zones of Sea*, (4), pp. 25–38. doi:10.22449/2413-5577-2022-4-25-38

Вертикальное перемешивание в деятельном слое Черного моря по данным мелкомасштабных измерений

А. Н. Морозов *, Е. В. Маньковская

Морской гидрофизический институт РАН, Севастополь, Россия
**e-mail: anmorozov@mhi-ras.ru*

Аннотация

Рассмотрены методические вопросы использования параметризации *G*03 для оценки коэффициента вертикальной турбулентной диффузии по данным о скорости течения и плотностной стратификации, собранным с разрешением 4 м по глубине. На основе экспедиционных материалов, полученных в 87-м рейсе НИС «Профессор Водяницкий», проходившем с 30 июня по 18 июля 2016 г. в центральном секторе северной части Черного моря, выполнена оценка значений этого коэффициента на верхней границе холодного промежуточного слоя и слое глубин 350–390 м. В качестве исходных данных о скорости течения были использованы результаты измерений в режиме выдержки акустического доплеровского профилометра течений у поверхности моря и в нижней точке зондирования. В верхнем слое моря при потенциальной плотности 14.2 кг/м^3 значение коэффициента составило $7.26\cdot10^{-6}$ м^2/с, что близко к его значению $6\cdot10^{-6}$ м^2/с в ядре холодного промежуточного слоя, оцененному из уравнения теплопроводности по результатам измерений экспедиций 2017 г. Соответствующий поток тепла в холодный промежуточный слой равен 1.79 Вт/м^2. Косвенная оценка коэффициента в сезонном термоклине составила $2.26\cdot10^{-7}$ м^2/с – значение, сопоставимое с коэффициентом молекулярной диффузии тепла. Поток соли при значении потенциальной плотности 14.2 кг/м^3 равен 2977 г/(м^2·год), соответствующий перенос соли через изопикническую поверхность – $1.1\cdot10^{15}$ г/год, или около 22 % массы соли, приносимой в Черное море нижнебосфорским течением за год. В слое глубин 350–390 м при значении потенциальной плотности около 16.9 кг/м^3 оценка коэффициента вертикальной турбулентной диффузии составила $2.66\cdot10^{-6}$ м^2/с. Соответствующий поток тепла равен $3.9\cdot10^{-3}$ Вт/м^2, или около 10 % геотермального потока. Поток соли $4.1\cdot10^{-6}$ г/(м^2·с) соответствует ее переносу через изопикническую поверхность в размере $3.9\cdot10^{13}$ г/год и составляет 0.75 % от массы соли, приносимой нижнебосфорским течением за год. Установлено отношение кинетической энергии мелкомасштабных процессов к их потенциальной энергии, которое равно 1.53 для верхнего слоя и 11 для нижней точки зондирования. Такая изменчивость определяет почти трехкратное усиление вертикального перемешивания в верхней точке измерений в соответствии с параметризацией *G*03.

Ключевые слова: Черное море, вертикальное перемешивание, сдвиг скорости течения скорость течения, поток тепла, поток соли

Благодарности: работа выполнена в рамках государственного задания по темам № 0555-2021-0003 «Оперативная океанология», № 0555-2021-0005 «Прибрежные исследования».

Для цитирования: *Морозов А. Н., Маньковская Е. В.* Вертикальное перемешивание в деятельном слое Черного моря по данным мелкомасштабных измерений // Экологическая безопасность прибрежной и шельфовой зон моря. 2022. № 4. С. 25–38. EDN TRZMDQ. doi:10.22449/2413-5577-2022-4-25-38

Introduction

Vertical fluxes of heat, salt, nutrients and other substances in the Black Sea water column have a significant impact on the functioning of the ecosystem of the upper active layer and partly determine the efficiency of reproduction of its resources used in the national economy (fishing, mussel farms, oyster plantations, etc.). Basically, vertical exchange is carried out by means of turbulent mixing. As a result, the estimation of the vertical turbulent diffusion coefficient in the Black Sea has been an urgent task of oceanology for many years [1)] [1–7].

The range of coefficient values given in the literature for the Black Sea extends from values close to the molecular heat diffusion coefficient of ~10^{-7} m^2/s [3] to the maximum value of $3 \cdot 10^{-2}$ m^2/s (in the work [1)]). Such a large range of coefficient values is determined both by the difference in methods for its assessment, and by the spatio-temporal difference in hydrophysical conditions and atmospheric effects. At present, it is generally accepted that the value of the vertical turbulent diffusion coefficient obtained from microstructural data is the most reliable [4]. However, the sources only state two cases of using microstructural probes in the deep part of the Black Sea [3, 4], which give the values of the coefficient in the upper stratified layer of the sea at the level of $O(10^{-6})$ m^2/s. A small number of this kind of data is due to the high cost of equipment, technological difficulties in carrying out measurements and data processing. At the same time, synchronous measurements of density and current velocity profiles performed with a small-scale resolution are currently widespread and are often used to estimate the vertical turbulent diffusion coefficient [6, 8–12].

From the summer of 2016 to the present day, the Marine Hydrophysical Institute has carried out more than 20 expeditions in the central sector of the northern part of the Black Sea [13, 14], where both CTD measurements and measurements of current velocity profiles using the Acoustic Doppler Current Profilers (ADCP) were taken. The purpose of this work is to study the characteristics of small-scale processes in the active layer of the Black Sea. The article discusses methodological issues of applying the G03 parameterization [10, 11] for estimating the vertical turbulent diffusion coefficient based on the data obtained as a result of ADCP exposure near the sea surface and at the bottom of sounding. The measurement data are used to estimate the heat and salt fluxes at the upper boundary of the cold intermediate layer [13] and at the lower boundary of the upper layer of shear baroclinic currents [6, 15]. It is expected that the proposed approach to estimating the vertical turbulent diffusion coefficient, applied to the entire array of data collected during expeditions of recent years, will make it possible to assess the seasonal variability of the intensity of vertical mixing at different depths in the active layer of the Black Sea.

[1)] Blatov, A.S., Bulgakov, N.P., Ivanov, V.A., Kosarev, A.N. and Tuzhilkin, V.S., 1984. *Variability of Hydrophysical Fields of the Black Sea*. Leningrad: Gidrometeoizdat, 240 p. (in Russian).

Data, instruments and methods

The expedition materials obtained during the 87th cruise of the R/V *Professor Vodyanitsky*, which took place from 30.06.2016 to 8.07.2016 in the central sector of the northern part of the Black Sea (31°–36.5° E, 43°–45° N), were used in the article [16]. CTD measurements were performed using the SBE 911plus probe, the results were interpolated to a grid with a step of 1 m. The current velocity profiles were measured using a lowered ADCP based on WHM300 manufactured by RDI, depth resolution (b) 4 m [17]. The total number of stations was 106. The work used data from 65 stations taken at a sea depth of more than 400 m. The current velocity vectors in the 30–60 m layer at these stations are shown in Fig. 1. The stations were evenly located in the area of the Rim Current and outside it closer to the center of the sea. The sequence of measuring the current velocity profile included 3–5 min exposures of the instrument near the sea surface and at the lower sounding point [14]. It is the data obtained during ADCP exposures at these horizons that are analyzed in this work.

Density profiles ($\rho = 1000 + \sigma_\theta$, where σ_θ is the potential density, kg/m^3) were previously subjected to low-frequency depth filtering using a triangular filter corresponding to ADCP spatial averaging, transfer function $H_{ADCP}(k) = (\sin(\pi bk)/(\pi bk))^4$ (k is the vertical wave number) [17]. Further, using linear interpolation, the density values were determined at the horizons for measuring the current velocity.

Fig. 2 shows the initial data in the form of a scattering diagram: the buoyancy frequency square is plotted along the abscissa ($N^2 = (g/\rho)(\Delta\sigma_\theta/\Delta z)$, where g is the acceleration of gravity; Δz is the depth increment (here – 4 m)); along the y-axis, the squared shear of the current velocity according to the data ADCP ($Sh^2_{ADCP} = (\Delta U/\Delta z)^2 + (\Delta V/\Delta z)^2$, where U, V are the eastern and northern components

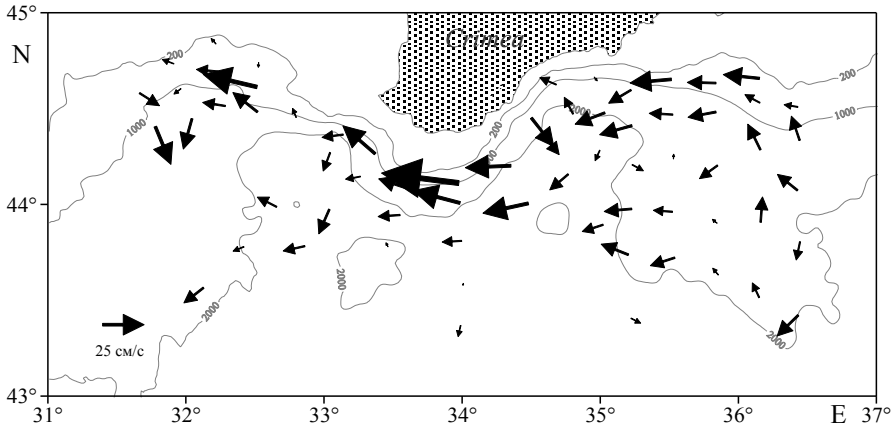

Fig. 1. Schematic station layout in the 87th cruise of the R/V *Professor Vodyanitsky* (arrows show current velocity vectors at the layer of 30–60 m)

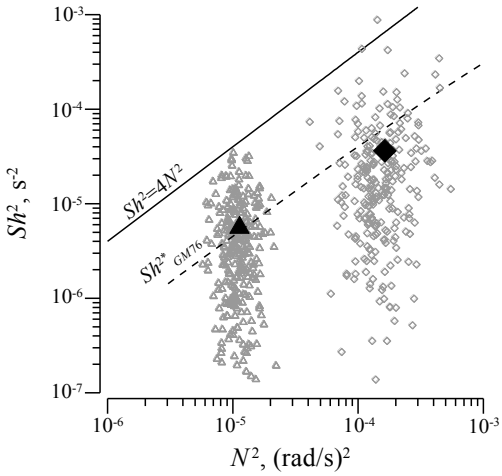

Fig. 2. Input data of CTD-soundings and ADCP measurements (grey diamonds are for the exposure near the sea surface, grey triangles are for that at the lower sounding point; black symbols – mean values)

of the current velocity vector). Transfer function of differentiation at a finite depth increment $H_{\mathrm{Dif}}(k) = (\sin(\pi\Delta z k)/(\pi\Delta z k))^2$ [18]. Gray diamonds correspond to the data obtained in the vicinity of the upper boundary of the cold intermediate layer (density 14.2 ± 0.15 kg/m^3) when the device is exposed near the sea surface. The number of readings is 256, the average depth of the isopycna with a potential density of 14.2 kg/m^3 is 44 m. The grey triangles correspond to the data collected when the instrument was exposed at the lower probing point. The number of readings is 566, the average density value is 16.9 kg/m^3, the average depth is 369 m. Black markers are average values $\langle N^2\rangle$ and $\langle Sh^2\rangle$, where $\langle\ldots\rangle$ is the operator of averaging over all samples.

The solid black line corresponds to the critical value of the gradient Richardson number (Ri = N^2/Sh^2), which is 0.25 [19]. At values of the Richardson number less than the critical one, a linear instability of the shear flow can occur, leading to the development of turbulence. It can be seen from the figure that in the initial data set, all values of the Richardson number at the lower sounding point are greater than the critical one, which can be perceived as the absence of turbulent mixing, since the necessary condition for shear flow instability is not met. This is due to the fact that the measurements were carried out with the spatial depth resolution inherent in ADCP and, in addition, the derivatives were calculated at finite depth increments. The vertical resolution of the shear measurement process, determined by the weakening of the transfer function $H_{ADCP}\cdot H_{\mathrm{Dif}}$ to a level of 3 dB, was about 12 m. It was shown in [20] that the enhancement of turbulence dissipation should be associated with small values of the Richardson number obtained at vertical increments of 3 m. At the same time, estimates of the value of the Richardson number on a 10-meter scale have little in common with the microstructure. In essence, this means that turbulence is mainly generated at vertical scales that are smaller than the vertical resolution with which our measurements were made.

The black dashed line represents the results of the ratio $Sh^{2*}_{GM76} = \int_0^1 F_{GM76}(N,k)\cdot H_{ADCP}(k)\cdot H_{\mathrm{Dif}}(k)\cdot dk$, where $F_{GM76}(N, k)$ – shear spectral

density for the canonical spectrum of internal waves GM76 [21, 22], as given in [23]. At the upper boundary of the cold intermediate layer $\langle Sh^2_{ADCP} \rangle = 3.7 \cdot 10^{-5}$ s^{-2}; $Sh^{2*}_{GM\,76} = 6.2 \cdot 10^{-5}$ s^{-2}. This confirms the fact that the intensity of internal waves in the Black Sea is weaker than in oceanic conditions, for which the canonical spectrum of GM76 was determined. For the ocean, there are two sources of internal waves approximately equal in power: tides and wind [24], while in the Black tide-free sea, the only source of internal waves is the wind [25]. At the lower point of the sounding, the average value of the squared measured shear ($\langle Sh^2_{ADCP} \rangle = 5.5 \cdot 10^{-6}$ s^{-2}) slightly (10 %) exceeds the value of $Sh^{2*}_{GM\,76} = 5 \cdot 10^{-5}$ s^{-2}, which is a less expected result. Early parameterizations for estimating the vertical turbulent diffusion coefficient from the data collected at fine-scale resolution were based either on the Richardson number [26] or on the relationship $K_V \infty \left(\left\langle Sh^2_{ADCP} \right\rangle / Sh^{2*}_{GM\,76} \right)^2$ [8], or on a more complex dependence on the Richardson number and the probability of observing its value less than the critical one [27, 28].

Results and discussion

In the framework of this article, to estimate the coefficient of vertical turbulent diffusion (K_V), the parameterization G03 [10] was used, which takes into account the deviation of the spectrum of internal waves from the canonical form [9] and the geographical location of the measurement area. The applied formulas for calculations are borrowed from [11]:

$$K_V = K_0 \frac{\left\langle Sh^2_{ADCP} \right\rangle^2}{\left(Sh^2_{GM\,76} \right)^2} \cdot h_1(R_\omega) \cdot j\left(\frac{f}{N} \right),$$

$$h_1(R_\omega) = \frac{3(R_\omega + 1)}{2\sqrt{2} R_\omega \sqrt{R_\omega - 1}},$$

$$j(f/N) = \frac{f \operatorname{arccos} h(N/f)}{f_{30} \operatorname{arccos} h(N_0/f_{30})},$$

where $K_0 = 5 \cdot 10^{-6}$ m^2/s; f is the local inertial frequency at 44° N; f_{30} is the inertial frequency at 30° N; $N_0 = 5.24 \cdot 10^{-3}$ rad/s. The ratio of flow velocity shear to strain variations (R_ω – the shear/strain variance ratio), or the ratio of kinetic and potential energy of small-scale processes, is defined as

$$R_\omega = \frac{\left\langle Sh^2_{ADCP} \right\rangle}{\left\langle N^2 \right\rangle \left\langle \xi^2_Z \right\rangle},$$

where $\langle \xi^2_z \rangle = \langle \delta^2 \rangle / \langle N^2 \rangle^2 = \langle (N^2 - N^2_{\text{Fit}})^2 \rangle / \langle N^2 \rangle^2$ is the mean square strain; N_{Fit} is the dependence characterizing stable features of density stratification.

Lower boundary of the upper layer of shear baroclinic currents. Fig. 3 shows some graphical material explaining the procedure for estimating the coefficient of vertical turbulent diffusion and calculating the heat and salt fluxes based on the data obtained at the lower point of sounding. Fig. 3, *a* shows the dependence of the buoyancy frequency square on the difference between the measurement depth and the isopycnal depth σ_θ = 16.9 kg/m^3 ($D_{16.9}$).The linear dependence N^2_{Fit} on distance was drawn by the least squares method (black line) and characterizes the stable state of density stratification. The normalized value of deformation at $D_{16.9} = 0$ $\langle Sh^2_{\text{Strain}} \rangle = \langle \xi_z^2 \rangle \cdot \langle N^2 \rangle \approx 5 \cdot 10^{-7}$ rad^2/s^2, while the mean value of the square of the measured shear of the current velocity at $D_{16.9} = 0$

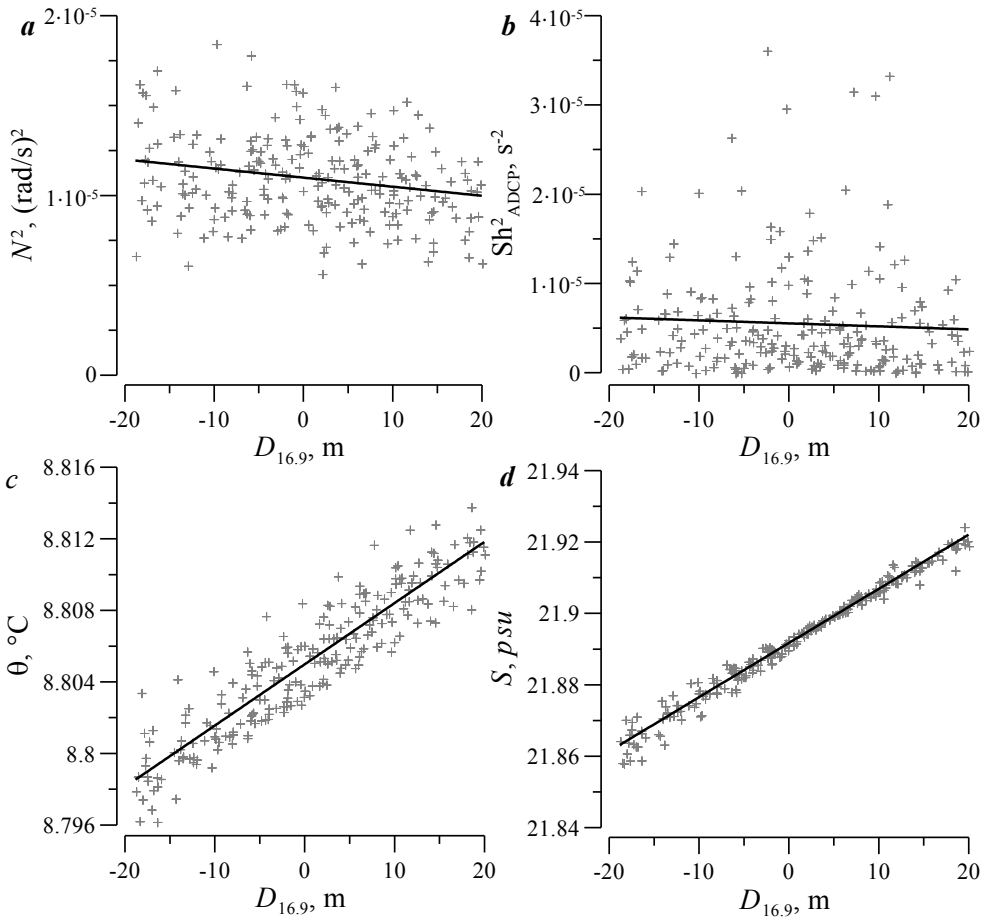

Fig. 3. Dependences of buoyancy frequency square (*a*); square of ADCP shear (*b*); temperature (*c*); salinity (*d*) on the distance to isopicna σ_θ = 16.9 kg/m^3 in the range of ±20 m. Crosses are for input data, black lines are for dependences

$\langle Sh^2_{ADCP} \rangle \approx 5.5 \cdot 10^{-6}$ s^{-2} (Fig. 3, *b*). The ratio of kinetic horizontal energy to potential energy $R_\omega = 11$, which is close to the estimate of this parameter for the 250–500 m layer in the Black Sea given in [5]. For spectrum GM76 $R_\omega = 3$. A significant difference in the values of the parameter is caused by the dominance of internal waves in the deep layers of the Black Sea near the inertial range [14, 29–31], which are more pronounced in the horizontal current velocity than in the deformation of isopycnal surfaces. Values of the parameter R_ω, which is in the range of 8–14, are also characteristic of the northern seas [32], and in some areas of the Atlantic Ocean, R_ω reaches 100 [12]. The value of the function $h_1(R_\omega) = 0.37$, which is ~ 2.5 times less than that for the canonical spectrum GM76. The calculated value of the coefficient $K_V = 2.66 \cdot 10^{-6}$ m^2/s, which is only ~ 2 times less than modern theoretical predictions [7], and ~ 60 times less than that given in earlier works [1, 2].

The salt flux was calculated from the ratio $F_{\text{Salt}} = \rho \cdot K_V \cdot S_Z$, where $S = \partial S/\partial z = 1.5 \cdot 10^{-3}$ psu/m is the salinity derivative (S) with respect to depth (Fig. 3, *d*). The corresponding value $F_{\text{Salt}} = 4.1 \cdot 10^{-6}$ g/(m^2·s). Assuming that the area of the horizontal section of the sea at a depth of 370 m is equal to $3 \cdot 10^5$ km^2 [33], we find that the salt flux amounting to $3.9 \cdot 10^{13}$ g/year rises through it. The lower Bosphorus current brings an average of 150 km^3 (V_B) of Marble Sea water with a salinity of about 34 psu [33] to the Black Sea, or about $5.1 \cdot 10^{15}$ g/year of salt. Thus, through the isopycnal surface $\sigma_\theta = 16.9$ kg/m^3, the amount of salt, which is 0.75 % of its inflow through the Bosphorus Strait against 35 % given in [3] rises. In other words, to maintain the salt balance, it is necessary that less than one percent of the salt brought by the lower Bosphorus current penetrate into the depth layer of more than 350 m.

The heat flux was calculated from the relation $F_{\text{Heat}} = \rho \cdot C_W \cdot K_V \cdot \theta_z$, where $C_W = 4.2 \cdot 10^3$ J/(°C·kg) is the heat capacity of water; $\theta_z = \partial\theta/\partial z = 3.4 \cdot 10^{-4}$ °C/m is the derivative of potential temperature (θ) with respect to depth (Fig. 3, *c*). The corresponding value $F_{\text{Heat}} = 3.9 \cdot 10^{-3}$ W/m^2, which is about 10 % of the geothermal heat flux ($F_{\text{HeatGeo}} = 40$ mW/m^2 [34, 35]). At an average water temperature of the lower Bosphorus current of 14 °C, the Black Sea receives $F_{\text{HeatBosph}} = \rho \cdot C_W \cdot (T_M - T_0) \cdot V_B = 9 \cdot 10^{18}$ J/year, at $T_0 = 0$ °C. $F_{\text{Heat16.9}} = 3.7 \cdot 10^{16}$ J/year and is transferred through the isopycnal surface with a potential density of 16.9 kg/m^3, which is about 0.41 % of the heat supplied with the lower Bosphorus current.

The almost twofold excess of the share of the salt flux (0.75 %) over the share of the heat flux (0.41 %) can be explained by the difference in the processes of exchange of substances with the environment when the waters of the Marble Sea are submerged to depths of more than 370 m. In particular, heat exchange occurs not only with the surrounding aquatic environment, but also through the bottom surface.

Upper boundary of the cold intermediate layer. Calculation of the vertical turbulent diffusion coefficient from the data obtained during ADCP exposure near the sea surface was carried out according to a complicated procedure. This is due to the fact that the characteristic scales of stable stratification variability are close to the vertical resolution of the measurements.

The temperature and salinity profiles (Fig. 4, *a*) were obtained as a result of low-frequency filtering of the initial data and were subsequently used to determine the corresponding vertical derivatives. The largest number of measurements N^2 is observed in the vicinity of the local minimum of the buoyancy frequency between the seasonal and permanent pycnocline at potential density values of 14.2 ± 0.15 kg/m^3 (256 readings in Fig. 4, *a* and *b*) [13]. In order to minimize the influence of the final resolution of measurements on the determination of parameters $\langle\delta^2\rangle$ and $\langle N^2\rangle$, their calculation was made for several samples of initial data falling into windows of different widths ($\Delta\sigma_\theta$) with symmetrical boundaries relative to the value of potential density $\sigma_\theta = 14.2$ kg/m^3. In the calculation of $\langle\delta^2\rangle$, stable stratification was represented by a second-order polynomial (dashed line in Fig. 4, *b*). The results of the determinations were well represented by linear dependences obtained by the least squares method with a decrease in the sampling window width from 0.35 to 0.15 kg/m^3 (corresponding dashed lines in Fig. 4, *c*). The lower threshold of the window width was determined from the condition that the amount of initial data should be at least 100. Further in the calculations, we used the values $\delta^2(0)$ and $N^2(0)$ obtained from the linear dependences at $\Delta\sigma_\theta = 0$. The average value of the squared shear did not show any dependence on the width of the sampling window. The measured value of the squared normalized deformation was about 1.2 of its value for the spectrum of GM76. On the contrary, the measured value of the squared shear of the current velocity (Fig. 4, *d*) is only about 0.6 of its value for the spectrum of GM76. The corresponding ratio of the kinetic and potential energies of small-scale processes $R_\omega = 1.53$, which is almost two times less than its value for the spectrum of GM76. This can be caused by the interaction of internal waves with vertical inhomogeneities of stable density stratification, which have characteristic scales close to the lengths of internal waves. The function value $h_1(R_\omega) = 2.53$ versus units for GM76 spectrum. Geographic correction $j = 1.55$. Vertical turbulent diffusion coefficient $K_V = 7.26 \cdot 10^{-6}$ m^2/s, which is quite close to its value ($\sim 6 \cdot 10^{-6}$ m^2/s) in the core of the cold intermediate layer at $\sigma_\theta = 14.5$ kg/m^3, calculated from the heat conduction equation [13].

The heat flux through the isopycnal surface with a potential density of 14.2 kg/m^3 ($F_{\text{Heat}14.2}$) was 1.79 W/m^2, which significantly exceeds the value of the geothermal flux. At a qualitative level, it is obvious that the seasonal pycnocline in the Black Sea weakens the exchange processes between the upper homogeneous mixed layer and the water column, but quantitative estimates are rarely given in the literature [36]. By equating the heat fluxes at the upper boundary of the cold intermediate layer and in the seasonal pycnocline, we can estimate the vertical turbulent mixing coefficient in the seasonal pycnocline itself from the relation $K_V(12) \approx T_z(14.2)/T_z(12) \cdot K_V(14.2) = 2.26 \cdot 10^{-7}$ m^2/s. The obtained value is close to the value of the heat molecular diffusion coefficient ($k_T = 1.4 \cdot 10^{-7}$ m^2/s). In essence, this means that in summer the heat flux from the upper homogeneous mixed layer into the water column through the seasonal thermocline is largely determined by molecular diffusion.

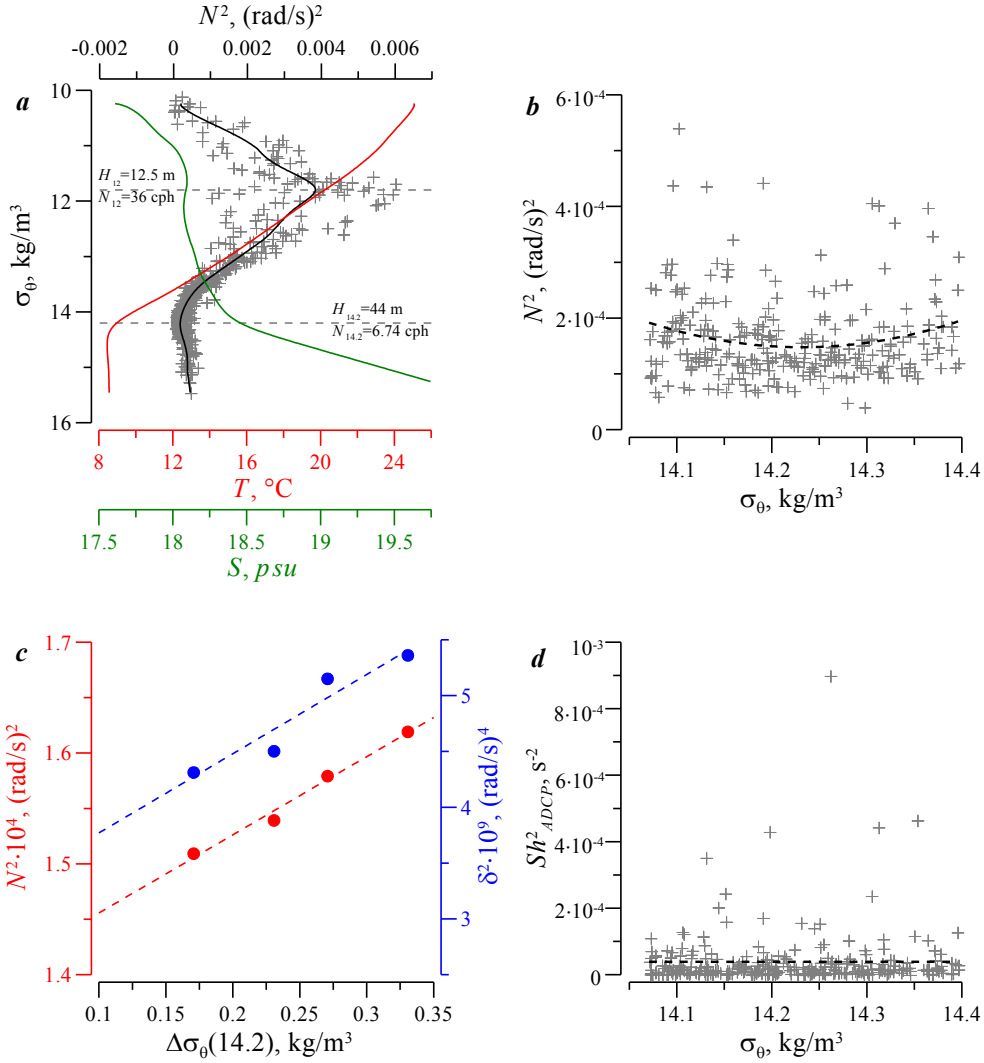

Fig. 4. Averaged profiles of temperature (red line), salinity (green line), and buoyancy frequency square (black line, crosses are for input data) (*a*); dependence of buoyancy frequency square on density in the neighbourhood of value 14.2 kg/m^3 (crosses are for input data, dashed line is for quadratic polynomial approximant) (*b*); dependences of buoyancy frequency square (red dots) and mean squared deviation from the mean (blue dots) on the sampling window width in the neighbourhood of density value of 14.2 kg/m^3 (dashed lines are for approximating linear dependences) (*c*); dependence of squared shear on density (dashed line is for the mean) (*d*)

The microstructural measurements taken in the Yellow Sea with similar parameters of the pycnocline also showed values of the vertical turbulent diffusion coefficient comparable to the molecular heat diffusion coefficient [37].

The salt flux through the isopycnal surface at the value of potential density σ_θ = 14.2 kg/m^3 is equal to 2977 g/(m^2·year), which gives a salt transfer of $1.1 \cdot 10^{15}$ g/year. This is about 22 % of the salt flow brought into the Black Sea by the lower Bosphorus current. A significant violation of the salt balance can be explained by the seasonal variability of both the exchange through the Bosphorus Strait [34] and the vertical turbulent diffusion coefficient [6].

Conclusion

The methodological issues of applying the G03 parametrization for estimating the vertical turbulent diffusion coefficient from the current velocity and stratification data collected near the sea surface and at the lower point of sounding with a small-scale resolution are considered.

For the upper boundary of the cold intermediate layer at a potential density of 14.2 kg/m^3, the corresponding estimate of the coefficient was $7.26 \cdot 10^{-6}$ m^2/s. This is close to its value in the core of the cold intermediate layer ($6 \cdot 10^{-6}$ m^2/s) obtained from the heat transfer equation based on the results of several expeditions in 2017. The corresponding vertical heat flux was 1.79 W/m^2. The salt transfer through the isopycnal surface with a potential density of 14.2 kg/m^3 is $1.1 \cdot 10^{15}$ g/year, or about 22 % of the mass of salt ($5.1 \cdot 10^{15}$ g/year) brought into the Black Sea by the lower Bosphorus current. An indirect estimate of the coefficient in the seasonal pycnocline amounts to $2.26 \cdot 10^{-7}$ m^2/s and shows its comparability with the heat molecular diffusion coefficient, which is in good agreement with the results of microstructural measurements for similar conditions.

For the lower boundary of shear baroclinic flows at a potential density of 16.9 kg/m^3, the estimate of the vertical turbulent diffusion coefficient was $2.66 \cdot 10^{-6}$ m^2/s, which is almost half the size of the theoretical estimate. The corresponding heat flux is $3.9 \cdot 10^{-3}$ W/m^2, or ~10 % of the geothermal heat flux. A salt flux of $4.1 \cdot 10^{-6}$ g/(m^2·s) corresponds to its transport through the isopycnal surface in the amount of $3.9 \cdot 10^{13}$ g/year and is 0.75% of the mass of salt brought by the lower Bosphorus current per year.

One of the results of the presented work is the establishment of the ratio of kinetic and potential energy of small-scale processes. Near the surface in the vicinity of the isopycna with a potential density of 14.2 kg/m^3, its value amounted to 1.53 and 11 for the lower sounding point at a potential density of 16.9 kg/m^3. As a result, the value of the vertical turbulent diffusion coefficient at the surface turned out to be three times higher than at the lower point of sounding, despite the fact that the ratio of the buoyancy frequency square to the squared shear in the lower layer is almost half the size.

The given estimates of the parameters are conditional, but nevertheless they can be useful in discussing their values obtained by other methods, in particular, from the results of numerical experiments.

REFERENCES

1. Kolesnikov, A.G. and Boguslavskii, S.G., 1978. On the Vertical Transport in the Black Sea. In: MHI, 1978. *Marine Hydrophysical Research*. Sevastopol: MHI. Iss. 2, pp. 33–46. (in Russian).
2. Boguslavsky, S.G., Zhorov, V.A. and Ivashchenko, I.K., 1994. Formation of the Vertical Salinity Profile in the Black Sea. *Physical Oceanography*, 5(6), pp. 443–449. https://doi.org/10.1007/BF02198510
3. Gregg, M.C. and Yakushev, E., 2005. Surface Ventilation of the Black Sea's Cold Intermediate Layer in the Middle of the Western Gyre. *Geophysical Research Letters*, 32(3), L03604. doi:10.1029/2004GL021580
4. Zatsepin, A.G., Golenko, N.N., Korzh, A.O., Kremenetskii, V.V., Paka, V.T., Poyarkov, S.G. and Stunzhas, P.A., 2007. Influence of the Dynamics of Currents on the Hydrophysical Structure of the Waters and the Vertical Exchange in the Active Layer of the Black Sea. *Oceanology*, 47(3), pp. 301–312. https://doi.org/10.1134/S0001437007030022
5. Morozov, A.N. and Lemeshko, E.M., 2014. Estimation of Vertical Turbulent Diffusion Coefficient by CTD/LADCP-Measurements in the Northwestern Part of the Black Sea in May, 2004. *Morskoy Gidrofizicheskiy Zhurnal*, (1), pp. 58–67 (in Russian).
6. Podymov, O.I., Zatsepin, A.G. and Ostrovsky, A.G., 2017. Vertical Turbulent Exchange in the Black Sea Pycnocline and its Relation to Water Dynamics. *Oceanology*, 57(4), pp. 492–504. https://doi.org/10.1134/S0001437017040142
7. Samodurov, A.S., Chukharev, A.M. and Kazakov, D.A., 2021. Basic Regularities of Vertical Turbulent Exchange in the Mixed and Stratified Layers of the Black Sea. *Physical Oceanography*, 28(4), pp. 376–391. doi:10.22449/1573-160X-2021-4-376-391
8. Gregg, M.C., 1989. Scaling Turbulent Dissipation in the Thermocline. *Journal of Geophysical Research: Oceans*, 94(C7), pp. 9686–9698. https://doi.org/10.1029/JC094iC07p09686
9. Polzin, K.L., Toole, J.M. and Schmitt, R.W., 1995. Finescale Parameterizations of Turbulent Dissipation. *Journal of Physical Oceanography*, 25(3), pp. 306–328. https://doi.org/10.1175/1520-0485(1995)025<0306:FPOTD>2.0.CO;2
10. Gregg, M., Sanford, T. and Winkel, D., 2003. Reduced Mixing from the Breaking of Internal Waves in Equatorial Waters. *Nature*, 422, pp. 513–515. https://doi.org/10.1038/nature01507
11. Kunze, E., Firing, E., Hummon, J.M., Chereskin, T.K. and Thurnherr, A.M., 2006. Global Abyssal Mixing Inferred from Lowered ADCP Shear and CTD Strain Profiles. *Journal of Physical Oceanography*, 36(8), pp. 1553–1576. https://doi.org/10.1175/JPO2926.1
12. Ferron, B., Kokoszka, F., Mercier, H. and Lherminier, P., 2014. Dissipation Rate Estimates from Microstructure and Finescale Internal Wave Observations along the A25 Greenland–Portugal OVIDE Line. *Journal of Atmospheric and Oceanic Technology*, 31(11), pp. 2530–2543. https://doi.org/10.1175/JTECH-D-14-00036.1
13. Morozov, A.N. and Mankovskaya, E.V., 2020. Cold Intermediate Layer of the Black Sea According to the Data of Field Research in 2016-2019. *Ecological Safety of Coastal and Shelf Zones of Sea*, (2), pp. 5–16. doi:10.22449/2413-5577-2020-2-5-16 (in Russian).
14. Morozov, A.N. and Mankovskaya, E.V., 2021. Modern Studies of Water Dynamics in the North-Western Part of Black Sea from LADCP Measurements. In: MSU, 2021. *InterCarto. InterGIS. GI Support of Sustainable Development of Territories: Proceedings of the International conference*. Moscow: Faculty of Geography MSU. Vol. 27, part 3, pp. 5–15. doi:10.35595/2414-9179-2021-3-27-110-120

15. Morozov, A.N., Lemeshko, E.M., Shutov, S.A., Zima, V.V. and Deryushkin, D.V., 2017. Structure of the Black Sea Currents Based on the Results of the LADCP Observations in 2004–2014. *Physical Oceanography*, (1), pp. 25–40. doi:10.22449/1573-160X-2017-1-25-40

16. Morozov, A.N. and Mankovskaya, E.V., 2019. Seasonal Variability of Currents Structure in the Black Sea Northern Part from Field Measurements in 2016. *Fundamental and Applied Hydrophysics*, 12(1), pp. 15–20. https://doi.org/10.7868/S2073667319010027 (in Russian).

17. Morozov, A.N. and Lemeshko, E.M., 2006. Methodical Aspects of the Application of Acoustic Doppler Current Profilers in the Black Sea. *Physical Oceanography*, 16(4), pp. 216–233. https://doi.org/10.1007/s11110-006-0027-8

18. Morozov, A.N., 2018. Statistic of the Richardson Number according to Observations from the Oceanographic Platform. *Ecological Safety of Coastal and Shelf Zones of Sea*, (2), pp. 39–46. doi:10.22449/2413-5577-2018-2-39-46 (in Russian).

19. Miles, J., 1961. On the Stability of Heterogeneous Shear Flows. *Journal of Fluid Mechanics*, 10(4), pp. 496–508. doi:10.1017/S0022112061000305

20. Toole, J. and Schmitt, R., 1987. Small-Scale Structures in the North-West Atlantic Sub-Tropical Front. *Nature*, 327, pp. 47–49. https://doi.org/10.1038/327047a0

21. Garrett, C. and Munk, W., 1975. Space-Time Scales of Internal Waves: A Progress Report. *Journal of Geophysical Research*, 80(3), pp. 291–297. https://doi.org/10.1029/JC080i003p00291

22. Cairns, J.L. and Williams, G.O., 1976. Internal Wave Observations from a Midwater Float, 2. *Journal of Geophysical Research*, 81(12), pp. 1943–1950. https://doi.org/10.1029/JC081i012p01943

23. Fer, I., 2006. Scaling Turbulent Dissipation in an Arctic Fjord. *Deep Sea Research Part II: Topical Studies in Oceanography*, 53(1–2), pp. 77–95. https://doi.org/10.1016/j.dsr2.2006.01.003

24. Munk, W. and Wunsch, C., 1998. Abyssal Recipes II: Energetics of Tidal and Wind Mixing. *Deep Sea Research Part I: Oceanographic Research Papers*, 45(12), pp. 1977–2010. https://doi.org/10.1016/S0967-0637(98)00070-3

25. Morozov, A.N., Mankovskaya, E.V. and Fedorov, S.V., 2021. Inertial Oscillations in the Northern Part of the Black Sea Based on the Field Observations. *Fundamentalnaya i Prikladnaya Gidrofzika*, 14(1), pp. 43–53. doi:10.7868/S2073667321010044 (in Russian).

26. Munk, W.H. and Anderson, E., 1948. Notes on a Theory of the Thermocline. *Journal of Marine Research*, 7(3), pp. 276–295.

27. Kunze E., Williams III, A.J. and Briscoe, M.G., 1990. Observations of Shear and Vertical Stability from a Neutrally Buoyant Float. *Journal of Geophysical Research: Oceans*, 95(C10), pp. 18127–18142. https://doi.org/10.1029/JC095iC10p18127

28. Polzin, K., 1996. Statistic of the Richardson Number: Mixing Models and Finestructure. *Journal of Physical Oceanography*, 26(8), pp. 1409–1425. https://doi.org/10.1175/1520-0485(1996)026<1409:SOTRNM>2.0.CO;2

29. Morozov, A.N., 2001. Spectral Parameters of Inertial Oscillations in the Black Sea. In: MHI, 2001. *Ekologicheskaya Bezopasnost' Pribrezhnoy i Shel'fovoy Zon i Kompleksnoe Ispol'zovanie Resursov Shel'fa* [Ecological Safety of Coastal and Shelf Zones and Comprehensive Use of Shelf Resources]. Sevastopol: MHI. Iss. 2, pp. 61–69 (in Russian).

30. Klyuvitkin, A.A., Ostrovskii, A.G., Lisitzin, A.P. and Konovalov, S.K., 2019. The Energy Spectrum of the Current Velocity in the Deep Part of the Black Sea. *Doklady Earth Sciences*, 488(2), pp. 1222–1226. https://doi.org/10.1134/S1028334X1910012X

31. Khimchenko, E., Ostrovskii, A., Klyuvitkin, A. and Piterbarg, L., 2022. Seasonal Variability of Near-Inertial Internal Waves in the Deep Central Part of the Black Sea. *Journal of Marine Science and Engineering*, 10(5), 557. https://doi.org/10.3390/jmse10050557

32. Naveira Garabato, A.C., Oliver, K.I.C., Watson, A.J. and Messias, M.-J., 2004. Turbulent Diapycnal Mixing in the Nordic Seas. *Journal of Geophysical Research: Oceans*, 109(C12), C12010. https://doi.org/10.1029/2004JC002411

33. Ivanov, V.A. and Belokopytov, V.N., 2013. *Oceanography of the Black Sea*. Sevastopol, 210 p.

34. Kutas, R.I., 2010. Geothermal Conditions of the Black Sea Basin and Its Surroundings. *Geophysical Journal*, 32(6), pp. 135–158 (in Russian).

35. Stanev, E.V., Chtirkova, B. and Peneva, E., 2021. Geothermal Convection and Double Diffusion Based on Profiling Floats in the Black Sea. *Geophysical Research Letters*, 48(2), e2020GL091788. https://doi.org/10.1029/2020GL091788

36. Morozov, A.N., Ivanov, V.A., Shutov, S.A., Zima, V.V., Deryushkin, D.V. and Lemeshko, E.M., 2016. Spatial Structure of Currents near Gerakleysky Peninsula According ADCP-Observations in 2015. In: MHI, 2016. *Ecological Safety of Coastal and Shelf Zones of Sea*. Sevastopol: MHI. Iss. 16, pp. 73–79 (in Russian).

37. Liu, Zh., Wei, H., Lozovatsky, I.D. and Fernando, H.J.S., 2009. Late Summer Stratification, Internal Waves, and Turbulence in the Yellow Se. *Journal of Marine Systems*, 77(4), pp. 459–472. https://doi.org/10.1016/j.jmarsys.2008.11.001

Submitted 26.09.2022; accepted after review 25.10.2022;
revised 02.11.2022; published 23.12.2022

About the authors:

Alexey N. Morozov, Senior Research Associate, Marine Hydrophysical Institute of RAS (2 Kapitanskaya St., Sevastopol, 299011, Russian Federation), Ph. D. (Tech.), **ORCID ID: 0000-0001-9022-3379**, **Scopus Author ID: 7202104940, ResearcherID: ABB-4365-2020**, *anmorozov@mhi-ras.ru*

Ekaterina V. Mankovskaya, Senior Research Associate, Marine Hydrophysical Institute of RAS (2 Kapitanskaya St., Sevastopol, 299011, Russian Federation), Ph. D. (Tech.), **ORCID ID: 0000-0002-4086-1687**, **Scopus Author ID: 57192647961, ResearcherID: AAB-5303-2019**, *emankovskaya@mhi-ras.ru*

Contribution of the authors:

Alexey N. Morozov – problem setting; processing, analysis and description of the study results; preparation of the article text and graphics

Ekaterina V. Mankovskaya – measurement data processing; collection of information to study; discussion of results; article text correction

All the authors have read and approved the final manuscript.

DOI:10.22449/2413-5577-2022-4-39-51

Sources of Errors of Satellite Data in Spring in Black Sea

E. N. Korchemkina *, A. O. Raykina

Marine Hydrophysical Institute of RAS, Sevastopol, Russia
** korchemkina@mhi-ras.ru*

Abstract

For the Black Sea, there are visible discrepancies between remote estimates of the optical characteristics of sea water and contact measurements. Despite the fact that modern atmospheric correction algorithms take into account non-zero brightness in the long-wavelength region, they do not completely solve the problem and require additional analysis. In this paper, we compare remote sensing data and data from simultaneous field measurements of the sea reflectance and atmospheric transparency in order to further improve the standard methods of atmospheric correction, taking into account the real aerosol optical depth. In this paper, we consider the measurement data of the spectral reflectance of the water column and the optical characteristics of the atmosphere, obtained during the cruises of the R/V *Professor Vodyanitsky* in the spring of 2019 and 2021 in the north-eastern part of the Black Sea. As a result of comparison with satellite data, it was found that satellite reflectance data in the Black Sea in spring are on average underestimated compared to contact measurements. The average values of the Angström parameter and the aerosol optical depth according to satellite data are twice as high as field measurements. The values of the Angström exponent, which are greatly overestimated compared to field measurements, lead to an excessive allowance for the influence of the atmosphere and, as a result, to an underestimation of the reflectance values.

Keywords: sea reflectance, atmospheric correction, atmospheric aerosol optical depth, Angström parameter, spectrophotometer, SPM sun photometer

Acknowledgement: the authors are grateful to junior research associate of the Department of Marine Optics and Biophysics D. V. Kalinskaya for processing data on atmospheric characteristics. The work was performed under state assignment of FSBSI FRC MHI on topic no. FNNN-2021-0003 “Operational oceanology”.

For citation: Korchemkina, E.N. and Raykina, A.O., 2022. Sources of Errors of Satellite Data in Spring in Black Sea. *Ecological Safety of Coastal and Shelf Zones of Sea*, (4), pp. 39–51. doi:10.22449/2413-5577-2022-4-39-51

Источники погрешности спутниковых данных в весенний период в Черном море

Е. Н. Корчёмкина *, А. О. Райкина

Морской гидрофизический институт РАН, Севастополь, Россия
**korchemkina@mhi-ras.ru*

Аннотация

Для Черного моря между дистанционными оценками оптических характеристик морской воды и контактными измерениями наблюдаются видимые расхождения. Несмотря на то что современные алгоритмы атмосферной коррекции учитывают ненулевую яркость в длинноволновой области, они целиком не решают проблемы и требуют дополнительного анализа. В работе сопоставлены данные дистанционного зондирования и одновременных экспедиционных измерений коэффициента яркости и прозрачности атмосферы для дальнейшего усовершенствования стандартных методов атмосферной коррекции с учетом реальной аэрозольной оптической толщины. Рассматриваются данные измерений спектрального коэффициента яркости толщи вод и оптических характеристик атмосферы, полученные в ходе экспедиций НИС «Профессор Водяницкий» весной 2019 и 2021 гг. по Черному морю. В результате сопоставления натурных данных со спутниковыми установлено, что спутниковые данные коэффициента яркости в Черном море в весенний период в среднем занижены по сравнению с контактными измерениями. Средние значения показателя Ангстрема и аэрозольной оптической толщины по спутниковым данным вдвое превышают натурные измерения. Сильно завышенные по сравнению с натурными измерениями значения показателя Ангстрема приводят к избыточному учету влияния атмосферы и, как следствие, к занижению значений коэффициента яркости.

Ключевые слова: коэффициент яркости моря, атмосферная коррекция, аэрозольная оптическая толщина, параметр Ангстрема, спектрофотометр, солнечный фотометр, *SPM*

Благодарности: авторы выражают благодарность м. н. с. отдела оптики и биофизики моря Д. В. Калинской за обработку данных о характеристиках атмосферы. Работа выполнена в рамках темы государственного задания FNNN-2021-0003 «Оперативная океанология».

Для цитирования: *Корчемкина Е. Н., Райкина А. О.* Источники погрешности спутниковых данных в весенний период в Черном море // Экологическая безопасность прибрежной и шельфовой зон моря. 2022. № 4. С. 39–51. EDN YQDXKA. doi:10.22449/2413-5577- 2022-4-39-51

Introduction

At present, satellite research methods are the most effective for global analysis of the state of the marine environment. Data from space colour scanners make it possible to obtain information about important optical parameters of the upper water layer (chlorophyll concentration, suspended matter content, ocean water transparency, etc.) in a wide range of spatial and temporal scales. These data are indicators of the ecosystem and serve as input parameters for Earth's climate assessment models [1–4]. However, for the Black Sea, there are visible discrepancies between the remote sensing data and the readings of contact measurements, since the standard algorithm for processing satellite observations has been developed for open ocean waters [5]. It is known that optical properties of the waters in the Black Sea and the ocean differ, in particular,

due to the increased absorption of light by yellow matter and the greater amount of suspended matter, including the suspended matter of terrigenous origin [6]. According to the work [1)], in the study area of the Black Sea, the contribution of yellow matter to the attenuation index reaches 28 % at a wavelength of 416 nm (and decreases with wavelength), and the combined contribution of scattering by coarse and fine suspension is 64 % at the same wavelength. For a wavelength of 506 nm, these contributions are 9 and 80 %, respectively.

The standard atmospheric correction algorithm assumes that in the long-wavelength part the brightness of the radiation emerging from the water column is zero (black pixel algorithm) [7]. This assumption is valid only for type 1 optically deep waters with a chlorophyll concentration of 0.3 mg/m^3 or less and is not suitable for waters containing higher concentrations of chlorophyll or mineral particles [2)]. Large errors are especially typical for coastal and river runoff areas [8, 9], which differ from open areas of the sea in a twofold greater contribution of inanimate suspension (20–30 %) to the total light absorption in the wavelength range of 400–500 nm [10–12].

In this case, the use of the black pixel algorithm to correct the non-zero contribution of water can lead to an overestimation of the optical depth of the aerosol, i.e., to the subtraction of too large an aerosol reflectance value from the reflectance at the upper boundary of the atmosphere. The resulting reflectance of the water column will then be too small, and in the blue region of the spectrum it may even turn out to be negative [2)].

Despite the fact that the modern atmospheric correction algorithm uses an iterative method for taking into account non-zero brightness [13], it does not completely solve the problem and requires additional analysis.

Previously, regional algorithms for the seas of Russia, including the Black Sea, have already been created based on *in situ* measurements [14, 15]. The paper [14] considers ways to reduce the effect of atmospheric correction errors on the accuracy of calculating the biooptical parameters of water. The method is based on the simultaneous calculation of aerosol contribution $\rho_a(\lambda_i)$ and the spectral coefficient of sea reflectance $\rho_w(\lambda_i)$ from the measured values of reflectance $\rho_t(\lambda_i)$ of the ascending radiation at the upper boundary of the atmosphere. Atmospheric correction errors are controlled by comparing the data obtained *in situ* and the values calculated from satellite data.

In [15], it is proposed to correct the sea reflectance spectra using the data on variability of the aerosol characteristics of the atmosphere, obtained on the basis of *in situ* measurements of the atmospheric characteristics with a sun photometer.

[1)] Mankovsky, V.I., Solov'iev, M.V. and Mankovskaya, E.V., 2009. [*Hydrooptical Properties of the Black Sea*]. A reference book. Sevastopol: MGI NAN Ukrainy, pp. 20–21.

[2)] Mobley, C.D., Werdell, J., Franz, B., Ahmad, Z. and Bailey, S., 2016. *Atmospheric Correction for Satellite Ocean Color Radiometry*. Greenbelt, Maryland: Goddard Space Flight Center, 85 p. doi:10.13140/RG.2.2.23016.78081

The analysis is based on the use of the error spectrum of aerosol optical depth (AOD) measurements with the SPM sun photometer. It is shown that the spectra corrected on the basis of statistical data are in good agreement with the results of direct measurements.

AOD is the main characteristic of aerosol, which determines the integral (in the atmospheric column) attenuation of direct solar radiation. It has spectral features that depend on the size and the refractive index of aerosol particles. AOD is one of the main parameters affecting the scattering and absorption of sunlight in the atmosphere. Comparison of AOD measured from the satellite and from the surface can provide useful additional information for satellite data processing and will enable to obtain more accurate reflectance spectra from remote estimates.

The purpose of this work is to compare remote sensing data and data of expeditionary measurements of the reflectance in order to further improve the standard methods for processing satellite measurements of the ascending water reflectance, taking into account the real AOD.

Data and methods

The paper considers the measurement data of the spectral reflectance (R) of the water column and the optical characteristics of the atmosphere obtained during the Black Sea expeditions of R/V *Professor Vodyanitsky* in the spring of 2019 and 2021. The measurements were carried out by the authors of the paper. The survey was carried out in the northern and north-eastern parts of the Black Sea (42.5°–45.8° N; 31.5–39.8° E) in the period from April 18 – May 13, 2019 (cruise 106) and from April 22 – May 8, 2021 (cruise 116). In 2019, the reflectance spectra of the water column were obtained at 89 sites, in 2021 – at 68 sites (Fig. 1). The spectral reflectance measurements were carried out from the shipboard with a spectrophotometer developed in the Department of Marine Optics and Biophysics of MHI RAS [16].

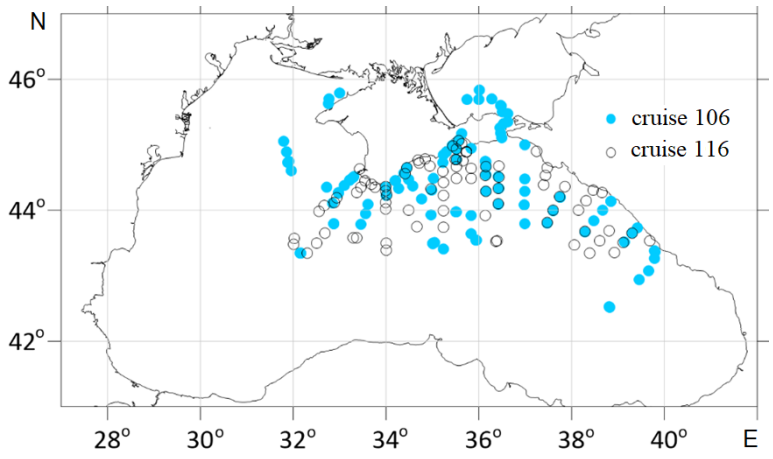

F i g . 1 . Measurement sites during the two cruises

The reflectance of the radiation rising from the sea at an angle of 30° to the nadir and the reflectance of a reference white screen at the same angle were measured. As a ratio of these quantities, the spectra of a dimensionless R were obtained in the wavelength range of 390–750 nm with a step of 1 nm and an error of 3 %.

AOD and Angström parameters α and β were determined from the data of spectral measurements of atmospheric transparency taken with the SPM sun photometer simultaneously with R measurements. The measurements were carried out simultaneously in 12 spectral channels from near UV to mid-IR, channel centres: 340, 379, 441, 501, 548, 675, 872, 940, 1020, 1244, 1556, and 2134 [17]. The Angström parameters were determined by approximating the obtained AOD data with the dependence $AOD(\lambda) = \beta \cdot \lambda^{-\alpha}$ in the wavelength range of 501–872 nm. In this work, only the α parameter will be considered as an indicator of the AOD spectral slope.

The work also uses the data of the second level of processing on the rising radiation from the sea (R_{rs}), on the aerosol optical depth (*aod*_869) and the Angström index in the wavelength range of 550–869 nm (*angstrom*), obtained using satellite scanners MODIS Aqua/Terra, Sentinel-3 A/B and VIIRS Suomi NPP/JPSS-1. During the analysis, these data were compared with the indications of *in situ* measurements. R_{rs} MODIS and VIIRS data are reduced to dimensionless values by multiplying by π. For a correct comparison with *in situ* data, pixels were selected without the *Straylight*, *Cloud_Margin*, *Cloud_Ambiguous* flags, coinciding in coordinates with the *in situ* measurement point within 0.01° and in time – within 3 h. In total, the study used data from 49 stations for cruise 106 and 39 for cruise 116 (for all satellites). The data obtained under conditions of a cloudless or slightly cloudy sky at sun angles exceeding 30° were selected.

Results and discussion

The average R spectra plotted from the *in situ* measurements of 106 and 116 cruises are shown in Fig. 2. Judging by the standard deviation (SD) shown on the graphs, the variability of the R spectra in the spring of 2019 was

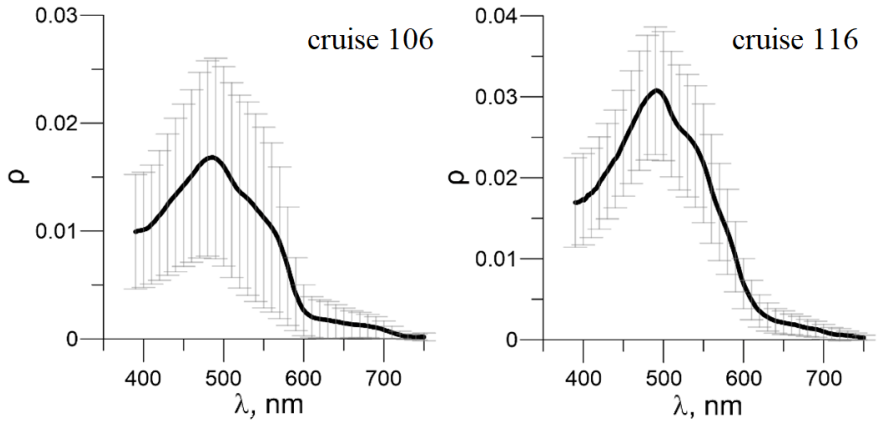

Fig. 2. Average reflectance spectra. Vertical bars show standard deviation of all measurements

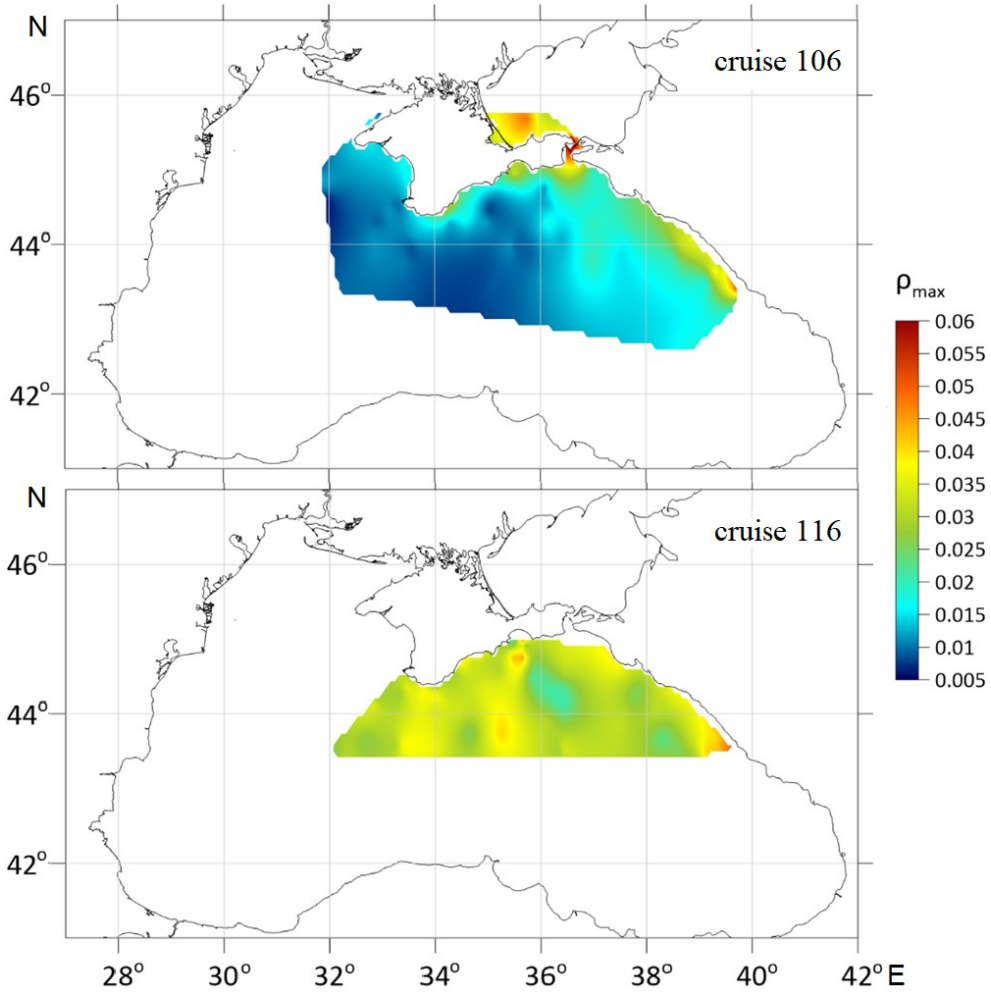

Fig. 3. Spatial distribution of maximal values of reflectance

significantly higher than in the same period of 2021. A similar situation can be observed in Fig. 3, which shows the spatial distribution of the maximum R values. It shows a significant difference between the R values in the coastal and deep-water areas of the sea during cruise 106, while in cruise 116, a more uniform distribution of optical properties was observed. The differences are most likely due to climatic and weather conditions (average temperature of the previous winter, amount of precipitation in the winter-spring period, etc.).

In 2019, the lowest R values were observed on the northwestern shelf and in the central deep-water part of the polygon. Increased values were observed in the eastern part of the polygon and along the southern coast of Crimea. All spectra have a similar characteristic shape, with the R maximum lying near 480 nm in the eastern deep-sea part and near 490 nm in the coastal part.

In the area of Sochi, a plume was observed due to the runoff of the Mzymty River. Here, the shape of the spectrum and the reflectance values changed, the maximum shifted towards long waves up to 497 nm, which can be explained by the influence of an increased concentration of suspended matter and inanimate organic matter coming with river runoff.

In 2021, the R variability in the study area was relatively low. There was no difference between the deep-water and coastal parts both in the shape of the spectra and in the values. The greatest variations were observed in the east of the study area; the scatter in the values of the R maxima ranged from 0.02 on the shelf outside the Feodosiya Bay to 0.049 in the bay itself.

Fig. 4 compares reflectance with remote sensing data. Basically, there is an underestimation of the satellite data compared to the*in situ* data, however, in some cases, a good match is observed for the open sea, an example of which dated 14.05.2021 is shown in Fig. 4, *d*. The underestimation is especially pronounced in the short-wavelength region, which is the main type of error introduced by incorrect selection of atmospheric correction parameters. Extrapolation of atmospheric aerosol parameters found from measurements in the near-IR range using an atmospheric model leads to the accumulation of errors with decreasing wavelength. In the case when the ascending reflectance of water in the near-IR region (for turbid waters) cannot be neglected, the ascending reflectance of the atmosphere is overestimated and the reflectance values of the water column are underestimated.

To analyze the AOD and the Angström parameter, their frequency histograms were constructed. Fig. 5 shows that the scatter of the AOD values and the Angström parameter according to satellite data is quite large, despite the fact that during the expedition no extreme phenomena were observed in the atmosphere (dust transport, fire smoke spread, etc.). Surface measurements show that the distribution of values occupies a fairly narrow range. The characteristics of the atmosphere according to satellite measurements are overestimated on average by a factor of 2–3, which leads to a regular underestimation of the values of the satellite reflectance, especially in short-wavelength channels.

Similar frequency distributions were constructed for the difference between *in situ* and satellite data, which was calculated using the formulas

$$\Delta(\mathrm{AOD}) = \mathrm{AOD}_{\text{in situ}} - \mathrm{AOD}_{\text{sat}},$$

$$\Delta(\alpha) = \alpha_{\text{in situ}} - \alpha_{\text{sat}},$$

$$\Delta(\mathrm{Rrs\_412}) = \mathrm{Rrs\_412}_{\text{in situ}} - \mathrm{Rrs}_{412\,\text{sat}}.$$

The obtained values of Δ(AOD), Δ(α), and Δ(Rrs_412) are shown in Fig. 6. It can be seen that the dominant negative values of Δ for AOD and the Angström parameter correspond mainly to positive values for the reflectance at a wavelength of 412 nm.

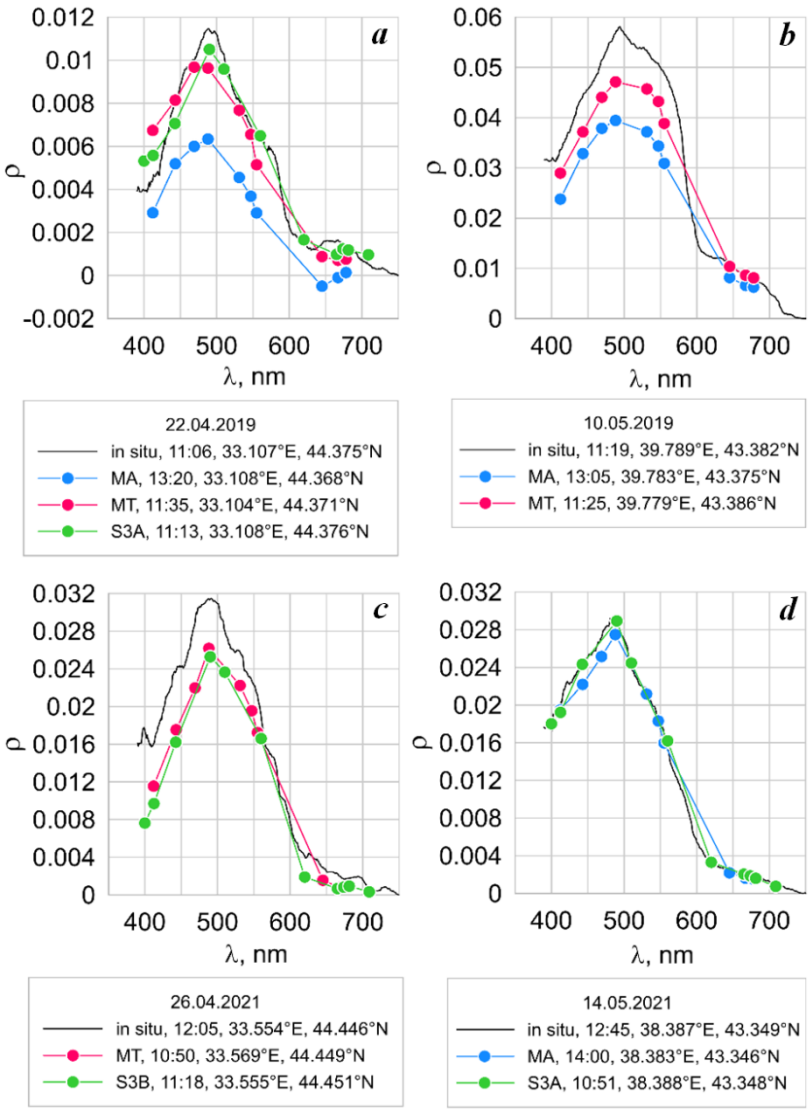

Fig. 4. Examples of comparison of satellite and *in situ* reflectances (MA – MODIS Aqua, MT – MODIS Terra, S3A/B – Sentinel-3 A/B)

To consider the average error of the standard atmospheric correction, such characteristics as the average error (*bias*) and the root mean square error of the model (RMSE) are chosen:

$$bias = \frac{1}{N}\sum_{i=1}^{N}\left(\mathrm{Rsr_i} - \mathrm{Rsr_i^{sat}}\right),$$

$$\mathrm{RMSE} = \sqrt{\frac{1}{N}\sum_{i=1}^{N}\left(\mathrm{Rsr_i} - \mathrm{Rsr_i^{sat}}\right)^2},$$

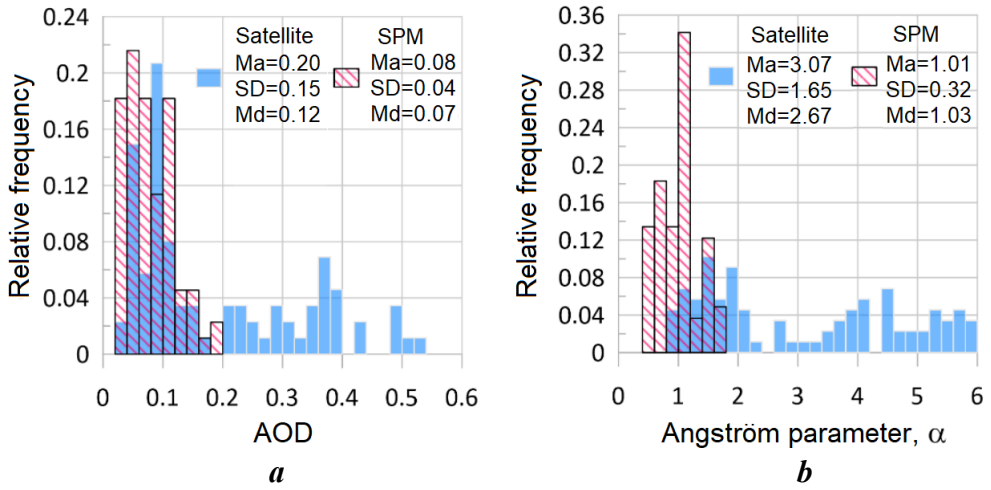

Fig. 5. Frequency distribution of aerosol optical depth (AOD) and Angstrom parameter from satellite and *in situ* (SPM) data (Ma – mean value, SD – standard deviation, Md – median)

which are a function of the difference between *in situ* and satellite Rrs after the correction by R_{rs}^{sat} data and depend on the wavelength. Fig. 7 shows their spectral dependences for the data from MODIS Aqua/Terra scanners. The data from other scanners in this study were used in a relatively small amount, not enough to build reliable RMSE and bias spectra.

The spectral bias values are positive for all wavelengths and decrease with wavelength. This indicates an underestimation of satellite data compared to *in situ* data on average over the entire spectral range (despite the fact that there are some cases when satellite values are higher than *in situ* data). At the same time, the values in the short-wavelength region are also the most subject to atmospheric

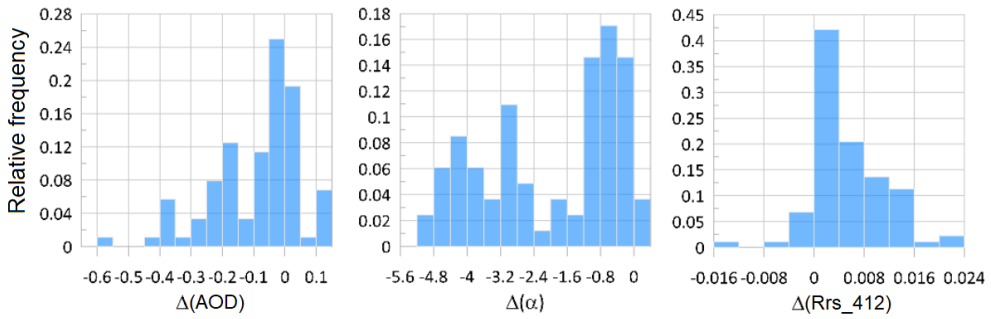

Fig. 6. Frequency distribution of discrepancy between *in situ* and satellite data

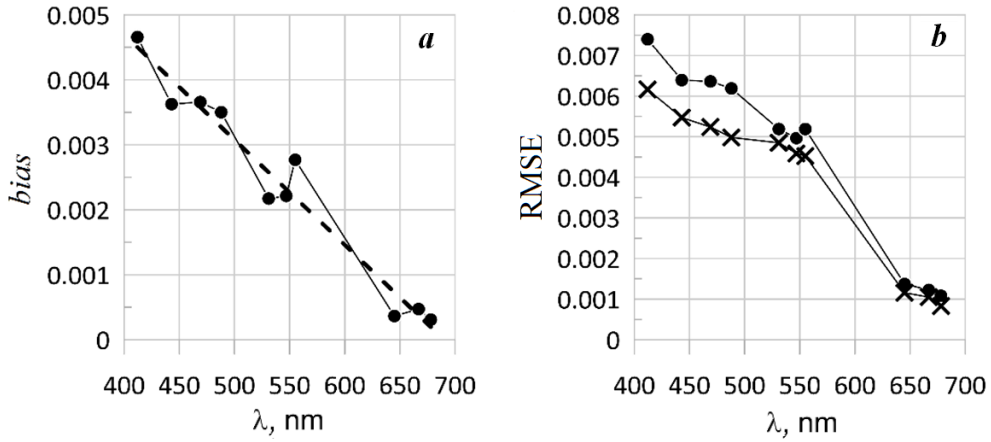

Fig. 7. Spectra of *bias* (*a*) and RMSE (circles are for RMSE before *bias* subtraction, crosses – after that) (*b*) for *in situ* and MODIS Aqua/Terra reflectances

correction errors. The same is evidenced by the RMSE values, which also decrease with the wavelength (shown by circles in Fig. 7, *b*).

The average bias spectrum approximated by a linear function (dashed line in Fig. 7, *a*) can be used as a correction for satellite data added to compensate for negative values in the shortwave region. If the bias value is added to the satellite R spectra, then the correspondence between the satellite data and *in situ* data becomes, on average, somewhat higher. This can be seen from the RMSE values in Fig. 7, marked with crosses, and in some examples shown in Fig. 8. However, this method will not completely eliminate individual cases when underestimation of the satellite data is too strong or when the values, on the contrary, are overestimated.

The presented bias values were obtained only from the data of the spring period of 2019 and 2021 and represent an attempt to correct the reflectance satellite data. Such model accuracy criterion as RMSE is reduced by 16 % for the wavelength of 412 nm, which shows a slight improvement in the accuracy of reconstructing satellite reflectance spectra. For better results, it is necessary to process a larger array of *in situ* data for different seasons and areas of the sea, which is not currently available.

The study used a strict rejection of satellite data according to the criterion of the possible presence of clouds, so the average correction value was calculated without their influence. However, even in the presence of illumination from clouds, the proposed approach will partially compensate for the contribution of additional reflectance, since it is either spectrally nonselective or, like the correction term, increases toward short waves.

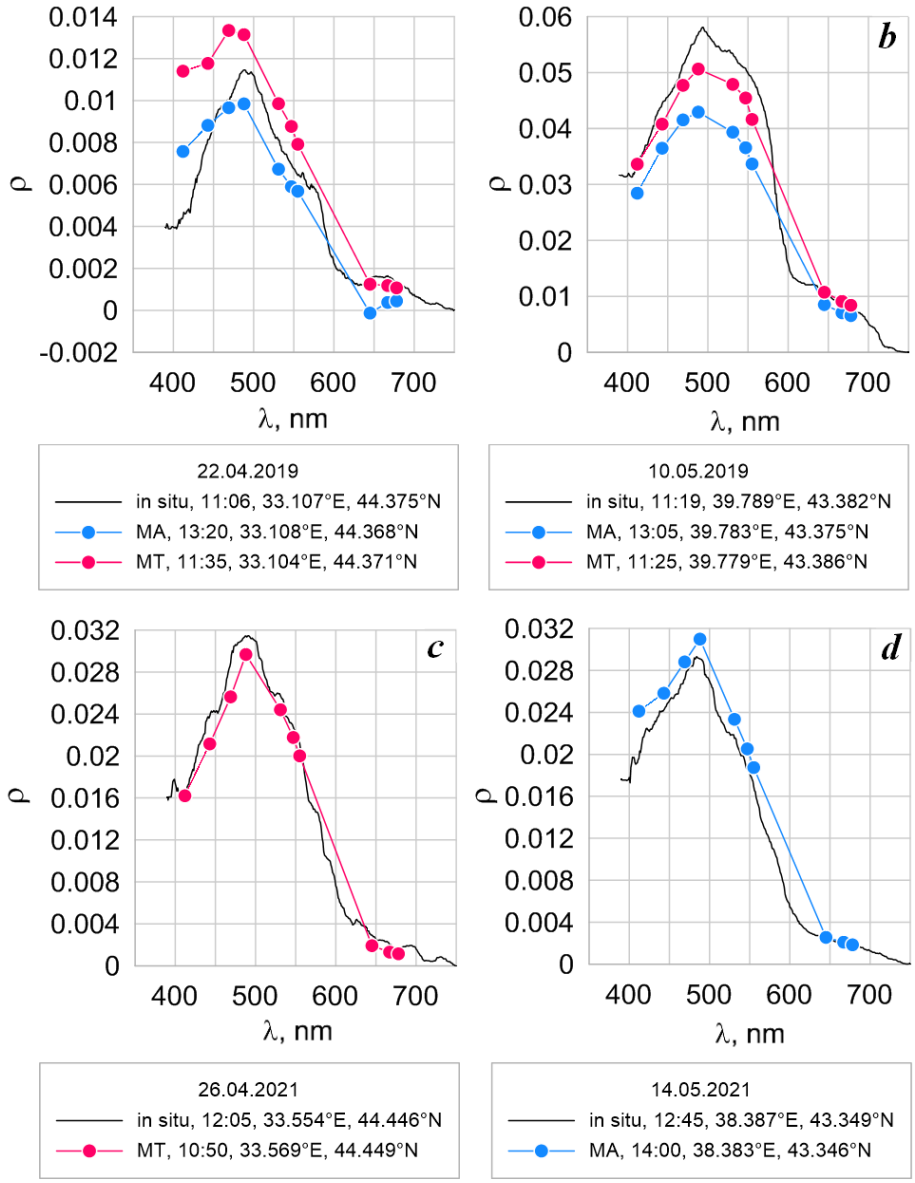

Fig. 8. Examples of comparison of corrected satellite and *in situ* reflectances (MA – MODIS Aqua, MT – MODIS Terra)

Conclusions

Comparison of the data of satellite color scanners with the results of *in situ* measurements made it possible to make a conclusion about the influence of errors in determining the parameters of aerosol over the Black Sea from satellite data on the possibility of reconstructing the radiation ascending from the sea.

1. The satellite data on the reflectance in the Black Sea in the spring period are on average underestimated compared to the contact measurements

2. The average values of the Angström and AOD values according to the satellite data are twice as high as the *in situ* measurements. The values of

the Angström parameter, which are greatly overestimated compared to the *in situ* measurements, lead to an excessive allowance for the influence of the atmosphere and, as a result, to an underestimation of the reflectance values.

3. The use of bias values as a correction term makes it possible to reduce the average error in calculating reflectance from satellite measurements.

REFERENCES

1. Pauly, D. and Christensen, V., 1995. Primary Production Required to Sustain Global Fisheries. *Nature*, 374, pp. 255–257. doi:10.1038/374255a0
2. Tilstone, G.H., Taylor, B.H., Blondeau-Patissier, D., Powell, T., Groom, S.B. and Rees, A.P., 2015. Comparison of New and Primary Production Models Using SeaWiFS Data in Contrasting Hydrographic Zones of the Northern North Atlantic. *Remote Sensing of Environment*, 156, pp. 473–489. doi:10.1016/j.rse.2014.10.013
3. Kato, S., Rose, F.G., Chang, F.-L., Painemal, D. and Smith, W.L., 2021. Evaluation of Regional Surface Energy Budget over Ocean Derived from Satellites. *Frontiers in Marine Science*, 8, 688299. doi:10.3389/fmars.2021.688299
4. Loeb, N.G., Johnson, G.C., Thorsen, T.J., Lyman, J.M., Rose, F.G. and Kato, S., 2021. Satellite and Ocean Data Reveal Marked Increase in Earth's Heating Rate. *Geophysical Research Letters*, 48(13), e2021GL093047. https://doi.org/10.1029/2021GL093047
5. Suetin, V.S., Korolev, S.N., Suslin, V.V. and Kucheryavyi, A.A., 2011. Comparative Analysis of the Methods Used for the Determination of the Optical Parameters of Waters in the Black Sea according to the Data of Satellite Measurements. *Physical Oceanography*, 21(2), pp. 106–114. https://doi.org/10.1007/s11110-011-9108-4
6. Kopelevich, O.V., Saling, I.V., Vazyulya, S.V., Glukhovets, D.I., Sheberstov, S.V., Burenkov, V.I. and Yushmanova, A.V., 2018. *Bio-Optical Characteristics of the Seas, Surrounding the Western Part of Russia, from Data of the Satellite Ocean Color Scanners of 1998-2017*. Moscow: IO RAS, 140 p. (in Russian).
7. Gordon, H.R. and Wang, M., 1994. Retrieval of Water-Leaving Radiance and Aerosol Optical Thickness over the Oceans with SeaWiFS: a Preliminary Algorithm. *Applied Optics*, 33(3), pp. 443–452. https://doi.org/10.1364/AO.33.000443
8. Moses, W.J., Sterckx, S., Montes, M.J., De Keukelaere, L. and Knaeps, E., 2017. Atmospheric Correction for Inland Waters. In: D. R. Mishra, I. Ogashawar and A. A. Gitelson, eds., 2017. *Bio-Optical Modeling and Remote Sensing of Inland Waters.* Amsterdam, The Netherlands: Elsevier, pp. 69–100. https://doi.org/10.1016/B978-0-12-804644-9.00003-3
9. Giardino, C., Brando, V.E., Gege, P.C., Pinnel, N., Hochberg, E., Knaeps, E., Reusen, I., Doerffer, R., Bresciani, M., Braga, F., Foerster, S., Champollion, N. and Dekker, A., 2019. Imaging Spectrometry of Inland and Coastal Waters: State of the Art, Achievements and Perspectives. *Surveys in Geophysics,* 40(3), pp. 401–429. https://doi.org/10.1007/s10712-018-9476-0
10. Moiseeva, N., Churilova, T., Efimova, T. and Krivenko, O., 2018. Light Absorption by non-Algal Particles and Colored Dissolved Organic Matter at the Wavelength of 490 nm in the Black Sea in the Autumn (2015 and 2016). In: SPIE, 2018. *Proceedings of SPIE.* Bellingham: SPIE. Vol. 10833: 24th International Symposium on Atmospheric and Ocean Optics: Atmospheric Physics, 108336B. https://doi.org/10.1117/12.2504650
11. Churilova, T., Suslin, V., Moiseeva, N. and Efimova, T., 2018. Dissolved and Suspended Matter Variability in Coastal Waters: Photosynthetic Available Light. In: SPIE, 2018. *Proceedings of SPIE.* Bellingham: SPIE. Vol. 10833: 24th International Symposium on Atmospheric and Ocean Optics: Atmospheric Physics, 1083365. https://doi.org/10.1117/12.2504637

12. Karabashev, G.S. and Evdoshenko, M.A., 2015. The Wavelength of Satellite Reflectance Maximum as a Remote Indicator of Water Exchange between Ecologically Different Aquatic Areas. *Oceanology,* 55(3), pp. 327–338. https://doi.org/10.1134/S0001437015030066
13. Bailey, S.W., Franz, B.A. and Werdell, P.J., 2010. Estimation of Near-Infrared Water-Leaving Reflectance for Satellite Ocean Color Data Processing. *Optics Express,* 18(7), pp. 7521–7527. https://doi.org/10.1364/OE.18.007521
14. Kopelevich, O., Burenkov, V.I. and Sheberstov, S.V., 2006. [The Development and Using of the Regional Algorithms for the Calculation of the Bio-Optical Characteristicsof Russian Seas from Ocean Color Satellite Data]. *Sovremennye Problemy Distantsionnogo Zondirovaniya Zemli iz Kosmosa*, 3(2), pp. 99–105 (in Russian).
15. Korchemkina, E.N. and Kalinskaya, D.V., 2022. Algorithm of Additional Correction of Level 2 Remote Sensing Reflectance Data Using Modelling of the Optical Properties of the Black Sea Waters. *Remote Sensing*, 14(4), 831. https://doi.org/10.3390/rs14040831
16. Lee, M.E., Shybanov, E.B., Korchemkina, E.N. and Martynov, O.V., 2015. Determination of the Concentration of Seawater Components Based on Upwelling Radiation Spectrum. *Physical Oceanography*, (6), pp. 15–30. doi:10.22449/1573-160X-2015-6-15-30
17. Sakerin, S.M., Kabanov, D.M., Rostov, A.P., Turchinovich, S.A. and Knyazev, V.V., 2013. Sun Photometers for Measuring Spectral Air Transparency in Stationary and Mobile Conditions. *Atmospheric and Oceanic Optics*, 26(4), pp. 352–356. https://doi.org/10.1134/S102485601304012X

Submitted 20.06.2022; accepted after review 12.08.2022;
revised 02.11.2022; published 23.12.2022

About the authors:

Elena N. Korchemkina, Senior Research Associate, Marine Hydrophysical Institute of RAS (2 Kapitanskaya St., Sevastopol, 299011, Russian Federation), Ph.D. (Phys.-Math.), **Researcher ID: I-1595-2015**, **ORCID ID: 0000-0003-0526-4083**, **Scopus Author ID: 23004799100**, *korchemkina@mhi-ras.ru*

Alina O. Raykina, engineer, Marine Hydrophysical Institute of RAS (2 Kapitanskaya St., Sevastopol, 299011, Russian Federation), *alina.raykina@gmail.com*

Contribution of the authors:

Elena N. Korchemkina – task statement, *in situ* data collection, data analysis, result interpretation, conclusion statement

Alina O. Raykina – data analysis, result interpretation and description, conclusion statement, article text writing

All the authors have read and approved the final manuscript.

DOI: 10.22449/2413-5577-2022-4-52-68

Hydrolithodynamic Conditions of Sediment Movement through the Strait of Baltiysk (Vistula Lagoon, Baltic Sea)

R. B. Zakirov*, B. V. Chubarenko, V. A. Chechko

Shirshov Institute of Oceanology, Russian Academy of Sciences, Moscow, Russia
**e-mail*: *kotruslan2@gmai.com*

Abstract

In the area of the strait connecting the Vistula Lagoon with the Baltic Sea, the work was carried out to refine the bottom topography, collect bottom sediments, measure currents in different seasons, and install a set of sediment traps at 4 levels in the 2-meter bottom layer. The sediment accumulation zones were identified on the basis of the bathymetric data according to geomorphological features. On the basis of *in situ* data, we studied the hydrolithodynamic conditions of suspended sediment movement through the strait and the general nature of sediment exchange. The suspended material moves through the strait both during inflows and outflows, while silt and fine sand are mainly transported from the lagoon into the sea, while fine, medium and coarse sands, on the contrary, are brought into the lagoon and feed the surge delta (a shallow area at the lagoonic end of the strait). Surge delta sediments mainly consist of fine and medium sand. It was assumed that the flow of sediments of sandy grain sizes does not reach the surge delta (the final deposition zone) in full, the part of the volume entering the strait is removed during regular maintaining dredging in the strait. Consequently, the surge delta develops more slowly than it could do naturally.

Keywords: strait, estuary, surge delta, lagoons, bottom sediments, suspended sediments, currents, sampling, field measurements

Acknowledgements: the authors are grateful to colleagues V.T. Paka, A.O. Korzh, A.A. Kondrashov for instrumentation support of current measurements, to A.N. Babakov for advice and partial preparation of sediment collection instruments, to V.S. Pinchuk and volunteer colleagues for participation in the expedition works. The fieldwork was carried out under cooperation agreement no. 4/2019 (1358) as of 3.07.2019 between Shirshov Institute of Oceanology RAS (Atlantic Branch) and Immanuel Kant Baltic Federal University and funded under RFBR project 19-35-90069 support, the interpretation of results is funded under state assignment of IO RAS (topic no. FMWE-2021-0016).

For citation: Zakirov, R.B., Chubarenko, B.V. and Chechko, V.A., 2022. Hydrolithodynamic Conditions of Sediment Movement through the Strait of Baltiysk (Vistula Lagoon, Baltic Sea). *Ecological Safety of Coastal and Shelf Zones of Sea*, (4), pp. 52–68. doi:10.22449/2413-5577-2022-4-52-68

Гидролитодинамические условия движения наносов через Балтийский пролив (Калининградский залив, Балтийское море)

Р. Б. Закиров*, Б. В. Чубаренко, В. А. Чечко

Институт океанологии им. П.П. Ширшова РАН, Москва, Россия
**e-mail: kotruslan2@gmai.com*

Аннотация

В районе пролива, связывающего Калининградский залив с Балтийским морем, проведены работы по уточнению рельефа дна, отбору донных отложений, измерению течений в разные сезоны и установке набора наносоуловителей на четырех горизонтах в придонном 2-метровом слое. По геоморфологическим признакам выделены зоны осадконакопления. На основе натурных данных изучены гидролитодинамические условия движения взвешенных наносов и общий характер седиментообмена залива с морем. Движение взвешенного материала через пролив осуществляется как при затоках, так и при оттоках, при этом илистая и мелкая песчаная взвесь преимущественно выносятся из залива в море, а мелкая, средняя и крупная песчаные фракции, наоборот, заносятся в залив и подпитывают нагонную дельту (мель со стороны залива). Отложения нагонной дельты состоят в основном из мелко- и среднезернистого песка. Предполагается, что поток песчаных наносов достигает нагонной дельты (как конечной зоны депонирования) не в полном объеме, часть объема извлекается в процессе регулярного дноуглубления в проливе. В результате этого нагонная дельта развивается медленнее, чем могла бы в естественных условиях.

Ключевые слова: пролив, эстуарий, нагонная дельта, лагуны, донные осадки, взвесь, течения, натурные измерения

Благодарности: авторы благодарны коллегам В. Т. Паке, А. О. Коржу, А. А. Кондрашову за аппаратурное обеспечение измерений течений, А. Н. Бабакову за советы и подготовку оснащения наносонакопителей, В. С. Пинчуку и коллегам-волонтерам за участие в экспедиционных работах. Полевые работы выполнены в рамках договора о сотрудничестве Института океанологии им. П. П. Ширшова РАН (Атлантическое отделение) с БФУ им. И. Канта от 3.07.2019 №4/2019 (1358) за счет поддержки проекта РФФИ 19-35-90069, интерпретация – за счет госзадания ИО РАН (тема № FMWE-2021-0016).

Для цитирования: *Закиров Р. Б., Чубаренко Б. В., Чечко В. А.* Гидролитодинамические условия движения наносов через Балтийский пролив (Калининградский залив, Балтийское море) // Экологическая безопасность прибрежной и шельфовой зон моря. 2022. № 4. С. 52–68. EDN ZKQZYX. doi:10.22449/2413-5577-2022-4-52-68

1. Introduction

The Kaliningrad Bay/Vistula Lagoon (Fig. 1) is the second largest transboundary lagoon-type water body [1] on the coast of the Baltic Sea. Although the Russian part of the water area (56.2 %) is called the Kaliningrad Bay on official maps, and the Polish part is called the Vistula Lagoon [2], in the article we shall use the name Vistula Lagoon in accordance with [3]. The lagoon is separated from the sea by a sandy Vistula Spit [2] and is freely connected to the sea by a natural channel, which has no official name, but in the scientific literature, starting from the

classic publication [3], it is listed as the Strait of Baltiysk [1)] (hereinafter referred to as the strait). Being the core of the natural and technical system [4] of the inlet section of the Kaliningrad Seaway Canal [2)], the strait is an important link in the system for ensuring the transport accessibility of Port of Kaliningrad. From autumn 2022, it has been no longer the only connection between the lagoon and the sea – a new artificially dug shipping canal has been opened in the southern part of the spit [3)], equipped with a lock that blocks free water exchange between the lagoon and the sea. The water area of the lagoon serves as a receiving reservoir for the rivers Pregolya, Paslenka, Prokhladnaya, Elblag, Bauda, Mamonovka-Bonuvka, Nelma, Nogat, etc., it receives both sea (17 km^3/year) and river (3.5 km^3/year) waters, and together with them terrigenous and biogenic material [3, 5, 6].

After almost complete regulation of the Nogat River flow in 1916, the flow of river waters and sediments into the lagoon water area sharply decreased and the role of water exchange through the Strait of Baltiysk increased [3]. The sedimentary balance of the lagoon water area was disturbed and, according to some assumptions, has not yet reached equilibrium [6]. According to the estimates [5, 7, 8], 76,500 tons of sedimentary material (60 % – biogenic suspended matter) are brought annually through the Strait of Baltiysk, and 348,400 tons per year are taken out of the lagoon into the sea (70 % – biogenic suspended matter). These estimates are based on short-term hydrological measurements of flows in the Strait of Baltiysk obtained during field work in 1951–1965 [3], and the results of numerical simulation [6, 8–10].

Based on the results of the bathymetric data analysis, we previously performed a morphometric description of the sand bank at the lagoon-ward end of the strait [11] and the erosional depression between the entrance pair breakwater piers of the seaward end of the strait [12], and based on the results of hydrological measurements, a relationship was revealed between the dynamics of the sea level and water exchange between the lagoon and the sea [13]. It was established [12] that the volume of erosion depression below the 12 m isobath is 1.13 mln m^3. In 2008–2016 the depression increased its size at a rate of 2450 m^3/year. The sand bank at the entrance to the Vistula Lagoon [11] has an annular shape with flush channels cutting through it; the volume of the sand bank above the 2.5 m isobath is estimated at 6.5 mln m^3, the deformation (during the period 2012–2019) was noted over its entire surface. The results obtained earlier testify to active hydrolithodynamic processes at the inlet and outlet of the strait.

[1)] The name “Baltic Strait” is absent in the Registry of Geographical Names of the Kaliningrad Oblast. In English-language literature (see Szydłowski, M., Artichowicz, W. and Zima, P., 2021. Analysis of the Water Level Variation in the Polish Part of the Vistula Lagoon (Baltic Sea) and Estimation of Water Inflow and Outflow Transport through the Strait of Baltiysk in the Years 2008–2017. *Water*, 13(10), 1328. doi:10.3390/w13101328), the name “Strait of Baltiysk” can be found (due to location near the city of Baltiysk).

[2)] The Kaliningrad Seaway Canal is stretched along the north coast of Vistula Lagoon from the strait to the mouth of the Pregolya River and is a navigable waterway connecting the port of Kaliningrad with the Baltic Sea.

[3)] The canal on the Polish part of the Vistula Spit was formally opened for navigation on 17 September 2022.

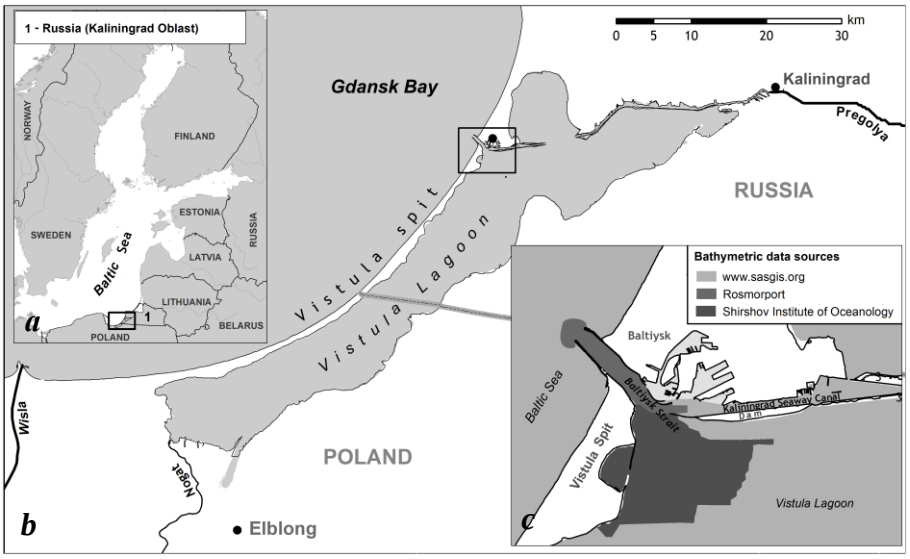

F i g . 1 . Study area: Baltic Sea (*a*); Vistula Lagoon in the South-Eastern Baltic (*b*); scheme of covering the study area with bathymetric data (*c*)

The flows over the sand bank [13] are subject to the regime features of the water exchange between the lagoon and the sea, they are bidirectionally oriented (toward the inflow of sea water and the outflow of water from the lagoon) and characterized by a frequent change of sign. A linear relationship was revealed between the value of the cumulative water exchange between the lagoon and the sea, as well as sea level fluctuations (regression coefficient $r = 0.84…0.98$).

At present, sediment flows through the strait have not been sufficiently studied; the field measurement data of 1951–1965 [3], on which modern estimates of suspended matter transport are based [6, 8], are already technically outdated and require clarification. The problem of balance in sediment exchange must be solved on the basis of data accumulation from the direct measurements of the suspended material flows.

The purpose of the work is to identify zones of sedimentation based on geomorphological features and experimentally, based on *in situ* data, to study the hydrolithodynamic conditions for the movement of suspended sediments in the area of the strait, which provides a free connection between the Vistula Lagoon and the Baltic Sea.

2. Research methodology

The paper implements a methodology for morphodynamic studies based on field measurements, sampling, processing and analysis of geological and geomorphological information.

The **digital topographic model** is based on bathymetric data from various sources: the single-beam echosounder measurements at the entrance to the Vistula Lagoon for 2012, the multibeam measurements at the offshore section of the Kaliningrad

Seaway Canal for 2011. The bathymetric data for the rest of the Vistula Lagoon and Gdansk Bay of the Baltic Sea were digitized using the library of SAS. Planet open geoinformation system (available at: www.sasgis.org) (Fig. 1, *c*). The processing and analysis of bathymetric data were performed using Esri ArcGIS 10.0 GIS software packages. A scheme of the bottom relief of the Strait of Baltiysk was prepared using standard surface mapping methods. Then, the sedimentation zones were identified based on morphological features, similarly to the sedimentation environment of the wave estuary [14–17].

The **sampling of bottom sediments** (layer 0.1–0.15 m) was carried out at three points (*B1*, *B2*, *B3* in Fig. 2) using a Van Veen single-rope clamshell bucket. The **sampling of suspended sediments** was carried out in accordance with methodological developments [18, 19]: a rigid pyramidal frame was installed at the bottom of the lagoon, on which cassettes with sediment traps of horizontal and vertical types were fixed at levels of 40, 100, 150, 200 cm from the bottom and 40, 100, 150, 200 cm from the bottom, respectively. The suspended sediments were collected at two points in the period from 28.06.2020 to 02.08.2020: at point *2* for 35 days, at point *7* for 18 days. At point *2*, only horizontal-type sediment traps were installed; at point *7*, both types of sediment traps were installed. Both horizontal- and vertical-type traps accumulate material regardless of the flow direction – the horizontal-type traps have side openings along the entire perimeter, the top end of the vertical-type traps is completely open.

The **granular composition** of the selected suspended matter and bottom material was determined by the mass content of particles of various sizes, expressed as a percentage relative to the weight of the dry sediment sample taken for analysis. The granular analysis was performed by sieve (fractions greater than 0.04 mm) and water-mechanical (fractions less than 0.04 mm) methods [20] by sifting a sandy sediment

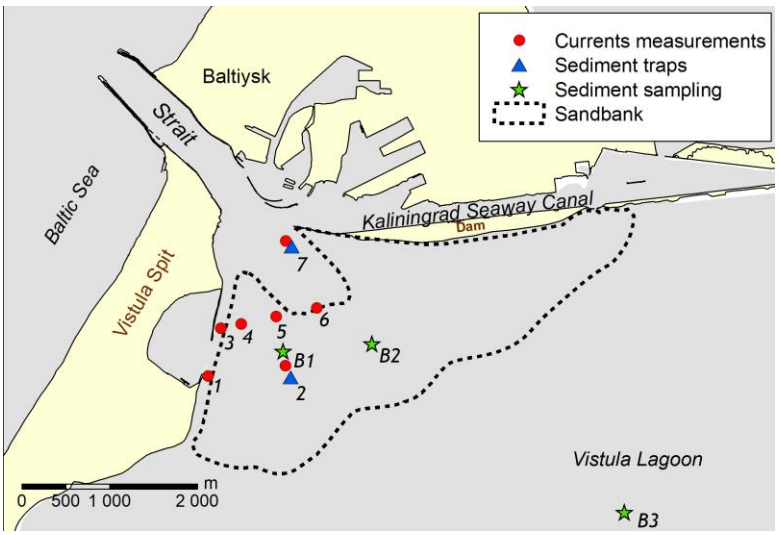

F i g . 2 . Measurement and sampling map

sample through a set of sieves of an AS 200 analytical sieving machine. Based on the granular analysis results in accordance with the Wentworth classification [21], the following fraction sizes were distinguished: coarse sand (1.0–0.5 mm), medium sand (0.5–0.25 mm), fine sand (0.25–0.125 mm), very fine sand (0.125–0.063 mm), silt (0.063–0.04 mm), clay (less than 0.04 mm).

The **flow measurements** were carried out in the water area of the Vistula Lagoon adjacent to the Strait of Baltiysk at seven points (points *1–7* in Fig. 2) by autonomous current-meters – inclinometers. They were developed at the AB IO RAS by a group managed by V.T. Paka [22] to measure bottom flows in the velocity range of 0.03–0.56 m/s (with a maximum relative error of 25 % for low velocities and 3–5 % for high velocities). The measurements were carried out in the following periods: winter 24.12.2019 – 13.02.2020 (51 days), spring 17.03.2020 – 21.04.2020 (35 days), and summer 28.06.2020 – 02.08.2020 (35 days).

The measurement data were preliminarily reduced to the same step with a discreteness of 1 measurement per 10 min, then the vector values of the flow velocities were converted into scalar ones: the vectors of the flow velocities ($\overline{V_a}$) were projected onto the OX axis, whose orientation was determined based on the idea of a bidirectional (outflow and inflow) nature of the flow in the water area close to the strait [23, 24]. Rather high correlation values were obtained between the flow velocities ($\overline{V}$) at different measurement points (see Table 1).

Conditions of the suspended matter transport. The sediment movement process can be represented as a sequence of three conditional phases – resuspension, transport and sedimentation (Fig. 3). Conditional flow velocity thresholds at which these phases arise can be obtained (Table 2) from the Hjulstrøm diagram [25]. On the basis of the obtained velocity ranges, according to the flow measurements, the intervals of the phases of resuspension, transport, and sedimentation for the grain size dimensions of sands, silt and clay (according to the Wentworth classification) were identified. Those phases of potential sedimentation and transport that were not supported by the previous phases of resuspension were not taken into account. The intervals obtained for the movement of suspended sediments were converted into percentages of the total duration of measurements separately for outflows and inflows. Their comparison makes it possible to integrally estimate the conditions of suspended matter transport in the case of reciprocating flows present in the study area.

Table 1. Correlation coefficients between flow velocities ($\overline{V}$)

Measurement period	Measurement point number	Correlation coefficient
24.12.19 – 13.02.20	*1* / *2*	0.99
17.03.20 – 21.04.20	*5* / *6*	0.99
28.06.20 – 02.08.20	*1* / *2*	0.94
28.06.20 – 02.08.20	*3* / *4*	0.92

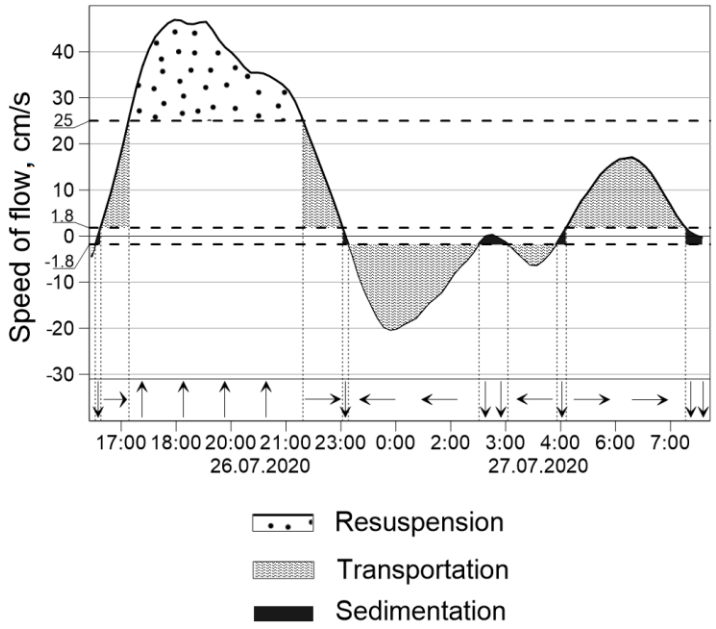

Fig. 3. Phases of the flow velocity at which potential resuspension, transport and sedimentation occur for particles of the grain size range 0.125–0.250 mm (fine sand). Horizontal dotted lines indicate the thresholds of resuspension and sedimentation for the selected range of grain size. Positive flow rate means inflow of water into the lagoon, negative – outflow. The arrows along the horizontal axis schematically indicate the processes of sedimentation (↓), transport (→;←) and resuspension (↑)

Table 2. Thresholds of the rate of resuspension and sedimentation according to the Hjulstrøm diagram [25] for various grain size dimensions

Sediment type (by Wentwort)	Particle size, mm	Resuspension threshold, cm/s	Sedimentation threshold, cm/s
Clay	0.040–0.063	25	0.5
Silt	0.063–0.125	20	0.9
Very fine sand	0.125–0.250	25	1.8
Fine sand	0.250–0.500	30	3.6
Medium sand	0.500–1.000	45	6.6

3. Results and discussion

Sedimentary environment. To characterize the hydrolithodynamic system of the strait, the classification widely used abroad [14–17] of sedimentary environments for estuaries was taken as a basis.

In the classification of sedimentary environments, a special type of estuaries is distinguished – a tidal estuary with a predominantly wave water exchange regime (wave estuary) [14, 17]. This type of estuaries is formed in the river–lagoon–strait–sea systems; it is characterized by the presence of a sandy barrier between the lagoon and the sea, channels (straits) through the barrier, a flooded tidal delta from the lagoonal side of the barrier, the central part of the estuary and the inner river delta.

The Vistula Lagoon is a lagoon-type tideless body of water where sea and fresh waters mix; therefore, by definition [14], it can be attributed to an estuarine system. In the Baltic Sea, the tidal movements are virtually absent, but surges of various genesis are very developed, ensuring the inflow of sea water into the lagoon and, accordingly, their outflow when surge conditions disappear [13]. Together with sea waters, marine sand is brought into the lagoon, it is deposited in the immediate vicinity of the strait and forms a sand bank [5, 11].

Similarly to the conceptual model of sedimentary environments of the wave estuary [14], and also by analogy with the identification of the "inner" delta in [26], the following zones were distinguished based on morphological features in the area of the Strait of Baltiysk (Fig. 4):

– Baltic Spit and the Strait of Baltiysk – the sand barrier and passage through it;

– sand bank at the lagoon-ward end of the strait – the surge delta (by analogy with the tidal one);

– the Vistula Lagoon – the central part of the estuary.

The surge delta is a shallow, which is formed at the mouth of the strait (channel) on the side of the lagoon. According to [15, 26], such accumulative formations are mainly composed of sediments, which are intercepted from the alongshore (from the sea side) sediment flow by reciprocating water movements through the strait (in the classical version [14] they are caused by tides, and in our case – by upsurges and downsurges). That is, in the case of the Vistula Lagoon, the surge delta serves as a zone of final deposition of sand deposits during their movement from the sea to the lagoon.

Granular composition of bottom sediments. The deposits of the accumulative area of the surge delta (point *B2*) contain 51 % of medium sands and 39 % of fine sands, and the deposits of the central gully (point *B1*) contain 84.8 % of fine sands (Table 3). The shares of coarse sands and very fine sands at points *B1* and *B2* are 5 % each. The predominance of medium and fine sands in the sediments of the accumulative area of the surge delta (point *B2*) indicates that the delta is mainly fed by these fractions. In the inner part of the lagoon, at point *B3*, the sediments contain 50 % of very fine sands, 29 % of fine sands, 10 % of medium sands and 10 % of silt.

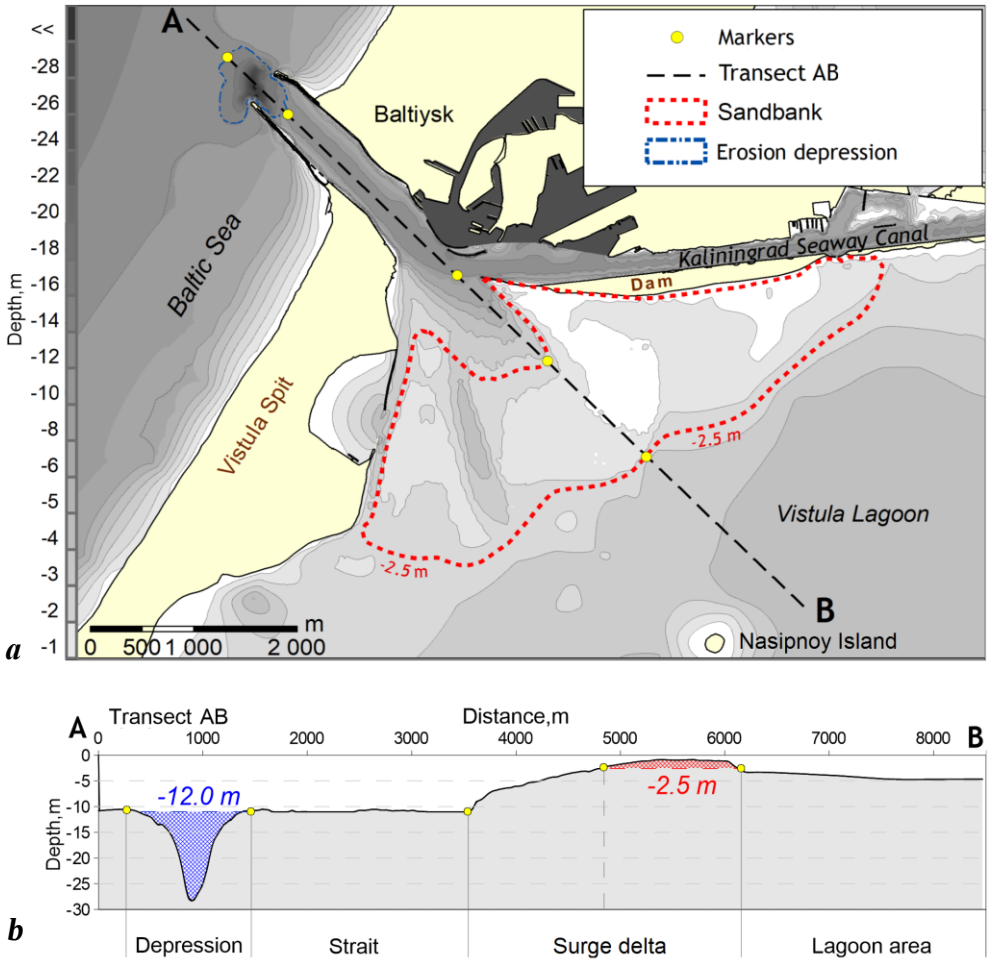

Fig. 4. Diagram of the morphological structure of the bottom relief of the sedimentary system of the Strait of Baltiysk: plan view (*a*) and profile *AB* view (*b*)

Vertical distribution of the suspended material. The experimental sampling of the suspended material at points *2* and *7* showed a gradual decrease in the mass of the accumulated material depending on the distance from the bottom (Table 4). Such a vertical distribution can be interpolated by an exponential curve with a fairly high regression coefficient (r from 0.85 to 0.98) and a small standard deviation (σ within 0.3–0.6 g):

$$m = A \cdot e^{-H/H_0},$$

where A (g) and H_0 (cm) are the parameters of the regression dependence.

For three exposures (Table 4), the coefficients A and H_0 are 22.3 g and 370 cm, 9.2 g and 670 cm, 24.7 g and 230 cm, respectively. These interpolations are characterized by regression coefficients and standard deviation values: 0.98 and 0.3 g, 0.85 and 0.3 g, 0.98 and 0.6 g, respectively.

Table 3. Particle size distribution of sedimentary material and suspended sediments at points *B1*, *B2*, *2*, *7* (%)

Sampling points	Sand				Silt	Clay
	coarse	medium	fine	very fine		
Sediments taken with a VanVeen grab						
B1	1	4	85	10	0	0
B2	4	51	40	5	0	0
B3	0	19	29	50	10	0
Suspended sediments accumulated in horizontal-type traps						
2	0	0	8	39	53	1
7	0	0	5	34	61	0
Suspended sediments accumulated in vertical-type traps						
7	0	1	16	44	40	0

Table 4. The mass of the suspended material according to the results of experimental sampling (m_{mea}) and interpolation (m_{int}) at points *2*, *7*

Level above the bottom, cm	Sampling method					
	Horizontal-type traps *		Horizontal-type traps **		Vertical-type traps **	
	m_{mea}, г	m_{int}, г	m_{mea}, г	m_{int}, г	m_{mea}, г	m_{int}, г
40	20.0	20.0	9.0	8.7	21.5	20.7
60	18.5	19.0	–	8.4	–	19.0
80	18.5	18.0	–	8.2	–	17.4
100	–	17.0	7.5	7.9	15.0	15.9
120	16.0	16.1	–	7.7	–	14.6
150	–	14.9	7.5	7.6	13.0	12.8
170	14.0	14.1	–	7.1	–	11.7
200	–	13.0	7.0	6.8	10.5	10.2

* Samples were taken at point *2*.

** Samples were taken at point *7*.

Note: the dash means samples were not taken.

Despite the difference in the duration of exposure of sediment traps at points *2* and *7* (687 and 432 hours), horizontal-type sediment traps at both points accumulated an approximately equal amount of material, which indicates a uniform distribution of the flow of suspended material over the entire area of the surge delta.

Although the characteristics of the interpolation curves describing the vertical distribution of suspended material differ at first glance, the data indicate that within the water column from the 40 cm to the 2 m level above the bottom, the amount of accumulated material varies within only 25 % of the maximum located at the 40 cm level above the bottom, which indicates a weak flow stratification along the vertical within a 2-meter water layer above the surge delta. This means that it is possible to estimate the transport from data obtained at only a few levels.

The mass of material in vertical-type sediment traps at point *7* also gradually increases from the upper to the lower levels. The characteristics of the vertical distribution are similar to those obtained for masses accumulated in horizontal-type traps. The only difference is that the mass in vertical-type traps grows faster (the values differ twice as much at the levels of 2 m and 40 cm above the bottom) than in horizontal-type traps where the difference was 1.3–1.4 times. It is natural, since the lower vertical-type traps integrate the entire vertical flow, which grows from level to level.

Granular composition of suspended sediments. According to the results of the grain size analysis of the suspended material taken into horizontal-type traps, i.e. from a horizontal flow, it was found that in summer seasonal conditions above the surge delta in a 2-meter layer from the bottom, the water flow carried 55–61 % of silty material, 34–39 % of very fine sand and 4–8 % of fine sand. Medium and coarse sands were not found in the horizontal-type traps. The sediment traps for vertical flows (vertical-type traps) accumulated 40 % of silty material, 44 % of very fine sand, 16 % of fine sand and up to 1 % of medium sand.

The silty material accumulated by the sediment traps could only be carried out of the lagoon into the sea, since it is scarce in marine sediments [27]. Very fine sands are widespread both in the sea and in the lagoon [7]; therefore, their accumulation in sediment traps (see Table 3) could be provided by both inflows from the sea and outflows from the lagoon. No medium sand was found in the sediment traps, which is consistent with the low water flow rates during the sampling period.

Estimates of the transport times of suspended material of different fractions. The summer installation of sediment accumulators did not provide sufficient information to assess the conditions for the transport of suspended material; therefore, the assessment was carried out on the basis of flow measurement data. Since a reliable relationship was found between the records of near-bottom velocities at points *1–7* (see Table 1), the water flow velocity averaged over the measurement data at these points was used to estimate the conditions for the transport of suspended matter.

At the first stage, the total time intervals of the successive phases of resuspension and transport of suspended material of different sizes were estimated, while the situations of inflow and outflow were analyzed separately, and the obtained values were converted into percentages (Table 5). The results showed that the velocity characteristics of the water flow both during inflow and outflow were sufficient for the transport of water suspension of all dimensions. Therefore, the general nature of the process of movement of suspended sediments through the strait can be expressed by the sum and difference in the durations of the potential transfer of the suspended material between inflows and outflows (Table 6).

The conditions for the transport of silt (32–54 %) and very fine sand (48–64 %) were preserved by the water flow for the longest time (as a percentage of the entire duration of the measurement), then, as the size increased, the duration of the transport of fine sand (32–44 %), medium sand (17–34 %) and coarse sand (1–3 %) followed (Table 6).

If we consider the movement of sediments through the strait as a reciprocating (or alternating) movement of material from the sea to the lagoon and back to the sea, then the difference in the duration of the transport of suspended material during inflows and outflows will characterize the balance of movement of suspended sediments through the Strait of Baltiysk in the period under consideration (Table 6).

Depending on the characteristics of the water flow, the silt and sandy material can be transported both from the lagoon to the sea and from the sea to the lagoon, but the possibility of involving the silt already carried into the sea is unlikely, since it is carried away by the alongshore flow. The velocity conditions for the transport (Table 6) of very fine sand were longer in winter and spring during outflows (by 8.1 and 0.2 %), and in summer – during inflows (by 2.4 %). The possibility

Table 5. The duration (in hours) of successive phases of resuspension and transfer of suspended sediments of different grain size according to flow velocity in the winter, spring, summer measurement periods (% is indicated from the total duration of measurements)

Sediment type	Winter (687 h)				Spring (432 h)				Summer (432 h)			
	Inflow		Outflow		Inflow		Outflow		Inflow		Outflow	
	h	%	h	%	h	%	h	%	h	%	h	%
Coarse sand	0	0	0	0	0	0	0	0	0	0	0	0
Medium sand	0	0	0	0	8	1	11	2	10	1	0	0
Fine sand	49	10	54	11	98	16	105	17	69	10	50	7
Very fine sand	101	21	91	19	140	23	121	20	115	17	102	15
Silt	130	27	131	27	167	28	215	36	175	25	158	23
Clay	101	21	91	19	134	22	189	31	116	17	104	15

Table 6. The sum of and the difference in the duration (% of the total measurement duration in hours) of the potential particle transport of various sizes in the time interval between inflows and outflows

Sediment type	Winter		Spring		Summer	
	Sum	Difference	Sum	Difference	Sum	Difference
Coarse sand	0	0	0	0	0	0
Medium sand	40	2	54	–9.1	32	1.8
Fine sand	54	–0.2	64	–8.1	48	2.4
Very fine sand	40	2	44	3.2	32	1.8
Silt	21	–0.9	34	–1.2	17	2.9
Clay	0	0	3.2	–0.6	1.4	1.4

of transporting fine sand lasted longer in winter, spring, and summer, and only during inflows (by 2, 3.2, and 1.8 %, respectively); medium sand – during inflows in winter and spring (by 0.9 and 1.2 %), and in summer – during outflows (by 2.9 %). Velocity conditions for the transport of coarse sand were noted only in spring and summer, while in spring the balance turned out to be in favor of outflows (by 0.6 %), and in summer – in favor of inflows (1.4 %).

In total, over all three measurement periods (73 days), the velocity conditions for the transport of silty material and very fine sand were longer during outflows (by 1.8 and 1.9 %), and fine, medium and coarse sands – during inflows (by 2.3, 0.5 and 0.4 %, respectively) (Fig. 5). It follows from this that during the flow measurements, the surge delta potentially accumulated material. To a greater extent, it was fed by fine sand, to a lesser extent, by medium and coarse sands.

4. Concluding remarks

The measurements carried out illustrated the features of the process of sediment transport through the Strait of Baltiysk in certain periods of the year. The *in situ* data on the accumulation of suspended material in traps made it possible to conclude that there is a slight vertical stratification of horizontal flows of suspended material (the values at the levels of 2 m and 40 cm above the bottom differ by 1.3–1.4 times). Due to the impossibility of covering all seasons of the year with direct observations, and also since the region under study is a transit region, the estimated difference in the duration of the potential transport of suspended material (according to the measured flow velocities) enables us to make assumptions about its general nature. The silty material is transported from the lagoon to the sea. The transfer of very fine sand is characterized by reciprocating motion. It can both be carried out and brought back into the lagoon, while very fine sand is not deposited on the surge delta, which

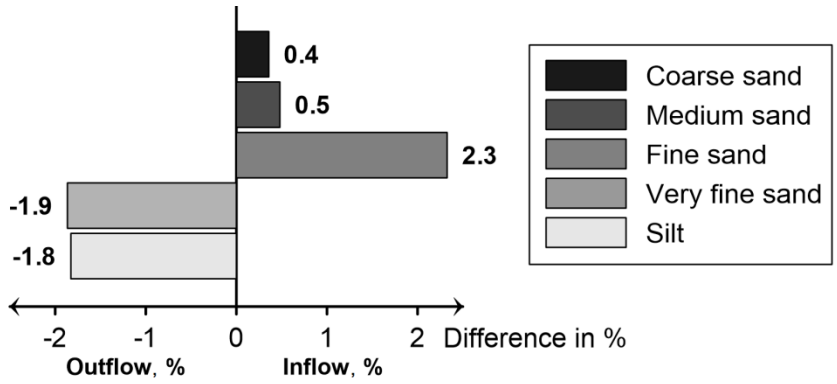

Fig. 5. Balance characteristic of the movement of suspended sediments through the Strait of Baltiysk: the difference in the total duration (%) of the suspension transfer between the inflows and outflows during three measurement periods (negative values – predominance of the outflow, positive ones – predominance of the inflow). Measurement duration was 73 days (100 %)

is the zone of final deposition for larger fractions. Surge delta deposits consist mainly of fine and medium sand with an insignificant content of coarse sand; their source is the alongshore sediment flow (from the seaward part of the Baltic Spit). The movement of sand of these dimensions is characterized as reciprocating, therefore, at a high intensity of water exchange, the sediments of the surge delta can again be involved in transport and carried back to the sea.

The low content of fine and medium sand in sediment traps corresponds to the fact that during the summer period of measurements, the water flow velocities sufficient for the mass transport of this type of suspended material were not observed.

The surge delta in the Vistula Lagoon, which is typical for the sedimentation situation in the sea-strait-estuary system, is increasing, but the current growth rate is so low that it does not explain the current size of the delta. The low rates of its development at present can be associated with regular dredging in the strait – the main flow of marine sediments is extracted during dredging at the approaches to the delta, which serves as the zone of final deposition.

Adhering to the indicated conceptual model of the sedimentary environment of the wind induced estuary, we can assume the following: if the surge delta actively develops further, then as it grows, it will increasingly clog the passage from the sea to the lagoon, and the flow of bottom sediments will be sent to the Kaliningrad Seaway Canal.

REFERENCES

1. Chubarenko, B. and Margoński, P., 2008. The Vistula Lagoon. In: U. Schiewer, ed., 2008. *Ecology of Baltic Coastal Waters*. Berlin, Heidelberg: Springer, pp. 167–195. doi:10.1007/978-3-540-73524-3_8
2. Kushevsky, V., Fedorov, G.M., Chubarenko, B.V. and Gritsenko, V.A., eds., 2014. [*The Region of the Vistula Lagoon: Current State and Development Scenarios*]. Kaliningrad: BFU im. Kanta, pp. 187–195 (in Russian).
3. Lazarenko, N.N. and Maevsky, A.P., eds., 1971. [*Hydrometeorological Regime of the Vistula Lagoon*]. Leningrad: Gidrometeoizdat, 279 p. (in Russian).
4. Zakirov, R.B. and Chubarenko, B.V., 2022. Entrance Section of the Kaliningrad Bay (Vistula Lagoon) as a Natural-Technical System. *Russian Journal of Applied Ecology*, (1), pp. 48–59. https://doi.org/10.24852/2411-7374.2022.1.48.59
5. Chechko, V.A. and Blazhchishin, A.I., 2002. Bottom Sediments of the Vistula Lagoon of the Baltic Sea. *Baltica*, 15, pp. 13–22. Available at: https://gamtostyrimai.lt/uploads/publications/docs/186_d0e78941be6818702231e507113c0959.pdf [Accessed: 05 December 2022].
6. Chubarenko, B.V. and Chubarenko, I.P., 2002. New Way of Natural Geomorphological Evolution of the Vistula Lagoon due to Crucial Artificial Influence. In: E. M. Emelyanov, ed., 2002. *Geology of the Gdansk Basin. Baltic Sea*. Kaliningrad: Yantarny Skaz, pp. 372–375.
7. Chechko, V., 2008. Spatial Structure and Evolution of Bottom Sediments in the Vistula Lagoon. In: B. Chubarenko, ed., 2008. *Transboundary Waters and Basins in the South-East Baltic*. Kaliningrad: Terra Baltica, pp. 244–249. Available at: http://atlantic.ocean.ru/images/publ/Transboundar.pdf [Accessed: 05 December 2022].
8. Chechko, V. and Chubarenko, B., 2006. Sediment Balance of the Vistula Lagoon. In: RSHU, 2006. *Managing Risks to Coastal Regions and Communities in a Changing World: Proceedings of International Coastal Conference EMECS'11-SeaCoasts XXVI, Saint Petersburg, 22–27 August, 2016*. Saint Petersburg: RSHU, pp. 174–185. doi:10.31519/conferencearticle_5b1b94303c55f9.63278465
9. Chubarenko, I.P. and Chubarenko, B.V., 2002. General Water Dynamics of the Vistula Lagoon. *Environmental and Chemical Physics*, 24(4), pp. 213–217.
10. Szydłowski, M., Kolerski, T. and Zima, P., 2019. Impact of the Artificial Strait in the Vistula Spit on the Hydrodynamics of the Vistula Lagoon (Baltic Sea). *Water*, 11(5), 990. https://doi.org/10.3390/w11050990
11. Zakirov, R.B. and Chubarenko, B.V, 2019. [Morphometric Characteristics of the Underwater Sand Bar at the Entrance to the Gulf of Kaliningrad as an Indicator of the Hydrodynamic Structure of the Bay's Water Exchange with the Sea]. In: MHI, 2019. [*Proceedings of the 4th All-Russian Scientific Conference for Young Scientists, Sevastopol, 22–26 April 2019*]. Sevastopol: FGBUN MGI, pp. 276–278 (in Russian).
12. Zakirov, R.B., Chubarenko, B.V., Sologub, S.P. and Shusharin, A.V., 2018. Dynamics of Scour Hole the Entrance to Kaliningrad Bay. *The Bulletin of Irkutsk State University. Series Earth Sciences*, 26, pp. 46–59. https://doi.org/10.26516/2073-3402.2018.26.46
13. Chubarenko, B. and Zakirov R., 2021. Water Exchange of Nontidal Estuarine Coastal Vistula Lagoon with the Baltic Sea. *Journal of Waterway, Port, Coastal, and Ocean Engineering*, 147(4), 05021005. doi:10.1061/(ASCE)WW.1943-5460.0000633

14. Reading, H.G., 1978. *Sedimentary Environments and Facies*. Oxford: Blackwell Scientific, 557 p.
15. Hayes, M.O., 1979. Barrier Island Morphology as a Function of Tidal and Wave Regime. In: S. P. Leatherman, ed., 1979. *Barrier Islands from the Gulf of St. Lawrence to the Gulf of Mexico*. New York: Academic Press, pp. 1–28.
16. FitzGerald, D.M. and Pendleton, E., 2002. Inlet Formation and Evolution of the Sediment Bypassing System: New Inlet, Cape Cod, Massachusetts. *Journal of Coastal Research*, 36(sp1), pp. 290–299. https://doi.org/10.2112/1551-5036-36.sp1.290
17. Baraboshkin, E.Yu., 2005. [*Practical Sedimentology (Terrigenous Reservoirs)*]. Tomsk: TPU, 153 p. (in Russian).
18. Antsiferov, S.M. and Kosyan, R.D., 1986. [*Suspended Sediments in the Upper Shelf*]. Moscow: Nauka, 224 p. (in Russian).
19. Lund-Hansen, L.C., Petersson, M. and Nurjaya, W., 1999. Vertical Sediment Fluxes and Wave-Induced Sediment Resuspension in a Shallow-Water Coastal Lagoon. *Estuaries*, 22(1), pp. 39–46. https://doi.org/10.2307/1352925
20. Budanova, T.E., Ozmidov, O.R. and Ozmidov, I.O., 2013. Modern Methods of Granulometric Analysis of Soils. *Engineering Survey*, (8), pp. 66–71 (in Russian).
21. Wentworth, C.K., 1922. A Scale of Grade and Class Terms for Clastic Sediments. *The Journal of Geology*. 1922. Vol. 30, iss. 5. P. 377–392. Available at: https://www.jstor.org/stable/30063207#metadata_info_tab_contents [Accessed: 16 November 2022].
22. Paka, V.T., Nabatov, V.N., Kondrashov, A.A., Korzh, A.O., Podufalov, A.P., Obleukhov, S.D., Golenko, M.N. and Shchuka, S.A., 2019. On the Improvement of the Tilting Bottom Current Meter. *Journal of Oceanological Research*, 47(2), pp. 220–229. https://doi.org/10.29006/1564-2291.JOR-2019.47(2).13 (in Russian).
23. Dubravin, V.F., Egorikhon, V.D., Chubarenko, B.V., Babakov, A.N. and Ivanov, S.N., 1997. [Bottom Currents of Kaliningrad Gulf]. In: KGU, 1997. [*Ecological Problems of the Kaliningrad Oblast*]. Kaliningrad: KGU, pp. 90–95 (in Russian).
24. Solov'ev, A.N., 1999. On the Manifestations of the Seiches Oscillations in the Baltic Sea in Kaliningrad Gulf on the Basis of Autonomous Nephelometer Data. *Okeanologiya*, 39(1), pp. 158–160 (in Russian).
25. Hjulstrøm, F., 1955. Transportation of Detritus by Moving Water. In: P. D. Trask, ed., 1955. *Recent Marine Sediments. A Symposium*. Tulsa, Oklahoma, pp. 5–31. https://doi.org/10.2110/pec.55.04.0005
26. Afanas'yev, V.V., Uba, A.V. and Levitsky, A.I., 2019. Migration of the Straits and Pelagic Sedimentation in the Lagoons. *Geosystems of Transition Zones*, 3(3), pp. 310–317 (in Russian).
27. Chechko, V.A., Chubarenko, B.V., Boldyrev, V.L., Bobykina, V.P., Kurchenko, V.Yu. and Domnin, D.A., 2008. Dynamics of the Marine Coastal Zone of the Sea Near the Entrance Moles of the Kaliningrad Seaway Channel. *Water Resources*, 35(6), pp. 652–661. https://doi.org/10.1134/S0097807808060043

Submitted 29.08.2022; accepted after review 20.09.2022;
revised 02.11.2022; published 23.12.2022

About the authors:

Ruslan B. Zakirov, Senior Engineer, P.P. Shirshov Institute of Oceanology of the Russian Academy of Sciences (36 Nakhimovsky Prosp., Moscow, 117997, Russian Federation), PhD student, **ORCID ID: 0000-0003-0125-374X, ResearcherID: AFB-2669-2022,** *kotruslan2@gmail.com*

Boris V. Chubarenko, Leading Research Associate, Head of the Laboratory of Coastal Systems, P.P. Shirshov Institute of Oceanology of the Russian Academy of Sciences (36 Nakhimovsky Prosp., Moscow, 117997, Russian Federation), Ph.D. (Phys.-Math.), **ORCID ID: 0000-0001-7988-1717, ResearcherID: I-6118-2016, Scopus Author ID: 6507102508**, *chuboris@mail.ru*

Vladimir A. Chechko, Senior Research Associate, P.P. Shirshov Institute of Oceanology of the Russian Academy of Sciences (36 Nakhimovsky Prosp., Moscow, 117997, Russian Federation), Ph.D. (Geol.-Miner.), **ORCID ID: 0000-0003-3030-1165, ResearcherID: AAF-9836-2020, Scopus Author ID: 15839153500**, *che-chko@mail.ru*

Contribution of the authors:

Ruslan B. Zakirov – problem statement, execution of the expedition work, processing and analysis of measurement data, preparation of images and article text

Boris V. Chubarenko – problem identification, planning of the expedition work and supplementary data collection, stylistic and substantial editing of the article text

Vladimir A. Chechko – coordination of the sedimentation issues

All the authors have read and approved the final manuscript.

DOI: 10.22449/2413-5577-2022-4-69-78

Marine Beach Litter Monitoring in the Russian Arctic

O. P. Netsvetaeva

Shirshov Institute of Oceanology, Russian Academy of Sciences, Moscow, Russia
Russian Arctic National Park, Arkhangelsk, Russia
e-mail: melob@bk.ru

Abstract

The remote and uninhabited islands of the Russian Arctic National Park, as many other coastal areas, are polluted with marine litter. It has become clear from surveys performed by various stakeholders in cooperation with the National Park. The purpose of this paper is to study marine litter pollution on the islands of the Russian Arctic National Park, and to demonstrate the Park's capabilities and intentions regarding this type of research. During the 2019–2021 field seasons, marine litter was collected and registered mainly by the Park's own staff on a network of representative beaches. These beaches are at Cape Zhelaniya (Severny Island of the Novaya Zemlya archipelago), Alexandra Land and Bell Island (Franz Josef Land). Over the years, the MSFD and OSPAR methods have been tested. The cleanup results for three years showed that the composition and amount of the collected marine litter items varies greatly from beach to beach. However, plastic items dominate significantly over other categories and make up over 80 %. Fishery is one of the most important sources of pollution of the studied beaches with marine litter.

Keywords: marine litter, plastic, Russian Arctic, Barents Sea, monitoring

Acknowledgements: the publication was prepared under science topic of Russian Arctic National Park no. 1-22-119-3. It based on the results of marine litter cleanups. The author is grateful for this data to Deputy Director for Research I. A. Mizin, state inspectors A. S. Morev, V. S. Zakharyin, O. V. Valkov, D. A. Barashnin (Russian Arctic National Park); A. A. Ershova, I. A. Krutikov (Russian State Hydrometeorological University), E. N. Basalai (The Polesie Agrarian Ecological Institute of the NAS of Belarus).

For citation: Netsvetaeva, O.P., 2022. Marine Beach Litter Monitoring in the Russian Arctic. *Ecological Safety of Coastal and Shelf Zones of Sea*, (4), pp. 69–78. doi:10.22449/2413-5577-2022-4-69-78

Мониторинг пляжного (берегового) мусора в Российской Арктике

О. П. Нецветаева

Институт океанологии им. П.П. Ширшова РАН, Москва, Россия
Национальный парк «Русская Арктика», Архангельск, Россия
e-mail: melob@bk.ru

Аннотация
Удаленные необитаемые острова национального парка «Русская Арктика», как и многие другие прибрежные территории, загрязнены морским мусором. Это стало ясно в результате ряда исследований, проведенных различными заинтересованными организациями в сотрудничестве с национальным парком. Цель настоящей работы заключается в исследовании загрязнения морским мусором островов национального парка «Русская Арктика», а также демонстрации возможностей и намерений парка относительно такого рода исследований. В полевые сезоны 2019–2021 гг. работы по сбору и учету морского мусора проводились в основном собственными силами парка на сети репрезентативных пляжей. Эти пляжи расположены на м. Желания (о. Северный архипелага Новая Земля), на о. Земля Александры и о. Белл (Земля Франца-Иосифа). В различные годы тестировались методики мониторинга морского мусора *MSFD* и *OSPAR*. Результаты уборок за три года показали, что видовой состав и количество собранных предметов морского мусора значительно различаются на исследованных пляжах. Однако пластиковый мусор превалирует над другими категориями, составляя в основном более 80 %. Одним из важнейших источников загрязнения рассмотренных пляжей морским мусором является рыболовство.

Ключевые слова: морской мусор, пластик, Русская Арктика, Баренцево море, мониторинг

Благодарности: публикация подготовлена в рамках научной темы национального парка «Русская Арктика» 1-22-119-3 и на основании результатов уборок морского мусора, в которых принимали участие заместитель директора по научной работе И. А. Мизин, госинспекторы А. С. Морев, В. С. Захарьин, О. В. Вальков, Д. А. Барашнин (национальный парк «Русская Арктика»); А. А. Ершова, И. А. Крутиков (Российский государственный гидрометеорологический университет), Е. Н. Басалай (Полесский аграрно-экологический институт НАН Беларуси).

Для цитирования: *Нецветаева О. П.* Мониторинг пляжного (берегового) мусора в Российской Арктике // Экологическая безопасность прибрежной и шельфовой зон моря. 2022. № 4. С. 69–78. EDN ZNNHDG. doi:10.22449/2413-5577-2022-4-69-78

Introduction

Marine litter is any persistent manufactured or recycled solid material that is dumped or left in the marine and coastal environment [1)]. Its distribution in the environment has now acquired colossal proportions: from coastal zones to remote areas of the oceans, from surface waters to the bottom layer and deep-water basins, and from the equator to the poles [1]. Thus, marine litter pollution is already considered a global problem affecting all the world's oceans, with a particular focus on plastics and microplastics [2)].

---

1) UNEP, 2005. *Marine Litter, an analytical overview*. Nairobi: UNEP, 58 p.

2) UNEP, 2009. *Marine Litter: A Global Challenge*. Nairobi: UNEP, 232 p.

In the Barents Sea and in the territories washed by it, as well as throughout the world, there is a negative trend towards an increase in marine litter pollution [2]. However, there are insufficient scientific data on the level of pollution, its characteristics, sources, damage caused, etc. The main reason for this state of affairs is inaccessibility of the region and high financial costs of expedition work. On the more accessible beaches of Europe, anyone can clean them up and count the marine litter. The results of each cleanup are recorded in a special smartphone application, and the data are accumulated in a single database [3)]. The studies of coastal pollution with marine litter in the Norwegian sector of the Arctic show that a significant proportion of litter (60–90 %) is plastic items [3, 4].

A pilot study of marine litter pollution of the beaches in the Russian Arctic National Park, conducted in 2017 as part of the scientific and practical expedition "Open Ocean: Archipelagos of the Arctic" together with the Marine Heritage: Explore and Preserve Association, showed that that the proportion of plastic litter on the islands of Franz Josef Land (FJL) was also high (84 %) [5]. In addition, on the islands of the Russian Arctic National Park, the collection and recording of marine litter was carried out as part of the Arctic Floating University [6] and MALINOR projects.

Tourists are actively encouraged to cleanup marine litter in the Russian Arctic National Park. This approach, when non-professionals under the guidance of specialists are engaged in the collection, classification and calculation of marine litter, can significantly increase the amount of data obtained in hard-to-reach regions where tourism activities are carried out. Besides, public participation in such events helps to raise public awareness of environmental issues and serious deficiencies in the waste management system that result in the pollution of even such remote and uninhabited northern territories. This awareness can be a key factor in promoting change in the behaviour of individual citizens. This may indirectly affect the improvement of waste management systems and the development of conscious consumption practices, which will reduce the amount of litter even before it enters the marine environment [7].

The results of studies in collaboration with other interested organizations showed that beach pollution with marine litter is relevant even for the hard-to-reach islands of the Russian Arctic. Therefore, in 2019, some work started on the collection and recording of marine litter using the National Park's own resources without the involvement of third-party organizations [8].

This article is based on the results of the works that the author reported on at a number of conferences [8–11].

Thus, the purpose of this work is to study marine litter pollution of the islands of the Russian Arctic National Park, as well as to demonstrate the capabilities and intentions of the park regarding this kind of research.

[3)] EEA. *Citizens Collect Plastic and Data to Protect Europe's Marine Environment*. 2018. [online] Available at: https://www.eea.europa.eu/themes/water/europes-seas-and-coasts/assessments/marine-litterwatch/briefing [Accessed: 03 December 2022].

Materials and Methods

To date, there is no single internationally approved methodology for the collection and recording of coastal marine litter. In each study, the authors choose a specific methodology based on the tasks and the territory under study, and also modify the existing ones. This state of affairs is, in the author's opinion, natural: the scientific community is in search of the best solutions in a new area of research.

During work in 2019, the park employees were guided by the MSFD methodology (Marine Strategy Framework Directive) [4]. The representatives of other organizations in the same year and earlier were guided by both this methodology and others. All currently existing methodologies of marine litter monitoring do not fundamentally differ from each other, nevertheless, some difficulties arose in interpreting the results and comparing them. Therefore, the question arose of choosing a unified marine litter monitoring methodology, which would be applied on the territory of the Russian Arctic. Such unification was important for systematic observations and possibility of comparing the results of studies conducted by different people at different time intervals.

In the 2020 field season, the marine litter monitoring was carried out according to the methodology adapted to the conditions of the park with a modified protocol (site survey sheet), taking into account the probability of detecting certain types of marine litter based on the results of previous observations. Two methodologies formed its basis:

1) OSPAR (Convention for the Protection of the Marine Environment of the North-East Atlantic, originally the Oslo (OS) and Paris (PAR) Conventions), widely used in monitoring marine litter on the coast of Norway, including the Svalbard archipelago – an area that is largely similar to the National Park's areas [5];

2) MSFD applied in the European seas and on their coasts.

The features of the adapted methodology are as follows:

– the methodology is presented in Russian, which significantly expands the circle of its Russian-speaking users who do not speak English;

– the methodology is described as concisely and clearly as possible, so that in the field one can quickly find the necessary information;

– the representative beaches are assigned identification numbers, where the letters indicate the archipelago where the beach is located, and the numbers indicate the ordinal number of the beach, for example, FJL001, NZ001. Systematic observations on the same beaches will make it possible to estimate the rate of accumulation of marine litter;

– when describing a trial site in the protocols, it is proposed to fill in the items that are important specifically for the territory of the park, for example, it is not necessary to indicate the distance to the nearest settlement, etc.;

---

[4] Hanke, G., Galgani, F., Werner, S., Oosterbaan, L., Nilsson, P., Fleet, D., Kinsey, S., Thompson, R. [et al.], 2013. Palatinus A;*Guidance on Monitoring of Marine Litter in European Seas*. Luxembourg: Publications Office of the European Union, 128 p.

[5] Wenneker, B., Oosterbaan, L. and ICGML, 2010. *Guideline for Monitoring Marine Litter on the Beaches in the OSPAR Maritime Area*. OSPAR Commission, 84 p.

– the protocol is reduced to five pages, the types of marine litter, which is extremely rare, are excluded. As a result, the amount of paper used will be reduced and record keeping in the field will be facilitated;

– each type of litter in the protocol corresponds to certain codes from the two methodologies (OSPAR and MSFD), which will facilitate comparison of the results of studies conducted according to these methodologies.

The essence of the methodology is as follows. It is necessary to select a representative beach, describe it and assign a unique identification number to it, and then lay a sampling site 100 m long and 5 m wide from the water's edge. Then, all marine litter larger than 2.5 cm should be collected, identified and recorded from the selected beach area. The total amount for each type of litter should be calculated in the protocol and the litter of the main categories should be weighed.

Altogether, seven representative beaches were examined (Table) with 13 sampling sites (Fig. 1) on two archipelagos of the Russian Arctic National Park in 2019–2021.

Results and discussion

2019. At three sampling sites laid in 2019 at Cape Zhelaniya (Severny Island of the Novaya Zemlya archipelago), the litter items classified as "plastic and other artificial polymers", which included "ropes, fragments of nets" and "plastic containers, packaging", account for a larger share of the litter collected at all three sites. However, the ratio of these two groups at the third site (NZ003), which is located

Register of representative beaches

Beach ID	Description of beach location	Date of cleanup
Severny Island (Novaya Zemlya)		
NZ001	The Barents Sea Coast west to Cape Zhelaniya	10.07.2019; 15.08.2020; 17.06.2021; 29.08.2021
NZ002	The Barents Sea Coast between Cape Zhelaniya and Cape Mavrikiya	12.08.2019; 15.08.2020; 29.08.2021
NZ003	Cape Zhelaniya, the Kara Sea coast, near the field base	13.09.2019; 17.06.2021
Alexandra Land (FJL)		
FJL001	At Cape Berdovskogo	24.07.2019
FJL002	At an unnamed cape between Cape Berdovskogo and Cape Zamanchivy	24.07.2019
FJL003	Severnaya Bay	30.07.2020
Bell Island (FJL)		
FJL005	South coast	23.06.2021

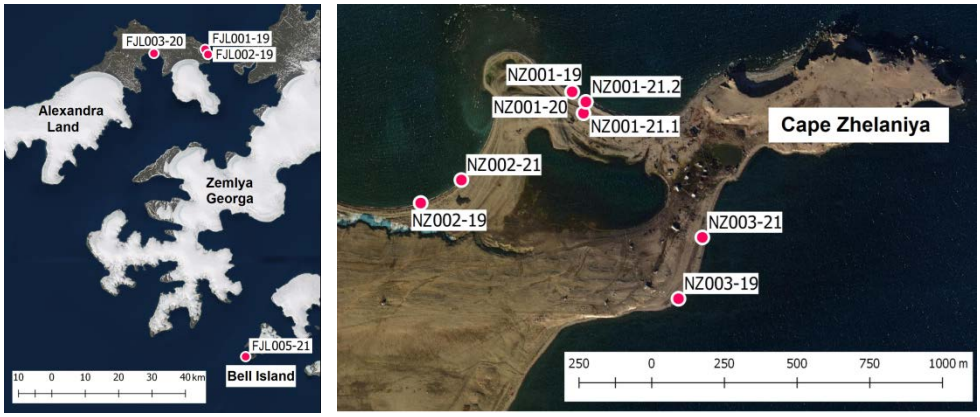

Fig. 1. Location of the sampling sites in 2019–2021

on the east coast, differs significantly (the share of nets is only 4 %) from their ratio at the sites of the western coast (NZ001 and NZ002), where the share of nets is 40 and 34 %, respectively. Considering that the source of this pollution is fishing, this distribution does not contradict previous studies and corresponds to the already outlined hypothesis [8] that marine litter on the western coast of Novaya Zemlya is associated with fishing in the Barents Sea. At the same time, almost no fishing is carried out in the Kara Sea, and the source of litter could be its unauthorized discharge from miscellaneous vessels or local pollution. Metal and glass objects were also found on the surveyed sites, but in much smaller quantities.

The items collected at two sites laid close to each other in the east of Alexandra Land are also mostly categorized as “plastics and other artificial polymers”. At the same time, in the more southern area (FJL002), all collected items (30.3 kg) are assigned to this category, and in the more northern area (FJL001), apart from plastic (4.7 kg), 40 % of metal litter (aluminum floats) with a total weight of 3 kg is found. In the “plastic and other artificial polymers” category, groups of items by name are distinguished. More than half of the plastic litter at both sites is nets; fish boxes have also been found in the more southerly site. The source of such marine litter is fishing, most likely in the Barents Sea. The other items (mounting foam, small plastic litter, cans) could have been thrown away on the spot or brought by ocean currents.

2020. A distinctive feature of the field work in 2020, in addition to some differences in the recording methodology, is weighing of all collected marine litter by category. In the previous year, it was possible to weigh items collected only on Alexandra Land (FJL).

Thus, at the first (NZ001) and the second (NZ002) sites located at Cape Zhelaniya, a total of 17.7 and 16.6 kg of marine litter was collected, respectively. At these two sites, in 2020, as in 2019, the products categorized

as “plastics and other artificial polymers” make up the majority of the collected litter, however, their share in 2020 is somewhat reduced due to the growth in the share of metal and the appearance of rubber waste. Weighing and recording were carried out only for large categories, so it is not possible to assess the scale of the impact of fishing by the number of collected nets and their remains.

On Alexandra Land, it was not possible to repeat the marine litter collection at the same sampling sites as in 2019 due to some logistical difficulties. Another sampling site was selected on the coast of Northern Bay (FJL003). The marine litter characteristics at this site are very different from the characteristics of litter collected in 2019 at the sites considered earlier, both at Cape Zhelaniya and at other sites on Alexandra Land. At FJL003, the majority, namely 64.5 %, are box boards and plastic products (canisters, packaging, pieces of plastic, a float) – 35.5 %, while neither nets nor fragments of nets were found. A total of 3.1 kg of marine litter was collected from this sampling site.

2021. The most detailed recording of marine litter was carried out in the field season of 2021 [9], which is due to the accumulated experience, analysis of previous studies and correction of shortcomings, as well as help from specialists experienced in this field, since some cleanups were carried out as part of a comprehensive Arctic Floating University – 2021 expedition.

A total of 1424 objects with a total weight of 125.8 kg were collected from five surveyed sampling sites. They included plastic, polystyrene – 1160 pcs. (23.1 kg); rubber – 30 pcs. (2.9 kg); clothes, textiles – 5 pcs. (3 kg); processed wood – 86 pcs. (10.1 kg); metal – 138 pcs. (85.7 kg); glass – 3 pcs. (0.5 kg); ceramics – 2 pcs. (0.5 kg). No hygienic and medical waste was found at any site.

The results of cleanups at different sites are very different from each other in terms of composition, quantity and weight of the collected items. Plastic objects prevail at all sites, while other litter categories are not found everywhere. Moreover, at all sites, except the one laid at Cape Zhelaniya from the direction of the Kara Sea, the proportion of plastic is from 83.7 to 100 %. On the mentioned site, the proportion of plastic and metal objects is 48 % each.

On Bell Island (FJL005-21), only 157 plastic items (11.1 kg), divided into 16 types, were found, but they were mainly pieces of plastic or polystyrene of 2.5–50 cm, rope (less than 1 cm in diameter) and lids.

At Cape Zhelaniya from the direction of the Kara Sea (NZ003-21), a total of 161 items (32 kg) was collected, of which 77 items accounted for plastic and metal, 5 – for rubber, and 2 – for ceramics. The plastic items are divided into 12 types, but basically, as in the previous case, these are pieces of plastic or polystyrene of 2.5–50 cm and lids, as well as strappings. The “metals” category includes various objects made of metal less than 50 cm in size.

In June, on the more northern beach at Cape Zhelaniya from the direction of the Barents Sea (NZ001-21.1), the largest number of marine litter was collected – 1085 pcs. (80.3 kg). This site also has the largest variety of litter

(six out of nine categories), namely plastic and polystyrene – 908 pcs., processed wood – 84 pcs., metal – 60 pcs., rubber – 25 pcs., clothes and textiles – 5 pcs., glass – 3 pcs. The maximum variety of collected items was found in the category "plastic and polystyrene" (19 subcategories). Mostly there were ropes (less than 1 cm in diameter), pieces of plastic or polystyrene of 2.5–50 cm and more than 50 cm, as well as lids and strappings.

Two months later, namely at the end of August, almost no marine litter was noted on the same beach (NZ001-21.2), except for eight items (0.6 kg). They were seven plastic items and a metal tube piece. Such a low amount of marine litter indicates that the main accumulation occurs in other periods: either in autumn or in early summer, since a year before, in June 2021, the marine litter was recorded on this beach, and then all collected items were removed.

On the beach, which is located to the south at Cape Zhelaniya from the direction of the Barents Sea (NZ002-21), the amount of the litter found is also small – 13 pcs. (1.9 kg). They are 11 plastic items and 2 processed wood items.

Fig. 2 represents a summary of the results of the marine litter recording for the three years considered.

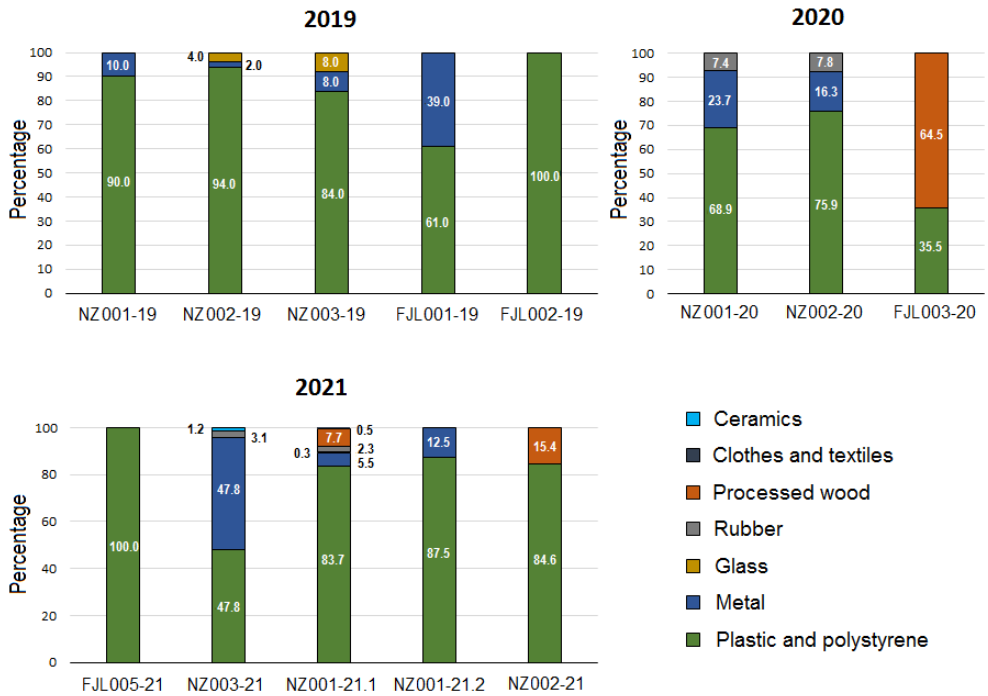

F i g . 2 . Marine litter distribution in 2019–2021

Conclusions

The activities carried out over three years to monitor the marine litter have shown that the Russian Arctic National Park is able to independently organize and regularly conduct such surveys, as well as assume the function of a coordinator of projects in this area.

However, a number of shortcomings have also been identified that need to be taken into account when planning field work in order to improve the monitoring system. For example, it is not enough to classify the collected items only into large categories (plastic, metal, glass, etc.), as was the case in the early years. Based on the data already available, it is clear that plastic objects make up the majority of all litter collected on the islands of the Russian Arctic National Park, and in the future it is important to introduce a more detailed classification into subcategories (nets, bags, ropes, etc.), which will help to identify sources of pollution. This classification was carried out in 2021.

Based on the results of the research, a unified methodology for monitoring marine litter on the islands of the Russian Arctic National Park was adopted and a network of reference beaches was selected, which is planned to be expanded annually.

The outlying islands of the Russian Arctic National Park are heavily polluted with marine litter, especially plastic (mostly over 80 %). The differences in litter composition between surveyed sites indicate differences in pollution sources. Fishing is one of the most important sources of pollution.

References

1. Galgani, F., Hanke, G. and Maes, T., 2015. Global Distribution, Composition and Abundance of Marine Litter. In: M. Bergmann, L. Gutow and M. Klages, eds., 2015. *Marine Anthropogenic Litter*. Cham: Springer, pp. 29–56. https://doi.org/10.1007/978-3-319-16510-3_2
2. Ivanova, L.V., Sokolov, K.M. and Kharitonova, G.N., 2018. Plastic Pollution Tendencies of the Barents Sea and Adjacent Waters under the Climate Change. *Arktika i Sever* [Arctic and North], (32), pp. 121–145. https://doi.org/10.17238/issn2221-2698.2018.32.121 (in Russian).
3. Bergmann, M., Lutz, B., Tekman, M.B. and Gutow, L., 2017. Citizen Scientists Reveal: Marine Litter Pollutes Arctic Beaches and Affects Wildlife. *Marine Pollution Bulletin*, 125(1–2), pp. 535–540. https://doi.org/10.1016/j.marpolbul.2017.09.055
4. Jaskólski, M.W., Pawłowski, L., Strzelecki, M.C., Zagórski, P. and Lane, T.P., 2018. Trash on Arctic Beach: Coastal Pollution along Calypsostranda, Bellsund, Svalbard. *Polish Polar Research*, 39(2), pp. 211–224. doi:10.24425/118746
5. Moseev, D.S. and Gavrilo, M.V., 2018. Anthropogenic Pressure on the Coasts of the Franz-Joseph Land Archipelago. In: E. Rumiantceva, G. Gogoberidze and M. Knyazeva, eds., 2018. *Arctic Shores: Shore-up to Sustainability*. Materials of the XXVII International Coastal Conference, Murmansk, September 24–29, 2018. Murmansk: MASU, pp. 253–256 (in Russian).
6. Vesman, A., Moulin, E., Egorova, A. and Zaikov, K., 2020. Marine Litter Pollution on the Northern Island of the Novaya Zemlya Archipelago. *Marine Pollution Bulletin*, 150, 110671. doi:10.1016/j.marpolbul.2019.110671

7. Taylor, A.R., Barðadóttir, Þ., Auffret, S., Bombosch, A., Cusick, A.L., Falk, E. and Lynnes, A., 2019. Arctic Expedition Cruise Tourism and Citizen Science: a Vision for the Future of Polar Tourism. *Journal of Tourism Futures*, 6(1), pp. 102–111. https://doi.org/10.1108/JTF-06-2019-0051

8. Korel'skiy, M.I. and Netsvetaeva, O.P., 2020. Analysis of the Marine Litter Distribution in a High-Altitude Arctic on the Coast of the Russian Arctic National Park Islands in 2019. In: FECIAR UrB RAS, 2020. [*Arctic Research: From Extensive Development to Integrated Development. Proceedings of the II International Scientific-Practical Conference (Arkhangelsk, November 11–14, 2020)*]. Arkhangelsk: Izdatelsky Tsentr A3+, pp. 371–375 (in Russian).

9. Netsvetaseva, O.P. and Mizin, I.A., 2021. Distribution of Marine Litter in the Russian Arctic National Park in Field Season of 2021. In: V. A. Lyubimov, exec. ed., 2021. *Collection of Works of the Arkhangelsk Centre of the Russian Geographical Society*. Arkhangelsk: KIRA. Iss. 9, pp. 207–213 (in Russian).

10. Netsvetaeva, O.P., Pogojeva, M.P. and Mizin, I.A., 2022. Marine Beach Litter Monitoring in the Russian Arctic. In: B. V. Chubarenko, ed., 2022. *Proceedings of the All-Russian Conference with International Participation "XXIX Coastal Conference: Field-Based and Theoretical Research in Shore Use Practice"*. Kaliningrad, April 18–24, 2022. Kaliningrad: Izdatelstvo IKBFU, pp. 475–477 (in Russian).

11. Ershova, A.A., Netsvetaeva, O.P., Mizin, I.A., Krutikov, I.A. and Basalay, E.N., 2022. Study of Marine Litter Accumulation of the Coasts of the Western Arctic Archipelagos. In: B. V. Chubarenko, ed., 2022. *Proceedings of the All-Russian Conference with International Participation "XXIX Coastal Conference: Field-Based and Theoretical Research in Shore Use Practice"*. Kaliningrad, April 18–24, 2022. Kaliningrad: Izdatelstvo IKBFU, pp. 460–463 (in Russian).

Submitted 31.05.2022; accepted after review 12.07.2022;
revised 02.11.2022; published 23.12.2022

About the author:

Olga P. Netsvetaeva, Junior Research Associate, North-West Branch, Shirshov Institute of Oceanology, Russian Academy of Sciences (36, Nahimovskiy Prosp., Moscow, Russia, 117997), Leading Research Associate, Russian Arctic National Park (36, Severnaya Dvina Emb., Arkhangelsk, Russia, 163051), Ph.D. (Geogr.), **ORCID ID: 0000-0002-5922-1399, ResearcherID: ABB-8322-2021, Scopus Author ID: 56606055100**, *melob@bk.ru*

The author has read and approved the final manuscript.

DOI: 10.22449/2413-5577-2022-4-79-89

Current System in Kruglaya Bay (Crimea) Based on Numerical Simulation and Observation Data

P. D. Lomakin*, Yu. N. Ryabtsev

Marine Hydrophysical Institute of RAS, Sevastopol, Russia
**e-mail: p_lomakin@mail.ru*

Abstract

On the basis of numerical modeling using the 3D barotropic linear Felsenbaum model, regularities of the structure of currents local system in Kruglaya Bay depending on the wind was revealed. It is established that, regardless of the wind flow direction, a number of general properties are inherent in the system of wind currents, and for each specific wind situation it has its own characteristics. It is shown that in the deep-water part of the investigated bay, the system of currents is two-layer, and in the shallow apex area, it is one-layer. Regardless of the wind situation, a topographic eddy cell is observed in the center of the bay in the area of extensive bottom uplift. The northern quarter winds cause a surge effect, developed circulation and ensure good water exchange with the open sea. The southern quarter winds are responsible for a weakly pronounced surge effect. Zonal winds generate weak zonal currents that impede water exchange between the bay and the sea. The simulation result is compared with the instrumental observations data of currents in Kruglaya Bay in northern quarter wind conditions. A good similarity is shown between the calculated system of currents and the flow scheme obtained from observational data.

Keywords: wind, currents, modeling, surge phenomena, Kruglaya Bay, Crimea

Acknowledgements: the research is performed under state task on topic no. 0555-2021-0005 “Complex interdisciplinary research of oceanologic processes, which determine functioning and evolution of the Black and Azov Sea coastal ecosystems”.

For citation: Lomakin, P.D. and Ryabtsev, Yu.N., 2022. Current System in Kruglaya Bay (Crimea) Based on Numerical Simulation and Observation Data. *Ecological Safety of Coastal and Shelf Zones of Sea*, (4), pp. 79–89. doi:10.22449/2413-5577-2022-4-79-89

Система течений в бухте Круглая (Крым) на основе численного моделирования и данных наблюдений

П. Д. Ломакин*, Ю. Н.Рябцев

Морской гидрофизический институт РАН, Севастополь, Россия
**e-mail: p_lomakin@mail.ru*

Аннотация
На основе численного моделирования с использованием трехмерной баротропной линейной модели Фельзенбаума выявлены закономерности структуры локальной системы течений в зависимости от ветра в бухте Круглой. Установлено, что, независимо от направления ветрового потока, системе ветровых течений в целом присущ ряд общих свойств, а для каждой конкретной ветровой ситуации она отличается собственными признаками. Показано, что в глубоководной части исследуемой бухты система течений двухслойная, а в мелководной кутовой области – однослойная. Независимо от ветровой ситуации в центре бухты, в районе обширного поднятия дна наблюдается топографическая вихревая ячейка. Ветры северной четверти вызывают нагонный эффект, развитую циркуляцию и обеспечивают хороший водообмен с открытой частью моря. Ветры южной четверти обусловливают слабо выраженный сгонный эффект. Зональные ветры генерируют слабые зональные течения, препятствующие водообмену между бухтой и морем. Результат моделирования сопоставлен с данными инструментальных наблюдений за течениями в бухте Круглой в условиях ветра северной четверти. Показано хорошее соответствие расчетной системы течений и схемы течений, полученной по данным наблюдений.

Ключевые слова: ветер, течения, моделирование, сгонно-нагонные явления, бухта Круглая, Крым

Благодарности: работа выполнена в рамках государственного задания по теме № 0555-2021-0005 «Комплексные междисциплинарные исследования океанологических процессов, определяющих функционирование и эволюцию экосистем прибрежных зон Черного и Азовского морей».

Для цитирования: *Ломакин П. Д., Рябцев Ю. Н*. Система течений в бухте Круглая (Крым) на основе численного моделирования и данных наблюдений // Экологическая безопасность прибрежной и шельфовой зон моря. 2022. № 4. С. 79–89. EDN ULTQHH. doi:10.22449/2413-5577-2022-4-79-89

Introduction

Kruglaya Bay (also known as Omega Bay) is situated on the southwestern coast of the Crimean Peninsula, in the southern part of the Sevastopol seashore, between Abramov Bay and Streletskaya Bay. The bay is meridionally oriented and freely communicates with the sea. The length of its axial line is about a mile, the width of the mouth area of the bay is ~ 0.3 miles, and the sea depth at the inlet is 13–17 m. The apex of the bay, with a horizontal scale of 150–200 m and a depth of 0.5–1.2 m, is bounded from the central area by two capes (Fig. 1).

One of the morphometric features of the studied bay, which determines the dynamics of water and suspended matter, as well as the structure of the fields of oceanological quantities, is a vast stony and partially covered with sand bottom uplift located in the central area, which is clearly distinguishable on satellite images in the visible range (Fig. 1, *b*). In stormy conditions and in the event of a large swell, its top emerges on the sea surface [1].

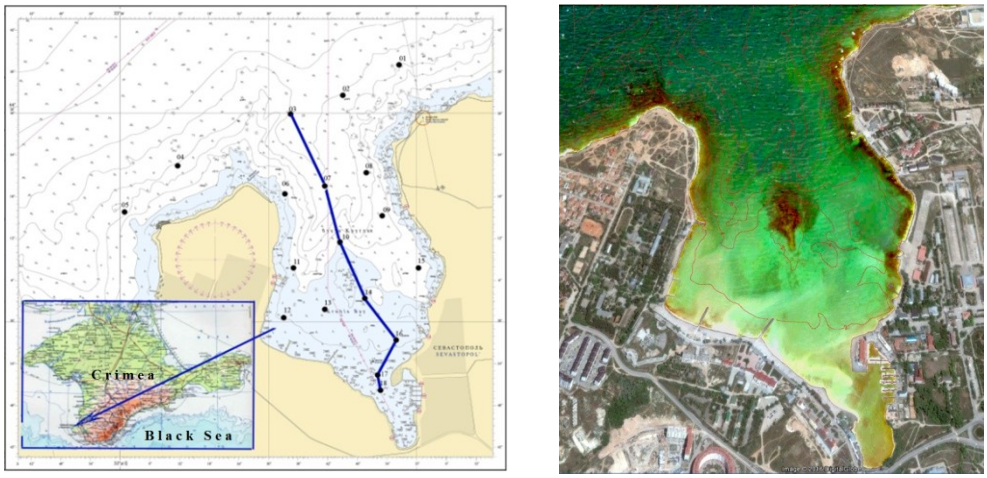

a ***b***

F i g . 1 . Geographic position of Kruglaya Bay with the oceanologic survey station map (*a*); satellite image of the bay (*b*)

Kruglyaya is one of the few bays of the Sevastopol seaside where city beaches are located. It is of interest from a recreational point of view, especially in modern conditions of increasing anthropogenic load, therefore, information about the hydrological regime of the bay, in particular about the regularities of the current system, seems to be very relevant.

Comprehensive oceanological studies are currently being carried out in this bay and adjacent seaside areas. For example, during the past three years, a number of surveys and a series of shore-based observations of the main hydrophysical and hydrochemical parameters of the environment have been carried out here. On the basis of the analysis of the data obtained, an understanding of currents, structure and temporal variability of the fields of the main oceanological quantities, sources of pollution, volumes of waste water, chemical composition of pollutants has been formed [1–5]. In [6], numerical modelling of the spreading process of suspended matter from a real-life source was carried out. In this article, the existing knowledge is expanded and supplemented by the result of numerical simulation of the local system of currents.

The aim of the work is to reveal regularities of the local current system depending on wind conditions in Kruglaya Bay on the basis of numerical simulation and to compare the obtained result with the data of instrumental observations of currents.

Initial data and research methods

The three-dimensional barotropic linear Felsenbaum model [7, 8], generalized for the case of taking into account Rayleigh friction, was used to calculate currents. It should be noted that numerical modelling of hydrological processes in similar basins is traditionally used to understand the regularities identified on the basis of field observations [9, 10].

In such models, the solution to the three-dimensional problem of flows is reduced to the solution to the two-dimensional problem for an integral current function. The current velocity components are calculated using analytical formulas that allow calculations to be made on a relatively fine grid and describe the characteristics of coastal currents and currents in bays. The details of the algorithm and the parameters used are described in the paper [8].

The numerical experiments were carried out for eight main winds of 8 m/s for 2 days. The currents were calculated layer by layer, from the upper to the bottom layer, under real bottom topography conditions.

The simulation result was compared with flow vector schemes obtained from two oceanological surveys conducted in August and November 2019 [1, 2].

Discussion of the results

The result of numerical simulation of the current system in the upper and bottom layers of the bay is demonstrated for meridional (Fig. 2, 3) and zonal (Fig. 4) winds.

The analysis of vector fields (Figs. 2–4) showed that regardless of the wind situation, the system of wind currents as a whole in Kruglaya Bay is characterized by a number of common features. At the same time, meridional and zonal winds determine their own features of the kinematic structure of waters.

Two qualitatively different kinematic structures of waters are observed in the bay under any wind direction. A two-layer structure – in the deep (central and open) area and a one-layer structure – in the shallow apex area. In the deep water, in the upper water layer the current vectors are oriented downwind, while in the bottom layer the current vectors are in the opposite direction. In the shallow apex area, both on the sea surface and near the bottom the current vectors are oriented downwind.

In each calculated wind situation in the area of the bottom uplift, an eddy cell with a predominantly anticyclonic component is observed in the field of current vectors in the entire water column. This topographic quasi-stationary eddy formation is formed as a result of the interaction of currents with the bottom uplift and prevents meridional exchange between the bay and the open water area of the Sevastopol seaside (Fig. 2–4).

It is shown below that winds of all directions (except the east) generate surge phenomena in the bay under consideration, the nature of which is determined by the direction of the wind flow, and the intensity is determined by the wind acceleration.

The northern and southern quarter winds cause, respectively, the upsurge and downsurge effects over the entire bay area. Zonal winds cause upsurge along the windward shore of the bay and downsurge – along the opposite leeward shore.

The northern quarter winds (northern, northwestern, northeastern) are characterized by maximum acceleration and cause an upsurge effect in Kruglaya Bay. Due to the acceleration of these winds, the current system in the bay is the most developed. The calculated current velocity is the highest, 10–17 cm/s at the surface and 5–12 cm/s near the bottom, compared to the situations caused by other winds. Northern winds provide ventilation for the entire bay and the best water exchange with the open part of the sea (Fig. 2).

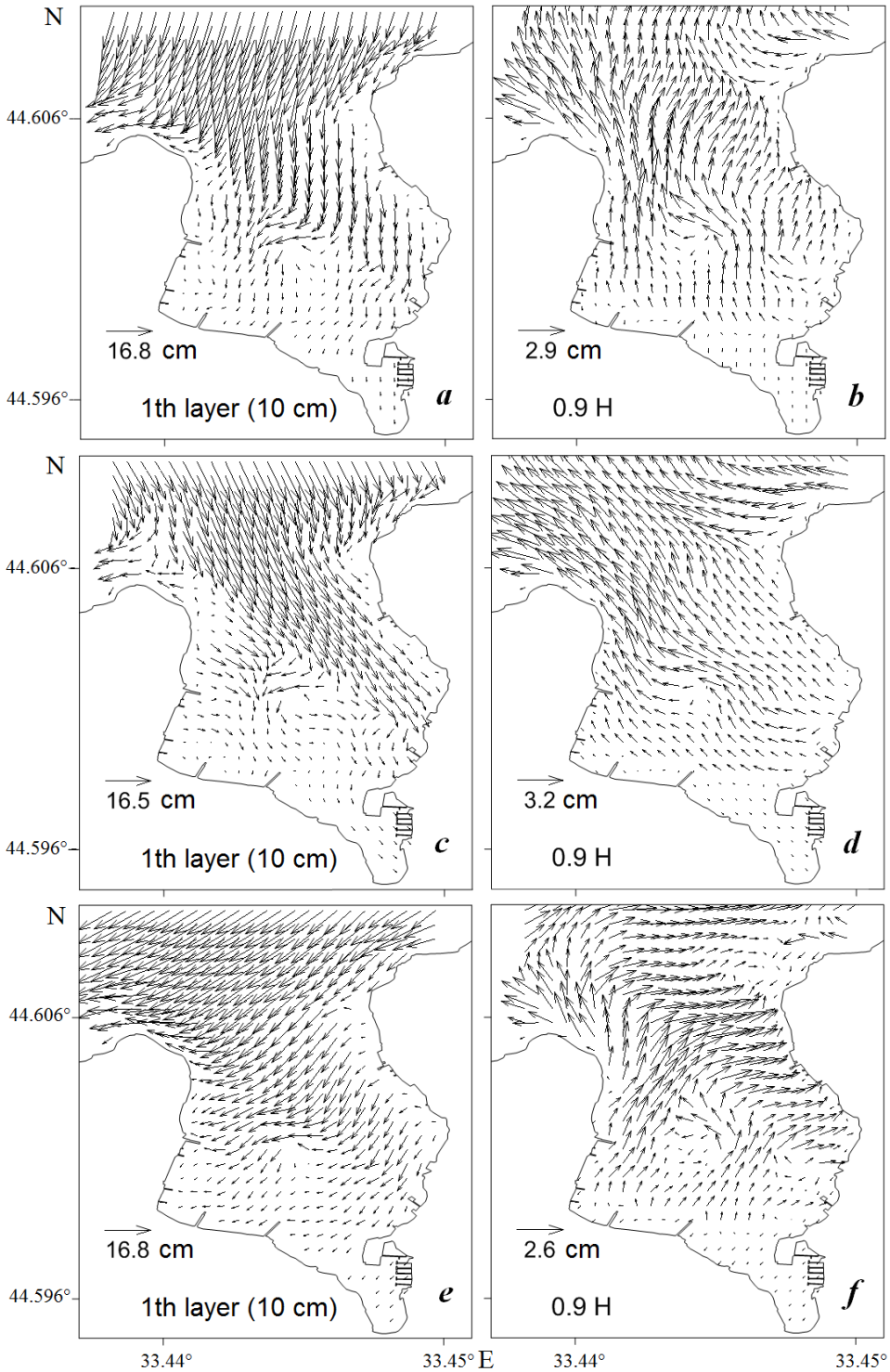

F i g . 2 . Vector field of currents generated in Kruglaya Bay by northern quarter winds in the upper (left) and bottom (right) layers: *a*, *b* – situation under north wind; *c*, *d* – under north-west wind; *e*, *f* – under north-east wind

The winds in the southern quarter (southern, southwestern, southeastern) cause a downsurge effect. However, due to limited wind acceleration, this effect is usually weakly expressed. According to episodic observations in the beach zone, the downsurge south winds in the studied bay do not cause more or less significant fluctuations in water temperature, their range is within 1°C.The calculated current velocity in the bay under south quarter winds is 7–15 cm/s in the upper layer and 3–7 cm/s near the bottom (Fig. 3).

The zonal (west and east) winds are characterized by minimal acceleration. The west wind causes a downsurge near the western shore of the bay and an upsurge near the eastern shore. The east wind causes a downsurge near the eastern shore and an upsurge near the western one. With zonal winds the calculated current velocity is minimal: 5–12 cm/s on the surface and 2–3 cm/s near the bottom; the zonal currents prevail and, consequently, the limited water exchange between the bay and the sea (Fig. 4).

Let us note an interesting, typical for Sevastopol, local atmospheric synoptic situation. When east winds blow over the Crimea near Sevastopol, an orographic effect leads to calm and windless weather, with east wind speeds not exceeding 3 m/s, as a rule. This phenomenon, well known to local meteorologists, has received the name of the *eastern position*.Therefore, in the city and in the area of the studied bay, there is never a moderate and strong east wind. The real weak wind flow observed at the eastern position is hardly capable of generating a more or less stable system of currents, and the calculation variant in Fig. 4, *c*, *d* – a purely theoretical situation that does not exist in nature.

All available empirical data confirm the known position [11] about predominantly wind driven nature of the currents in Sevastopol bays.

Fig. 5 shows diagrams of current vectors plotted from the results of two expeditions to Kruglaya Bay, which were carried out in August and November 2019. The first survey was carried out under weak northeast wind conditions, the second – under weak northwest wind conditions.

Before proceeding to the analysis of the local current system in the bay under study based on actual observations, the following should be taken into account. The current generated by a weak wind is unstable. Its characteristics change in accordance with variations in wind flow parameters, which were necessarily present during each survey (~10 hours).

Therefore, the time-differentiated vectors may refer to different fragments of the kinematic structure changed during the surveys, and not correspond to the real water circulation.

Judging by the current vectors directed along the normal to the shore at the stations that were located directly near the shoreline, the currents in the studied bay have a rather pronounced seiche component. A significant random component is also probable. In other words, vector diagrams obtained from the data of instrumental observations of currents (Fig. 5) do not constitute a complete picture but only give an approximate idea of real water circulation in Kruglaya Bay under conditions of a weak northern quarter wind. Only the information on current velocity appears to be reliable.

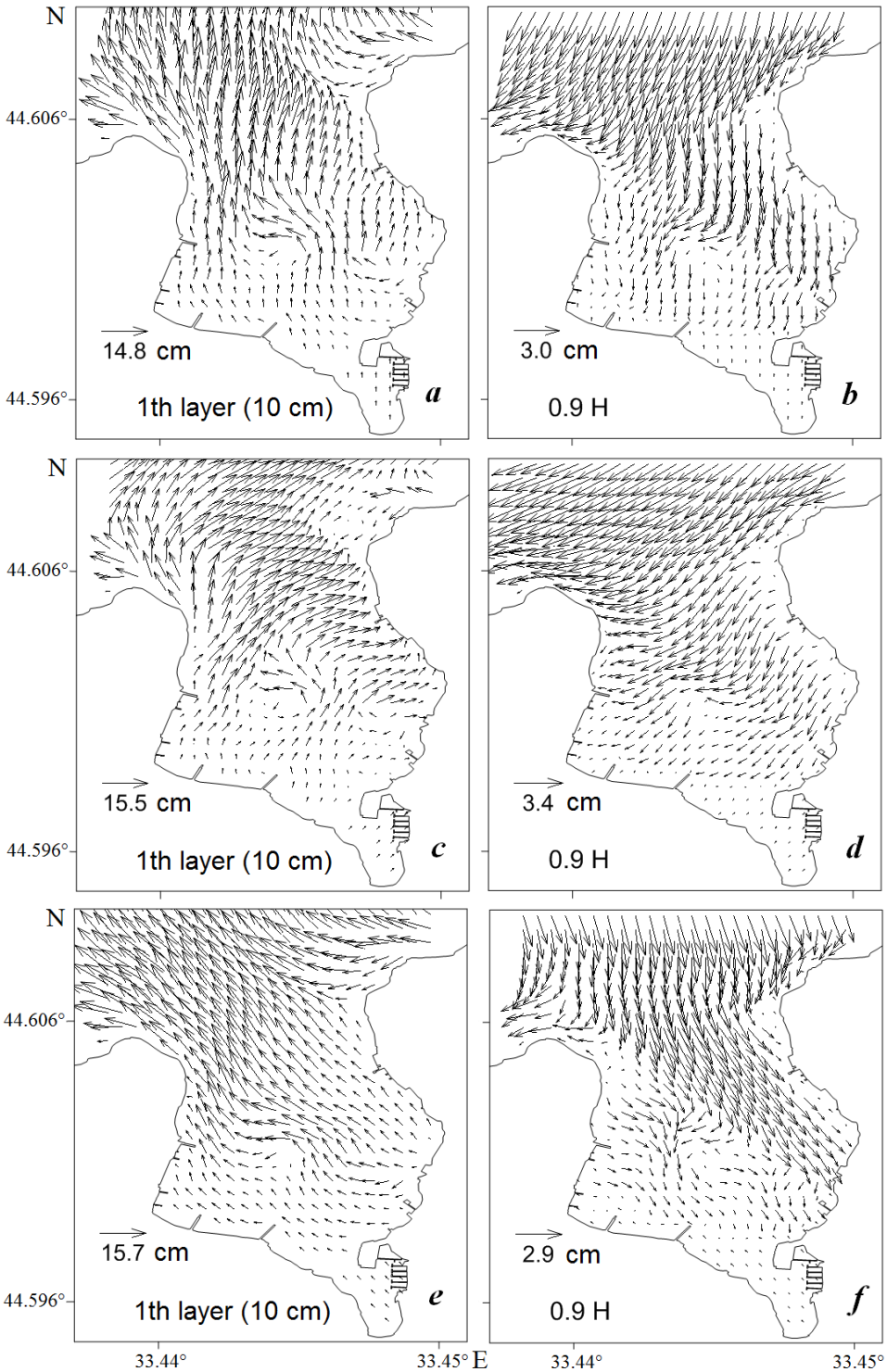

Fig. 3. Vector field of currents generated in Kruglaya Bay by southern quarter winds in the upper (left) and bottom (right) layers: *a*, *b* – situation under south wind; *c*, *d* – under south-west wind; *e*, *f* – under south-east wind

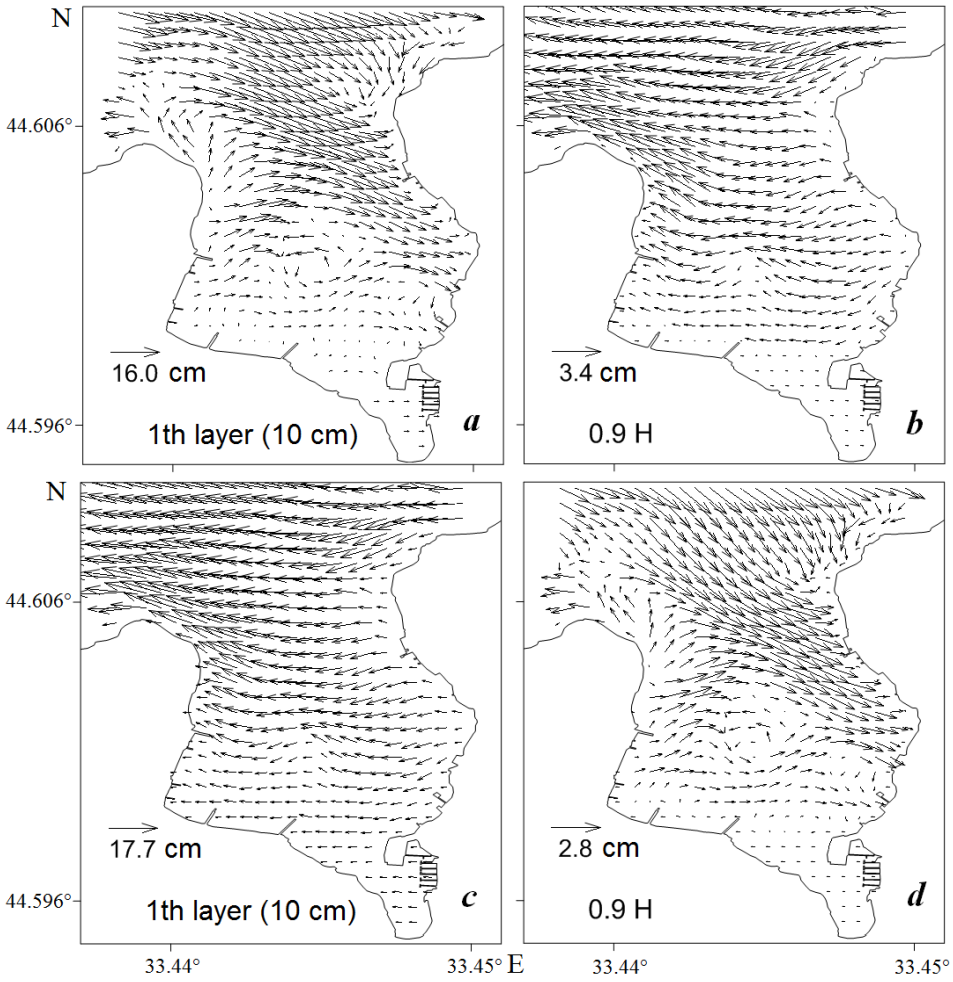

Fig. 4. Vector field of currents generated in Kruglaya Bay by zonal winds in the upper (left) and bottom (right) layers: *a*, *b* – situation under west wind; *c*, *d* – under east wind

The articles [1, 2] carried out a detailed study of instrumental observations of currents in Kruglaya Bay using an indirect method based on an analysis of the structure of the fields of oceanological quantities. The structure of the thermohaline field and the fields of concentration of total suspended matter and dissolved organic matter were analyzed together with the vector schemes.

As a result, the properties of the local current system generated by the northern quarter wind in Kruglaya Bay were confirmed. These properties were identified by numerical modelling and are shown in Fig. 2.

In particular, they are two-layer kinematic structure in the deep part of the bay; intensive upsurge effect; well-developed meridional circulation in the deep part with current velocity of 15–40 cm/s in the upper layer and 10–15 cm/s near the bottom and about 5 cm/s in the apex area. During both surveys in the area of bottom

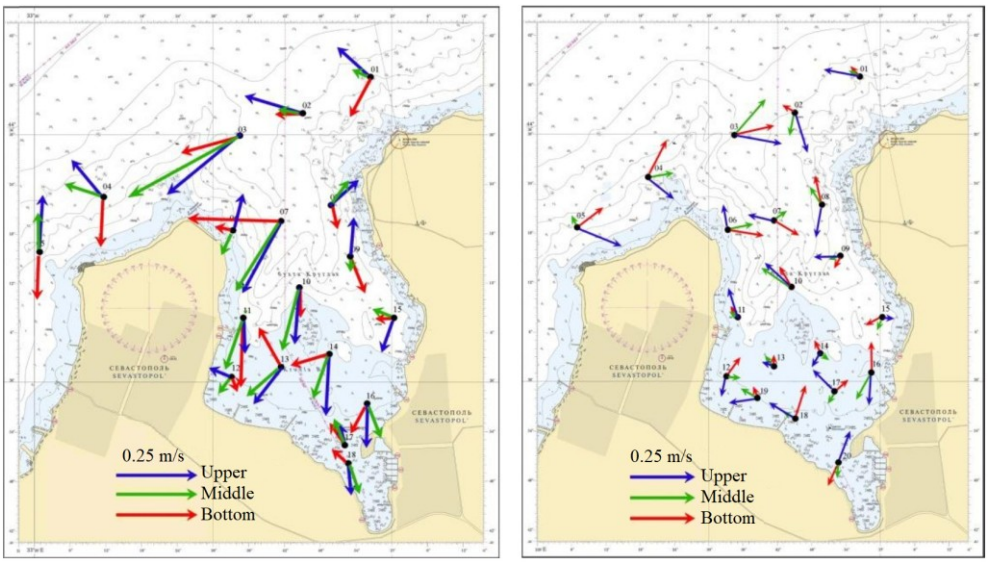

a ***b***

F i g . 5 . Current vectors in Kruglaya Bay: on 28 August (*a*) and 14 November (*b*) 2019

uplift in the field of vectors of currents and in the structure of actual fields of oceanological values, distinct eddy formation was recorded (Fig. 5), which presence was shown by all variants of model experiment (Fig. 2–4).

On the whole, the longshore anticyclonic circulation of water and suspended matter prevails in the studied bay. This is confirmed by the depth distribution along the three piers located on the western shore of the bay, as well as the specific shore properties at the base of these structures. The piers intercept the north-oriented alongshore flow of suspended matter, washing the western shore of the bay. The water depth along the southern side of the piers is significantly shallower than along the northern side. At the base of the piers the shore is scoured from the south while to the north there is a pronounced zone of downstream erosion.

Conclusion

Numerical modeling method has been used to reveal regularities in the structure of the local current system in Kruglaya Bay determined by the eight main types of wind.

It is established that regardless of the wind flow direction, the system of wind currents in the studied bay has the following properties: a two-layer structure in the deep-water region and a one-layer structure in the shallow apex area. In the upper water layer of the deep water, the current vectors are oriented downwind, in the bottom layer – the current vectors are oriented against the wind. In the shallow apex area on the sea surface and near the bottom, the current vectors are oriented downwind. In the central part of the bay, in the area of bottom uplift, a quasi-stationary topographic eddy formation is observed.

The northern, southern and zonal winds form fields of current vectors with specific features. The northern quarter winds cause an upsurge effect in Kruglaya Bay. Due to maximum acceleration under these winds, the current system in the bay is most developed and ensures good water exchange with the open sea area. The southern quarter winds determine the downsurge effect, which is weakly pronounced due to limited acceleration. The zonal winds have minimal acceleration and generate weak zonal currents that impede water exchange between the bay and the sea.

The result of simulations of the current system in the bay generated by the northern quarter winds is confirmed by data from expedition surveys. In particular, such properties as two-layer kinematic structure in the deep-water area of the bay and one-layer structure in the apex area, developed meridional circulation, intensive upsurge effect, formation of an eddy cell in the area of bottom uplift were confirmed.

An anticyclonic longshore circulation of water and suspended matter prevails in the studied bay.

REFERENCES

1. Lomakin, P.D. and Chepyzhenko, A.I., 2019. Currents and Fields of the Total Suspended Matter and Dissolved Organic Matter Content in the Waters of the Sevastopol Seaside in August 2019. *Monitoring Systems of Environment*, (4), pp. 60–65. doi:10.33075/2220-5861-2019-4-60-65 (in Russian).
2. Lomakin, P.D. and Chepyzhenko, A.I., 2020. Research and Control of Water Circulation and Structures of the Thermohaline Field in Omega Bay (Crimea) in the Summer-Autumn Period 2019. *Monitoring Systems of Environment*, (3), pp. 15–22. doi:10.33075/2220-5861-2020-3-15-22 (in Russian).
3. Gruzinov, V.M., Dyakov, N.N., Mezenceva, I.V., Malchenko, Yu.A., Zhohova, N.V. and Korshenko, A.N., 2019. Sources of Coastal Waters Pollution near Sevastopol. *Oceanology*, 59(4), pp. 523–532. doi:10.1134/S0001437019040076
4. Latushkin, A.A., Chepyzhenko, A.I., Prazukin, A.V., Chepyzhenko, A.A. and Firsov, Yu.K., 2021. Hydrophysical Research in the Kruglaya Bay (Sevastopol). *Ecological Safety of Coastal and Shelf Zones of Sea*, (3), pp. 107–122. doi:10.22449/2413-5577-2021-3-107-122 (in Russian).
5. Lomakin, P.D., Popov, M.A. and Chepyzhenko, A.A., 2021. Assessment of Sea Water State Using Colored Dissolved Organic Matter Concentration in the Omega Bay (Crimea) in Summer of 2020. *Russian Meteorology and Hydrology*, 46(11), pp. 786–791. doi:10.3103/S106837392111008X
6. Lomakin, P.D., Ryabtsev, Yu.N. and Chepyzhenko, A.I., 2021. Research of Sources and Distribution of Suspended Matter in Omega Bay (Crimea) Based on Expeditional Data and Numerical Simulation. *Monitoring Systems of Environment*, (3), pp. 59–67. doi:10.33075/2220-5861-2021-3-59-67 (in Russian).
7. Shapiro, N.B., 2006. Modeling of the Currents on the Seaside nearby Sevastopol City. In: MHI, 2006. *Ekologicheskaya Bezopasnost' Pribrezhnoy i Shel'fovoy Zon i Kompleksnoe Ispol'zovanie Resursov Shel'fa* [Ecological Safety of Coastal and Shelf Zones and Comprehensive Use of Shelf Resources]. Sevastopol: ECOSI-Gidrofizika. Iss. 14, pp. 119–134 (in Russian).
8. Shapiro, N.B. and Yushchenko, S.A., 2000. Simulation of Wind Currents in Sevastopol Bays. *Physical Oceanography*, 11(1), pp. 47–64. doi:10.1007/BF02524495
9. Fomin, V.V. and Repetin, L.N., 2005. Numerical Simulation of Wind Currents and Propagation of Impurities in the Balaklava Bay. *Physical Oceanography*, 15(4), pp. 232–246. doi:10.1007/s11110-005-0045-y

10. Belokopytov, V.N., Kubryakov, A.I. and Pryakhina, S.F., 2019. Modelling of Water Pollution Propagation in the Sevastopol Bay. *Physical Oceanography*, 26(1), pp. 3–12. doi:10.22449/1573-160X-2019-1-3-12

11. Mikhailova, E.N., Shapiro, N.B. and Yushchenko, S.A., 2001. Modelling of the Propagation of Passive Impurities in Sevastopol Bays. *Physical Oceanography*, 11(3), pp. 233–247. doi:10.1007/BF02508870

Submitted 22.06.2022; approved after review 16.08.2022;
revised 02.11.2022; published 23.12.2022

About the authors:

Pavel D. Lomakin, Leading Research Associate, Marine Hydrophysical Institute of RAS(2 Kapitanskaya St., Sevastopol, 299011, Russian Federation), Dr.Sci. (Geogr.), professor, **ResearcherID: V-7761-2017, Scopus Author ID: 6701439810, IstinaResearcherID: 18321047**, *p_lomakin@mail.ru*

Yuri N. Ryabtsev, Research Associate, Marine Hydrophysical Institute of RAS (2 Kapitanskaya St., Sevastopol, 299011, Russian Federation), **ORCID ID: 0000-0002-9682-9969, SPIN-code: 7853-4597**, *ruab@mail.ru*

Contribution of the authors:

Pavel D. Lomakin – general statement of the problem, selection and interpretation of expeditionary data, interpretation of the overall result, writing the article

Yuri N. Ryabtsev– performance of numerical experiments, interpretation of simulation results, interpretation of the overall result

All the authors have read and approved the final manuscript.

DOI: 10.22449/2413-5577-2022-4-90-103

Restoration of the Biocoenosis of the Black Sea Scallop *Flexopecten glaber* (Bivalvia: Pectinidae) off the Coast of Crimea (Laspi Area)

N. K. Revkov*, N. A. Boltachova

A.O. Kovalevsky Institute of Biology of the Southern Seas of RAS, Sevastopol, Russia
**e-mail: nrevkov@yandex.ru*

Abstract

The paper presents a description of the quantitative representation, taxonomic structure and formation features of the Black Sea scallop *Flexopecten galaber* biocoenosis in the south-western section of the Crimean shelf (Laspi area), after its depopulation off the coast of Crimea, which coincided with the period of ecological crisis of the Black Sea ecosystem during the second half of the 20th century. The material was benthic samples collected by SCUBA divers using a manual grab sampler in October 2020. A total of 64 macrozoobenthos species were identified in the scallop biocoenosis formed in the biotope of slightly silted sand with shell debris at a depth of 13–34 m. The total list of species was represented by Crustacea (12 species), Mollusca (21), Polychaeta (26), Miscellaneous group (5) and by not identified to species level of Acari, Gromia, Nematoda, Nemertea, Turbellaria. The mean abundance and biomass (after removing the mantle cavity fluid of bivalves) values of macrozoobenthos reached 11,231±2,424 ind./m^2 and 247.7±156.3 g/m^2, respectively. It is assumed that the forerunner to the *Flexopecten* biocoenosis in the area of its detection was the *Gouldia* biocoenosis. The zoobenthos biomass (with mantle cavity fluid of bivalves) in the *Flexopecten* biocoenosis (351 g/m^2) was similar to that values in the *Chamelea* biocoenosis at comparable depths off the coast of Crimea in the 1930s (388 g/m^2), 1957 (354 g/m^2), and 1981–2004 (475 g/m^2); *Chamelea* biocoenosis is classified as one of the most abundant coastal belt biocoenosis of the Black Sea basin. The recovery of *F. glaber* beds observed off the coast of Crimea and its transformation into a coenoses-forming species are in line with the modern recovery processes in the benthos of various areas of the Black Sea shelf, after the crisis period of 1980–1990s, which are associated with de-eutrophication and the improvement of the ecological status of its water areas.

Keywords: *Flexopecten galaber*, macrozoobenthos, Black Sea, biocoenosis

Acknowledgments: the work was carried out under state assignment of the Federal Research Center of the IBSS on the topic “Regularities of formation and anthropogenic transformation of biodiversity and bioresources of the Azov-Black Sea basin and other regions of the World Ocean” (registration no. 121030100028-0). The authors are very grateful to O.Yu. Vyalova for collecting the material, L.V. Bondarenko for taxonomic identification of crustaceans, L.V. Lukyanova for assistance in laboratory processing.

For citation: Revkov, N.K. and Boltacheva, N.A., 2022. Restoration of the Biocoenosis of the Black Sea Scallop Flexopecten glaber (Bivalvia: Pectinidae) off the Coast of Crimea (Laspi Area). *Ecological Safety of Coastal and Shelf Zones of Sea*, (4), pp. 90–103. doi:10.22449/2413-5577-2022-4-90-103

Восстановление биоценоза черноморского гребешка *Flexopecten glaber* (Bivalvia: Pectinidae) у берегов Крыма (район Ласпи)

Н. К. Ревков*, Н. А. Болтачева

ФГБУН ФИЦ «Институт биологии южных морей им. А. О. Ковалевского РАН», Севастополь, Россия

**e-mail: nrevkov@yandex.ru*

Аннотация

Представлено описание количественного развития, таксономической структуры и особенностей формирования биоценоза черноморского гребешка на юго-западном участке крымского шельфа (район Ласпи) после его депопуляции у берегов Крыма, совпавшей с периодом экологического кризиса черноморской экосистемы второй половины XX в. Материалом послужили бентосные пробы, собранные в октябре 2020 г. ручным водолазным дночерпателем на четырех станциях полигона. В биоценозе гребешка, сформировавшемся в биотопе слабо заиленного песка с ракушей на глубине 13–34 м, отмечены 64 представителя макрозообентоса. Из них Crustacea – 12, Mollusca – 21, Polychaeta – 26, сборная группа Miscellaneous – 5 видов и не идентифицированные до вида представители Acari, Gromia, Nematoda, Nemertea, Turbellaria. Средняя численность и биомасса макрозообентоса (без учета мантийной жидкости двустворчатых моллюсков) составили 11 231 ± 2424 экз./м^2 и 247.7 ± 156.3 г/м^2 соответственно. Предполагается, что предшественником биоценоза *Flexopecten* в районе его обнаружения был биоценоз *Gouldia*. При аналогичных методиках взвешивания (с учетом мантийной жидкости двустворчатых моллюсков) биомасса зообентоса в биоценозе *Flexopecten* (351 г/м^2) оказалась сходной с аналогичными параметрами развития бентоса на сопоставимых глубинах у берегов Крыма в 1930-х гг. (388 г/м^2), 1957 г. (354 г/м^2) и 1981–2004 гг. (475 г/м^2) в биоценозе *Chamelea*, относимом к наиболее развитым прибрежным поясным биоценозам Черноморского бассейна. Наблюдаемое восстановление поселений *F. glaber* и его превращение у берегов Крыма в ценозообразующий вид согласуется с современными восстановительными процессами в бентосе различных участков черноморского шельфа в посткризисный (после 1980–1990-х гг.) период деэвтрофикации бассейна Черного моря и улучшения экологического состояния его акваторий.

Ключевые слова: биоценоз, *Flexopecten glaber*, макрозообентос, Черное море

Благодарности: работа выполнена в рамках государственного задания ФИЦ ИнБЮМ по теме «Закономерности формирования и антропогенная трансформация биоразнообразия и биоресурсов Азово-Черноморского бассейна и других районов Мирового океана» (№ гос. регистрации 121030100028-0). Авторы выражают большую признательность О. Ю. Вяловой за сбор материала, Л. В. Бондаренко – за определение группы ракообразных, Л. В. Лукьяновой – за помощь в лабораторной обработке материала.

Для цитирования: *Ревков Н. К., Болтачева Н. А.* Восстановление биоценоза черноморского гребешка *Flexopecten glaber* (Bivalvia: Pectinidae) у берегов Крыма (район Ласпи) // Экологическая безопасность прибрежной и шельфовой зон моря. 2022. № 4. С. 90–103. EDN WQVQWD. doi:10.22449/2413-5577-2022-4-90-103

Introduction

The Black Sea scallop *Flexopecten glaber* (Linnaeus, 1758) is the only representative of the family Pectinidae (class Bivalvia) in the Black Sea [1)]. It forms aggregations from the water's edge to depths of 40 m in biotopes of dense shell, silty-sandy sediments with an admixture of shell debris and coarse sandy-pebble sediments [1]. At the beginning of the 20th century, *F. glaber* was abundant in all oyster beds and deeper layers of coastal sand near Sevastopol [2]. In the area of the Kerch Strait, the scallop together with *Ostrea edulis* Linnaeus, 1758 formed its own biocoenosis as a leading benthic form, and near the open coasts of Crimea, it was included in different biocoenoses as a characteristic or secondary species [1]. However, already in the 1950s and 1960s, the Black Sea population of *F. glaber* tended to decrease. On the soft bottom sediments (not including oyster beds), the Black Sea scallop was a member of only two biocoenoses – *Gouldia* (15–32 m depth, biotope of shells with sand and a slight admixture of silt, western coast of Crimea) [3] and *Parvicardium – Gouldia – Pholoe inornata* (10–25 m depth, gravel-sandy sediments, Southern coast of Crimea) [4]. Subsequent events in the 1970s (the beginning of eutrophication in the Black Sea basin, the death of oyster beds) followed by a peak of ecological crisis in the Black Sea ecosystem in the late 1980s and early 1990s determined the actual depopulation of *F. glaber*, so this species was included in the Red Book of the Republic of Crimea and the Red Data Book of Sevastopol as species declining in abundance [2), 3)].

An improvement in the ecological state of the Black Sea basin in the early 2000s resulted in the recovery of populations of some benthic species whose abundance and habitat had previously decreased [5, 6]. Since 2010, information has started to appear about the discovery of *F. glaber* aggregations in various parts of the Crimean coast (Donuzlav Bay, Kazachya and Laspi bays) [7, 8] and the mass settlement of their larvae on collectors of mussel and oyster farms [9, 10], which led to practical recommendations for the development of aquaculture of this species off the coast of Crimea [10].

The return of the scallop into the benthos of the region was expected, but required monitoring in terms of possible changes in the structural indicators of benthos development. The work aims at describing the biocoenosis of the Black Sea scallop formed in the water area of one of the sites in Southwestern Crimea (Laspi area).

Material and methods

The work was conducted in October 2020 near the coast of Southwestern Crimea (Laspi area, Mechty Bay). Benthic samples were taken by SCUBA divers using a manual grab sampler (S = 0.04 m^2) at four points of the study area: Station *1* (19 m

---

[1)] Scarlato, O.A. and Starobogatov, Ya.I., 1972. [Bivalvia Class]. In: F. D. Mordukhay-Boltovskoy, ed., 1972. [*Fauna Field Guide for the Black Sea and Sea of Azov*]. Vol. 3. Kiev: Naukova Dumka, pp. 178–249 (in Russian).

[2)] Revkov, N.K., 2015. [The Black Sea Scallop Flexopecten glaber ponticus Bucquoy, Dautzenberg et Dollfus, 1889]. In: S. P. Ivanov and A. V. Fateryga, eds., 2015. *Red Book of the Republic of Crimea. Animals*. Simferopol: ARIAL, 39 p. (in Russian).

[3)] Revkov, N.K., 2018. [The Black Sea Scallop Flexopecten glaber (Linnaeus, 1758)]. In: I. V. Dovgal and V. V. Korzhenevskiy, eds., 2018. *The Red Data Book of Sevastopol*. Sevastopol: ROST-DOAFK, 432 p. (in Russian).

deep), Station *2* (34 m), Station *3* (27 m) and Station *4* (13 m) (Fig. 1). The substrate in the sampling area was represented by slightly silty amphioxus sand with shell debris (amphioxus is coarse, well aerated sand typical of the *Branchiostoma* (=*Amphioxus*) *lanceolatum* habitat [2]). It was washed through a 0.5 mm sieve; after washing, the remaining sample was fixed in 4 % neutralised formalin. The material was further processed in the laboratory under a binocular microscope. The organisms were counted and weighed with an accuracy of 0.001 g. Their number and wet biomass were recalculated per 1 m^2 of bottom. The bivalve mass was determined after the removal of mantle cavity fluid. The species-level identification of benthic fauna was made using guides (Fauna Guide [4)] and [11]), and taxa were verified by WoRMS [5)]. The average values (from four sampling points) of abundance and biomass of large taxa with an indication of a standard error of measurements are presented in the table.

The faunal homogeneity of zoobenthos was assessed on a transformed (species presence/absence) species abundance matrix using the Bray-Curtis similarity coefficient in the *Cluster* program of PRIMER-6 package. The dominant species of benthic macrofauna was determined based on the density index (DI) value as follows

$$DI_i = N_i^{0.25} \cdot B_i^{0.75} \cdot p_i,$$

where N_i – specific abundance, ind./m^2; B_i – specific biomass, g/m^2; p_i – occurrence frequency of species i (0–1).

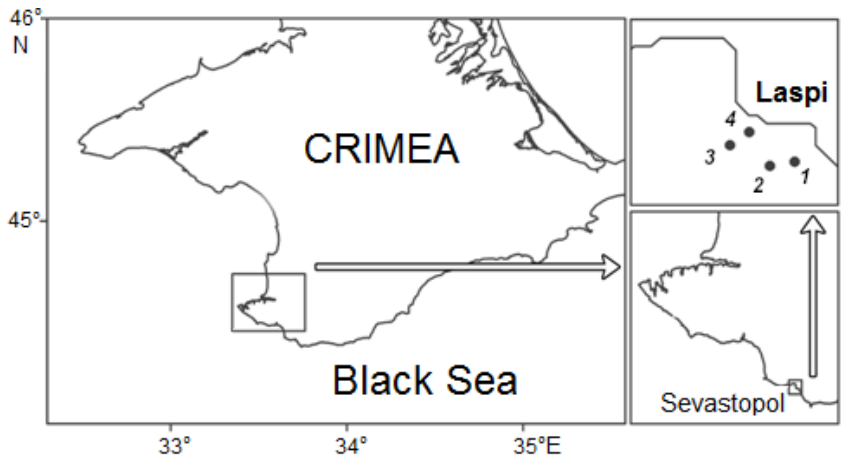

F i g . 1 . Schematic map of sampling locations in Laspi area

[4)] IBSS, 1968–1972. [*Fauna Field Guide for the Black Sea and Sea of Azov. Wild Invertebrata*]. 3 volumes. Kiev: Naukova Dumka, (in Russian).

[5)] WRMS. *An Authoritative Classification and Catalogue of Marine Names*. 2022. [online] Available at: http://www.marinespecies.org [Accessed: 01 December 2022].

The DI_i used in this work is an extension of the lineage of taxa quantification indices using the parameters of their occurrence frequency (p_i), specific abundance (N_i) and specific biomass (B_i) $(N_i \cdot B_i)^{1/2}$ [12]; $(N_i \cdot B_i)^{1/2} \cdot p_i$ [13]; $(N_i \cdot B_i \cdot p_i)^{1/3}$ [6]; $(B_i \cdot p_i)^{1/2}$ [14–16], collectively known as "density indices" and widely used in benthic studies of the Azov and Black Sea basin in the 1930s–1980s. The modern adjustment of indices came from studies on hydrobiont energy, where respiration costs of the i-th hydrobiont species per specific area are estimated by the formula $Q_i = N_i^{0.25} \cdot B_i^{0.75} \cdot k$ [17, 18]. This gave grounds to speak about the semantic load of the expression $N_i^{0.25} \cdot B_i^{0.75}$ as an estimated (approximate) equivalent of the energy role of hydrobionts and the possibility of using it in studies of structural organization of the benthos [19–21].

When comparing the current macrozoobenthos biomass with similar data from previous years, the biomass in the *Flexopecten* biocoenosis was recalculated taking the mantle cavity fluid of bivalves into account according to [22]. In the text, the names of the biocoenoses are abbreviated to the generic names of their dominant species.

Results

All stations in the study area had a high faunal homogeneity with a Bray – Curtis similarity of over 50 %. This allowed assigning them to a single biocoenosis, *Flexopecten glaber*, due to its dominant DI position. The DI value of *F. glaber* (143.05) was more than six times higher than that of the subdominant species, namely the clams *Bittium reticulatun* (22.76), *Gouldia minima* (20.93) and *Anadara kagoshimensis* (18.33). The DI-ranked range of species in the *Flexopecten* biocoenosis is considered in more detail in the discussion of the obtained material.

In total, 64 representatives of macrozoobenthos were observed in the *Flexopecten* biocoenosis at the level of species taxa. Among them are Crustacea – 12, Mollusca – 21, Polychaeta – 26, mixed group "Miscellaneous" – 5 species (see Appendix). Representatives of Acari, Gromia, Nematoda, Nemertea, Turbellaria as well as some specimens of polychaetes of families Nereididae, Phyllodocidae and Syllidae were not identified to species.

Average abundance and biomass of macrozoobenthos in the scallop biocoenosis were 11,231 ± 2,424 ind./m^2 and 247.7 ± 156.3 g/m^2, respectively (Table). Polychaetes and mollusks were the most abundant (Fig. 2, *a*). Among them mollusks *Bittium reticulatum*, *Caecum armoricum*, *C. trachea*, polychaetes *Pholoe inornata*, *Polygordius neapolitanus* and *Sigambra tentaculata* prevailed (density over 500 ind./m^2). In terms of biomass, the mollusks were the absolute leaders (Fig. 2, *b*), with the subdominant species after the leading biocoenosis species *Flexopecten glaber* being *Anadara kagoshimensis*, the recent (since 1969 [23]) alien species to the Black Sea.

[6] Arnoldi, L.V., 1949. [Materials for Quantitaive Studies of the Black Sea Zoobenthos. II. Karnikit Bay]. In: IBSS, 1949. *Trudy Sevastopolskoy Biologicheskoy Stantsii* [Proceedings of the Sevastopol Biological Station]. Vol. 7. Moscow, Leningrad: Izd-vo AN SSSR, pp. 127–192 (in Russian).

Mean density (*N*) and biomass (*B*) of the main macrozoobenthos taxa in the *Flexopecten glaber* biocoenosis

Taxon	*N*, ind./m^2	*B*, g/m^2
Annelida	5,131 ± 1,152	4.2 ± 1.3
Crustacea	644 ± 108	2.4 ± 0.6
Mollusca	4,169 ± 1,182	239.2 ± 156.8
Miscellaneous	1,288 ± 491	1.8 ± 0.6
Total	11,231 ± 2,424	247.7 ± 156.3

Note: the mollusk biomass is given exclusive of the mantle cavity fluid mass in bivalves.

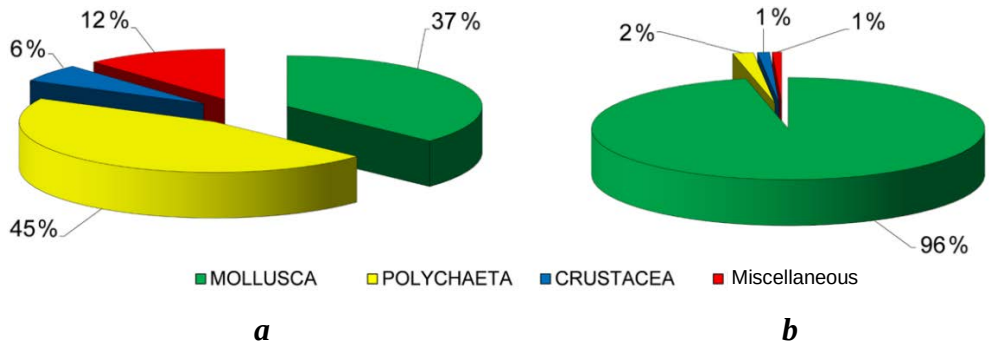

Fig. 2. Relative representation of the basic taxons of macrofauna (*a* – by biomass, *b* – by abundance) in the benthos of the study water area

Ten species in the scallop biocoenosis had an occurrence frequency of 100 % (recorded at all stations). These are the hermit crab *Diogenes pugilator*, the mollusks *Bittium reticulatum*, *Caecum armoricum*, *C. trachea*, *Lucinella divaricata*, *Mytilaster lineatus*, polychaetes *Micronephthys longicornis*, *Pholoe inornata*, *Sigambra tentaculata* (an alien species to the Black Sea [24]) and Nemertea. Two of the species – the index species of the biocoenosis *Flexopecten glaber* itself and the lancelet *Branchiostoma lanceolatum* – are included in the regional Red Data Books (those of Sevastopol and the Republic of Crimea). The former is as a species declining in abundance, the latter is as an rare species [2), 3), 7)].

[7)] Alyomov, S.V., 2018. Branchiostoma lanceolatum (Pallas, 1774). In: I. V. Dovgal and V. V. Korzhenevskiy, eds., 2018. *The Red Data Book of Sevastopol*. Sevastopol: ROST-DOAFK, 356 p. (in Russian).

Discussion

Flexopecten biocoenosis within a benthic biocoenotic classification off the coast of Crimea. As a result of the recovery processes in the population of *F. glaber* off the coast of Crimea after actual depopulation of this mollusk during the Black Sea ecosystem crisis in the second half of the 20th century, the scallop formed its own biocoenosis on the southwestern Crimean shelf area. A similar format of the *F. glaber* domination in benthos was observed in the first half of the 20th century in the oyster beds [1, 2]. In other biotopes near the open coasts of Crimea (silty ground, sand, shell debris, pebbles), *F. glaber* was a member of the characteristic (in biocoenoses *Ostrea – Mytilus*, *Modiolus adriaticus – Mytilus*, *Pitar – Gouldia – Chamelea*) and secondary (in biocoenoses *Loripes – Mytilaster – Modiolus adriaticus*, *Bittium – Mytilaster*, *Chamelea – Polititapes*, *Chamelea – Lucinella*, *Lucinella – Pitar – Chamelea – Gouldia*, *Spisula – Acanthocardia – Pitar*, *Gouldia*, *Parvicardium – Gouldia – Pholoe inornata*) benthos species [1, 3, 4].

Without giving the specifics of the methods of selection of the above biocoenoses, it can be stated that previously the Black Sea scallop was most frequently found in those of them, where the coenosis forming species were *Chamelea gallina* and *Gouldia minima*. These variations in scallop occurrence frequency becomes clear if we refer to a generalised scheme of the biocoenotic subdivision of the Black Sea benthos on the soft bottoms. Within the scallop depths (from 0 down to a depth of 40 m) there are three main biocoenoses: *Mytilus*, *Chamelea* and *Gouldia* [16]. The first two are categorised as regional (or belt), they occur at particular depths and in particular substrates almost along the entire Black Sea coast. The third one belongs to a group of local biocoenoses usually occupying small areas in particular parts of the sea [25]. The *Chamelea* biocoenosis develops in a biotope of sandy sediments (7–30 m depth), the *Gouldia* biocoenosis in sandy-silty sediments (20–50 m) and the *Mytilus* biocoenosis in silty sediments (20–53 m) [16].

It seems quite logical to assume that *F. glaber* population off the coast of Crimea will be recovering in biotopes favourable for the scallop development, and hence in the biocoenoses existing within these biotopes. These biocoenoses are *Mytilus*, *Chamelea* and *Gouldia*.

The observed recovery of *F. glaber* beds and its transformation off the coast of Crimea into a coenosis-forming species is consistent with the current recovery processes (after the 1980–1990s crisis) in the benthos of various parts of the Black Sea shelf associated with the de-etrophication of the Black Sea basin and the improvement in the ecological status of its water areas [22, 26–29].

The biotope of the Gouldia biocoenosis as one of the zones of formation of the modern Flexopecten biocoenosis. In the selected *Flexopecten* biocoenosis, out of the three main coenosis-forming species noted above (within depths up to 40 m) near the coast of Crimea (*M. galloprovincialis*, *Ch. gallina* and *G. minima*), *G. minima*, which ranked third in DI after *F. glaber* and the gastropod *Bittium reticulatum* (Fig. 3), had the greatest development.

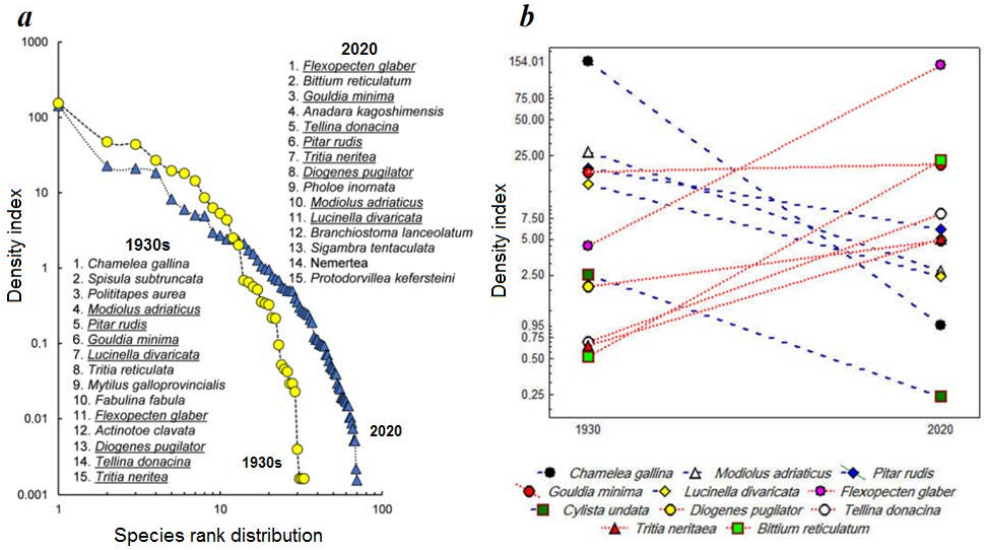

Fig. 3. Curves of the species rank distribution (*a*) and the quantitative representation of the principal macrozoobenthos species (*b*) according to the Density Index (DI) in the *Flexopecten* biocoenosis (Laspi area, depth 13–34 m) in 2020, and in the muddy-sand benthos grouping (area Cape Fiolent – Cape Sarych, depth 12–25 m) in the 1930s (on materials by L. V. Arnoldi [13]). The underlined species are shared by the two study periods

Estimated calculations show that if we exclude *F. glaber* and *A. kagoshimensis* (as an alien species that has recently appeared near the coast of Crimea) from the current benthic structure of the considered study area, the resulting reconstructed *Gouldia* biocoenosis will have a macrozoobenthos biomass of 52 ± 10 g/m^2 (during comparison, the weight of mantle cavity fluid of bivalve mollusks was taken into account), which is comparable to the average benthos biomass (30 g/m^2 [16]) in the *Gouldia* biocoenosis of the 1950s near the coast of Crimea and the Caucasus. Moreover, the relative stability of the *Gouldia* quantitative indices is noticeable when comparing data for Laspi area in 2020 with similar parameters of the 1930s for Southwestern Crimea (Fig. 3).

The *Flexopecten* biocoenosis that we selected is located in a mixed biotope (slightly silty amphioxus sand with shell debris), including components of different sediment fractions that are characteristic of the development biotopes of the main biocoenoses mentioned above. The *Flexopecten* biocoenosis was the closest to the *Gouldia* (32 species shared) and *Chamelea* (30) biocoenoses; the *Mytilus* biocoenosis was more distant (21). Twenty-five species were not previously seen in any of the three biocoenoses near the coast of Crimea, but were present in the scallop biocoenosis. They are seven crustaceans: *Chondrochelia savignyi*, *Elaphognathia bacescoi*, *Eurydice pontica*, *Liocarcinus navigator*,

Melita palmata, *Microdeutopus versiculatus*, *Palaemon elegans*, bryozoans *Cradoscrupocellaria bertholletii*, *Cryptosula pallasiana*, bivalve *Anadara kagoshimensis*, six gastropods: *Caecum armoricum*, *Ebala pointeli*, *Retusa umbilicata*, *Steromphala adriatica*, *Vitreolina incurve*, and six polychaetes: *Lindrilus flavocapitatus*,
Lysidice ninetta, *Lysidice unicornis*, *Nereiphylla pusilla*, *Polyophthalmus pictus* and *Schistomeringos rudolphi*.

Based on the above specific substrate features, species composition and quantitative species development, we believe that the nearest native predecessor of *Flexopecten* biocoenosis in the considered local biotope of silty amphioxus sand with shell debris at 13–34 m depth could be the *Gouldia* biocoenosis. Previously, a mixed representation of psammophilic, pelophilic and euryedaphic forms of benthos was noted for it [16].

In the list of species of the Black Sea *Gouldia* biocoenosis given by M. I. Kiseleva [16], *F. glaber* is absent. However, we note that in earlier publications she indicates the presence of *F. glaber* in this biocoenosis both in the western (Tarkhankut Peninsula, near Cape Uret, a biotope with shell debris, sand and a small admixture of silt at a depth of 10–25 m; species occurrence frequency at the station is 5 %, the abundance being 10 ind./m^2 and the biomass 13.1 g/m^2) [3], and in the southern part of the Crimean shelf (biocoenosis *Parvicardium – Gouldia – Pholoe inornata*) [4]. This discrepancy seems to be caused solely by a technical error of "species dropout" during aggregation of materials. The presence of the scallop in the *Gouldia* biocoenosis of the 1950s and in our data of 2020 indicates the return of the species position (and, as our data show, even its improvement) in a biotope favourable for its development.

Peculiarities of the quantitative development of zoobenthos in the Flexopecten biocoenosis. To assess the level of biomass achieved in the current *Flexopecten* biocoenosis near the coast of Southwestern Crimea, we compare these values with similar data in the *Chamelea* biocoenosis, which forms some of the highest biomass in the benthos of the soft bottoms at depths down to 32 m [30].

The earliest quantitative materials on the region, including the area of interest in Laspi area, are presented in the work of L. V. Arnoldi [13]. Based on biotopic features, he subdivided the benthos of the Southern coast of Crimea (from Cape Fiolent to Cape Sarych) into four main groups: 1) coastal clear sand (depths 1–12 m, *Chamelea – Lucinella – Spisula* group), 2) silt and sand (12–25 m, Chamelea group), 3) mussel muds (26–50 m, *Mytilus* group) and 4) phaseolina muds (51–110 m, *Modiolula – Molgula* group). The group of interest out of the four identified is the second one. The mean macrozoobenthos biomasses of the 1930s *Chamelea* and 2020 *Flexopecten* groups were comparable: 388 g/m^2 vs. 351 g/m^2, respectively. In the current *Flexopecten* biocoenosis, the index form of the 1930s *Chamelea gallina* (DI = 154.01) was placed in the secondary species group

(20th position by DI = 0.95) (see Fig. 3). We note in particular that the level of quantitative development of *Gouldia minima* remained almost unchanged during the compared periods (DI = 18.04 in the 1930s vs. DI = 20.93 in 2020), and in the modern period, *Anadara kagoshimensis* (DI = 18.33), which has successfully established itself near the Crimean coast since the 1990s, joined the leading benthos group along with its native representatives [31].

In 1957, near the open south coast of Crimea in the *Chamelea* biocoenosis (9–25 m; a biotope of fine sand) the macrozoobenthos biomass was low and almost equal to that of the *Flexopecten* biocoenosis (354 g/m^2 vs. 351 g/m^2) [4]. In the second half of the 20th century, during the period of hypereutrophication of the Black Sea basin [32], there was an increase in zoobenthos biomass values in the *Chamelea* biocoenosis associated with a positive response of *Ch. gallina* itself to an increase in available food [35–37]. Accordingly, in 1981–2004 the zoobenthos biomass in the *Chamelea* biocoenosis near the coast of Crimea reached a historical maximum average value of 495 g/m^2 [30].

Thus, in our case, when the formation of the *Flexopecten* biocoenosis in the studied area of the Southwestern Crimea was based on the *Gouldia* biocoenosis, the macrozoobenthos biomass level achieved in the scallop biocoenosis became comparable with that of the main biocoenosis of the sand sublittoral – *Chamelea*. Given the different biotopic relationship between the two biocoenoses (the *Flexopecten* biocoenosis formed on the basis of the silty-sandy *Gouldia* biocoenosis, and the *Chamelea* biocoenosis is located on sandy bottom), the resultant significant expansion of the sublittoral zone with high benthic biomass should be noted.

In this paper we consider one of the possible options for *F. glaber* to realize its biotic potential near the Crimean coast in the process of returning to the regional fauna "through" the *Gouldia* biocoenosis. Other variants may be related to the passage of *F. glaber* through different conditions in other existing biocoenoses.

Conclusion

The paper describes appearance of the Black Sea scallop *Flexopecten glaber* biocoenosis in an area of Southwestern Crimea in a biotope of slightly silty amphioxus sand with shell debris in the depth range 13–34 m. The biocoenosis includes 63 species of benthic macrofauna with a predominance of Polychaeta (26 species) and Mollusca (21 species) groups. It is suggested that the native predecessor of the *Flexopecten glaber* biocoenosis in the area of its detection was the *Gouldia minima* biocoenosis.

With similar weighing methods (taking mantle fluid from bivalves into account), the zoobenthos biomass of the *Flexopecten glaber* biocoenosis (351 g/m^2) was similar to that of the benthos at comparable depths near the southern coasts of Crimea in the 1930s (388 g/m^2), 1957 (354 g/m^2) and 1981–2004 (495 g/m^2) in the *Chamelea gallina* biocenosis, which has one of the highest levels of biomass on the Black Sea shelf.

Appendix

List of macrozoobenthos species in *Flexopecten glaber* biocoenosis

ANNELIDA	
Aonides paucibranchiata Southern, 1914	*Nereiphylla pusilla* (Claparède, 1870)
Capitella capitata (Fabricius, 1780)	*Perinereis cultrifera* (Grube, 1840)
Eunice vittata (Delle Chiaje, 1828)	*Pholoe inornata* Johnston, 1839
Exogone naidina Örsted, 1845	Phyllodocidae g.sp.
Goniadella bobrezkii (Annenkova, 1929)	*Platynereis dumerilii* (Audouin & Milne Edwards, 1834)
Harmothoe imbricata ((Linnaeus, 1767)	*Polygordius neapolitanus* Fraipont, 1887
Harmothoe reticulata (Claparède, 1870)	*Polyophthalmus pictus* (Dujardin, 1839)
Heteromastus filiformis (Claparède, 1864)	*Prionospio cirrifera* Wirén, 1883
Lagis neapolitana (Claparède, 1869)	*Protodorvillea kefersteini* (McIntosh, 1869)
Lindrilus flavocapitatus (Uljanina, 1877)	*Schistomeringos rudolphi* (Delle Chiaje, 1828)
Lysidice ninetta Audouin & Milne-Edwards, 1833	*Sigambra tentaculata* (Treadwell, 1941)
Lysidice unicornis (Grube, 1840)	*Spirobranchus triqueter* (Linnaeus, 1758)
Micronephthys longicornis (Perejaslavtseva, 1891)	Syllidae g.sp.
Mysta picta (Quatrefages, 1866)	*Syllis hyalina* Grube, 1863
Nereididae g.sp.	
CRUSTACEA	
Ampelisca diadema (Costa, 1853)	*Eurydice pontica* (Czerniavsky, 1868)
Apseudopsis ostroumovi Bacescu & Carausu, 1947	*Liocarcinus navigator* (Herbst, 1794)
Athanas nitescens (Leach, 1814 [in Leach, 1813–1815])	*Melita palmata* (Montagu, 1804)
Chondrochelia savignyi (Kroyer, 1842)	*Microdeutopus versiculatus* (Spence Bate, 1857)
Diogenes pugilator (P. Roux, 1829)	*Palaemon elegans* Rathke, 1836
Elaphognathia bacescoi (Kussakin, 1969)	*Pisidia bluteli* (Risso, 1816)
MOLLUSCA	
Anadara kagoshimensis (Tokunaga, 1906)	*Steromphala adriatica* (Philippi, 1844)
Ebala pointeli (de Folin, 1868)	*Gouldia minima* (Montagu, 1803)
Vitreolina incurva (Bucquoy, Dautzenberg & Dollfus, 1883)	*Lepidochitona cinerea* (Linnaeus, 1767)
Bittium reticulatum (da Costa, 1778)	*Lucinella divaricata* (Linnaeus, 1758)
Caecum armoricum de Folin, 1869	*Moerella donacina* (Linnaeus, 1758)
Caecum trachea (Montagu, 1803)	*Mytilaster lineatus* (Gmelin, 1791)
Chamelea gallina (Linnaeus, 1758)	*Mytilus galloprovincialis* Lamarck, 1819
Tritia neritea (Linnaeus, 1758)	*Parvicardium exiguum* (Gmelin, 1791)
Retusa umbilicata (Montagu, 1803)	*Pitar rudis* (Poli, 1795)
***Flexopecten glaber* (Linnaeus, 1758)**	*Rissoa parva* (da Costa, 1778)
Modiolus adriaticus Lamarck, 1819	

Miscellaneous	
Acari	*Leptosynapta inhaerens* (O.F. Müller, 1776)
Cylista undata (Müller, 1778)	Nematoda
Branchiostoma lanceolatum (Pallas, 1774)	Nemertea
Gromia	*Cradoscrupocellaria bertholletii* (Audouin, 1826)
Cryptosula pallasiana (Moll, 1803)	Turbellaria

REFERENCES

1. Nevesskaya, L.A., 1965. [*Late Quarternary Mollusks of the Black Sea, their Taxonomy and Ecology*]. Moscow: Nauka, 391 p. (in Russian).
2. Zernov, S.A., 1913. [*On Study of Life of the Black Sea*]. 280 p. (in Russian).
3. Kiseleva, M.I. and Slavina, O.Ya., 1964. [Benthic Biocenoses at the West Coast of Crimea]. In: SBS, 1964. [*Proceedings of the Sevastopol Biological Station*]. Sevastopol: Flag Rodiny. Iss. 15, pp. 152–177 (in Russian).
4. Kiseleva, M.I. and Slavina, O.Ya., 1963. [Benthic Biocenoses at the South Coast of Crimea]. In: SBS, 1963. [*Proceedings of the Sevastopol Biological Station*]. Kiev: Izd-vo Akademii Nauk Ukrainskoy SSR. Iss. 16, pp. 176–191 (in Russian).
5. Revkov, N.K., Timofeev, V.A. and Revkova, T.N., 2019. The Long-Term Changes of *Upogebia pusilla* (Crustacea: Decapoda) Population on the Northern Shelf of the Black Sea (Crimea). *Ekosistemy*, 19, pp. 123–132 (in Russian).
6. Filimon, A., 2020. First Record of *Flexopecten glaber* (Linnaeus, 1758) (Bivalvia: Pectinidae) from the Romanian Black Sea Shelf. *Cercetări Marine*, 50, pp. 186–191.
7. Pereladov, M.V., 2016. Biotope Structure and Modern Status of Oyster (*Ostrea edulis*) settlement in Donuzlav Lake, Crimea Peninsula, the Black Sea. *Trudy VNIRO*, 163, pp. 36–47 (in Russian).
8. Bondarev, I.P., 2019. New Data on Biology and Ecology of *Flexopecten glaber* (Linnaeus, 1758) (Bivalvia, Pectinidae) in the Black Sea. *Aquatic Bioresources and Environment*, 2(2), pp. 36–44. https://doi.org/10.47921/2619-1024_2019_2_2_36 (in Russian).
9. Pirkova, A.V. and Ladygina, L.V., 2017. Meiosis, Embryonic, and Larval Development of the Black Sea Scallop *Flexopecten glaber ponticus* (Bucquoy, Dautzenberg & Dollfus, 1889) (Bivalvia, Pectinidae). *Marine Biological Journal*, 2(4), pp. 50–57. doi:10.21072/mbj.2017.02.4.05 (in Russian).
10. Revkov, N.K., Pirkova, A.V., Timofeev, V.A., Ladygina, L.V. and Schurov, S.V., 2021. Growth and Morphometric Characteristics of the Scallop *Flexopecten glaber* (Bivalvia: Pectinidae) Reared in Cages off the Coast of Crimea (Black Sea). *Ruthenica, Russian Malacological Journal*, 31(3), pp. 127–138. doi:10.35885/ruthenica.2021.31(3).3 (in Russian).
11. Kiseleva, M.I., 2004. *Polychaetes (Polychaeta) of the Azov and Black Seas*. Apatity: Print. Kola Science Centre RAS, 409 p. (in Russian).
12. Zenkevitch, L.A. and Brozky, V.A., 1937. Some Data on the Ecology of Dominants in the Bentos of the Barents-Sea. *Uchenye Zapiski MGU*, 13, pp. 203–226 (in Russian).

13. Arnoldi, L.V., 1941. Quantitative Characteristics of the Zoobenthos of the Black Sea. *Trudy Zoologicheskogo Insituta Akademii Nauk SSSR* [Proceedings of the Zoological Institute of USSR], 7(2), pp. 94–113 (in Russian).
14. Vorobiov, V.P., 1949. [*Benthos of the Sea of Azov*]. Simferopol: Krymizdat, 193 p. (in Russian).
15. Stark, I.N., 1960. [Annual and Seasonal Dynamics of Benthos in the Sea of Azov]. In: AzNIIRKh, 1960. *Proceedings of AzNIIRKh*. Rostov-on-Don. 1(1), pp. 167–229 (in Russian).
16. Kiseleva, M.I., 1981. [*Benthos of Soft Bottoms of the Black Sea*]. Kiev: Naukova dumka, 168 p. (in Russian).
17. Kucheruk, N.V. and Savilova, T.A., 1985. Quantitative and Ecological Characteristics of the Bottom Fauna in the Shelf and Upper Slope of the North-Peruvian Upwelling Region. *Bulletin of Moscow Society of Naturalists. Biological Series*, 90(6), pp. 70–79 (in Russian).
18. Maltsev, V.I., 1990. Use of a Functional Abundance Index for Structural Studies of Zoocoenoses. *Hydrobiological Journal*, 26(1), pp. 105–106.
19. Revkov, N.K. and Nikolaenko, T.V., 2002. Biodiversity of Zoobenthos in the Coastal Zone of the South Coast of Crimea (Laspi Bay Area). *Russian Journal of Marine Biology*, 28(3), pp. 151–162. doi:10.1023/A:1016879418490
20. Denisenko, S.G., Denisenko, N.V., Lehtonen, K.K., Andersin, A.-B. and Laine, A.O., 2003. Macrozoobenthos of the Pechora Sea (SE Barents Sea): Community Structure and Spatial Distribution in Relation to Environmental Conditions. *Marine Ecology Progress Series*, 258, pp. 109–123. doi:10.3354/meps258109
21. Revkov, N.K., Boltacheva, N.A. and Bondarenko, L.V., 2014. Long-Term Changes of Zoobenthos in Yalta Gulf (Black Sea, Southern Coast of Crimea). *Marine Ekological Journal = Morskoj Ehkologicheskij Zhurnal*, 13(2), pp. 49–62 (in Russian).
22. Revkov, N.K., Boltacheva, N.A., Timofeev, V.A., Bondarev, I.P. and Bondarenko, L.V., 2018. Macrozoobenthos of the Zernov's Phyllophora Field, Northwestern Black sea: Species Richness, Quantitative Representation and Long-Term Variations. *Nature Conservation Research*, 3(4), pp. 32–43. doi:10.24189/ncr.2018.045
23. Kiseleva, M.I., 1992. [Comparative Characterization of Benthic Communities off the Coast of the Caucasus]. In: V. E. Zaika, ed., 1992. [*Long-Term Changes in the Zoobenthos of the Black Sea*]. Kiev: Naukova dumka, pp. 84–99 (in Russian).
24. Kiseleva, M.I., 1964. On the Finding of the Polychaet *Ancistrosyllis tentacullata* Treadwell in the Black and Red Seas. *Zoologocheskiy Zhurnal*, 43(10), pp. 1557–1558 (in Russian).
25. Kiseleva, M.I., 1979. [Bottom Biocoenoses and their Biomass]. In: V. N. Greze, ed., 1979. *Productivity of the Black Sea.* Kiev: Naukova dumka, pp. 218–239 (in Russian).
26. Cociasu, A., Dorogan, L., Humborg, C. and Popa, L., 1996. Long-Term Ecological Changes in Romanian Coastal Waters of the Black Sea. *Marine Pollution Bulletin*, 32(1), pp. 32–38. doi:10.1016/0025-326X(95)00106-W
27. Begun, T., Teacă, A. and Gomoiu, M.-T., 2010. State of Macrobenthos within Modiolus phaseolinus Biocoenosis from Romanian Black Sea Continental Shelf. *Geo-Eco-Marina*, 16, pp. 5–18. doi:10.5281/zenodo.56945
28. Todorova, V. and Konsulova, T., 2000. Long Term Changes and Recent State of Macrozoobenthic Communities along the Bulgarian Black Sea Coast. *Mediterranean Marine Science*, 1(1), pp. 123–131. doi:10.12681/mms.283

29. Petrova, E. and Stoykov, S., 2013. Biocenological Investigations of the Macrozoobenthos in the Northern Part of the Bulgarian Black Sea Coast in Depths up to 30 m. *Bulgarian Journal of Agricultural Science*, 19(suppl. 1), pp. 16–20.

30. Revkov, N.K., Abaza, V., Dumitrache, C., Todorova, V., Konsulova, T., Mickashavidze, E., Varshanidze, M., Sezgin, M., Ozturk, B. [et al.], 2008. The State of Zoobenthos. In: T. Oguz, 2008. *State of the Environment of the Black Sea (2001–2006/7)*. Istanbul, 2008. Chapter 8, pp. 243–290. Available at: https://repository.marineresearch.org/handle/299011/6659 [Accessed: 06 December 2022].

31. Revkov, N.K., Boltacheva, N.A., Nikolaenko, T.V. and Kolesnikova, E.A., 2002. Zoobenthos Biodiversity over the Soft Bottom in the Crimean Coastal Zone of the Black Sea. *Oceanology*, 42(4), pp. 536–546.

32. Yunev, O.A., Konovalov, S.K. and Velikova, V., 2019. *Anthropogenic Eutrophication in the Black Sea Pelagic Zone: Long-Term Trends, Mechanisms, Consequences*. Moscow: GEOS, 164 p. (in Russian).

33. Revkov, N.K., Valovaya, N.A., Kolesnikova, E.A., Nikolaenko, T.V. and Shalyapin, V.K., 1999. [On Response of the Black Sea Macrozoobenthos to Eutrophication]. In: MHI, 1999. *Ekologicheskaya Bezopasnost' Pribrezhnoy i Shel'fovoy Zon i Kompleksnoe Ispol'zovanie Resursov Shel'fa* [Ecological Safety of Coastal and Shelf Zones and Comprehensive Use of Shelf Resources]. Sevastopol: ECOSI-Gidrofizika, pp. 199–212 (in Russian).

34. Revkov, N.K., 2011. [Macrozoobenthos of the Ukrainian Shelf of the Black Sea]. In: V. N. Eremeev, A. V. Gaevskaya, G. E. Shulman, Ju. A. Zagorodnyaya, eds., 2011. *Biological Resources of the Black Sea and Sea of Azov*. Sevastopol: ECOSI-Gidrofizika, pp. 140–162 (in Russian).

35. Boltacheva, N.A. and Zaika, V.E., 2018. [Mollusks *Chamelea gallina* and *Mytilus galloprovincialis* of the Upper Sublittoral: Long-Term Changes]. In: N. S. Kostenko, ed., 2018. *The Biology of the Black Sea Offshore Area at the South-Eastern Crimea*. Simferopol: PP ARIAL, pp. 87–96. doi:10.21072/978-5-907032-04-0 (in Russian).

Submitted 3.07.2022; accepted after review 10.08.2022;
revised 02.11.2022; published 23.12.2022

About the authors:

Nikolai K. Revkov, Leading Research Associate, A.O. Kovalevsky Institute of Biology of the Southern Seas of RAS (2 Nakhimov Av., Sevastopol, 299011, Russian Federation), Ph.D. (Biol.), **ORCID ID: 0000-0001-8308-5262**, **Scopus Author ID: 6508089586**, **ResearcherID: H-6119-2016,** *nrevkov@yandex.ru*

Natalya A. Boltachova, Leading Research Associate, A.O. Kovalevsky Institute of Biology of the Southern Seas of RAS (2 Nakhimov Av., Sevastopol, 299011, Russian Federation), Ph.D. (Biol.), **ORCID ID: 0000-0003-0618-1992**, **Scopus Author ID: 36149089700**, *nboltacheva@mail.ru*

Contribution of the authors:

Nikolai K. Revkov – statement of the study problem, analysis of the results and their interpretation, preparation of graphic materials, formation of the article

Natalya A. Boltachova – analysis of the composition and abundance of polychaete worms, analysis and discussion of the results, editing of the manuscript

All the authors have read and approved the final manuscript.

DOI: 10.22449/2413-5577-2022-4-104-116

Colour Vision of the Amphipod *Chaetogammarus olivia* H. Milne Edwards, 1830 under Acute Light Exposure

V. A. Grintsov [1]*, **A. V. Kuznetsov** [1, 2], **S. N. Zheleznova** [1], **V. I. Ryabushko** [1]

[1] *Kovalevsky Institute of Biology of Southern Seas of RAS, Sevastopol, Russia*
[2] *Sevastopol State University, Sevastopol, Russia*
**e-mail: vgrintsov@gmail.com*

Abstract

Light pollution in urbanized industrial areas disrupts the biological rhythms in animals. Artificial light penetrates the coastal zone, even to the bottom. The study of marine invertebrates' colour vision expands our understanding of animal perception of signals from the environment and is useful in urban landscape planning with artificial lighting. Amphipods are common in the seas and fresh waters, as well as on land; some live in the surf zone, which has led to the development of specific sensory systems, because air transmits light and sound differently than water. We studied colour perception in invertebrates living near the water's edge. The amphipods *Chaetogammarus olivii* H. Milne Edwards, 1830 were placed in a long narrow channel, part of which was closed from direct sunlight. *C. olivii* preferred to remain in the shade, where males formed dense clusters and females with eggs more often kept apart despite the active movement through the channel. Experiments revealed a similarity between the distribution of *C. olivii* in channels with colourful gradient LED lighting and the response to the laser beam. Animals avoided intense white, blue, and purple light, to a lesser extent green light, and did not respond to red light, while running away from light sources in complete darkness. Light pulses with durations and pauses of 1 s each, which may correspond in frequency characteristics to a weak surf, had no effect on *C. olivii* in contrast to random flashes of light. Perhaps the coastal inhabitants' ability to swiftly locate themselves in water or air is caused by their photoreception of blue and violet light. Modern light pollution is capable of disorienting animals in the dark, which may negatively affect the ecological situation of the splash zone.

Keywords: Amphipoda, colour vision, opsins, light smog, behavior

Acknowledgements: the authors are grateful to M. I. Silakov for drawing our attention to the light pollution issue, to A. V. Pirkova, E. V. Lisitskaya and R. G. Gevorgiz for discussion of the manuscript, and to Prof. I. V. Dovgal and Prof. Randy Nelson for useful suggestions. The work was performed under state assignment of FRC IBSS on topics: “Regularities of formation and anthropogenic transformation of biodiversity and bioresources of the Azov-Black Sea basin and other regions of the World Ocean”

(state registration no. 118020890074-2) and “Study of control systems of biotechnological complex production processes aimed at development of scientific basis for obtaining biologically active agents and technical products of marine origin” (state registration no. 121030300149-0).

For citation: Grintsov, V.A., Kuznetsov, A.V., Zheleznova, S.N. and Ryabushko, V.I., 2022. Colour Vision of the Amphipod Chaetogammarus olivia H. Milne Edwards, 1830 under Acute Light Exposure. *Ecological Safety of Coastal and Shelf Zones of Sea*, (4), pp. 104–116. doi:10.22449/2413-5577-2022-4-104-116

Цветовое зрение амфипод *Chaetogammarus olivii* H. Milne Edwards, 1830 в условиях острого светового воздействия

В. А. Гринцов [1]*, А. В. Кузнецов [1, 2], С. Н. Железнова [1], В. И. Рябушко [1]

[1] *Институт биологии южных морей им. А.О. Ковалевского РАН, Севастополь, Россия*

[2] *Севастопольский государственный университет, Севастополь, Россия*

**e-mail: vgrintsov@gmail.com*

Аннотация

Световое загрязнение урбанизированных промышленных районов приводит к нарушению биологических ритмов у животных. В прибрежной зоне искусственный свет проникает даже на дно. Изучение цветового зрения морских беспозвоночных расширяет наше представление о восприятии животными сигналов из окружающей среды и полезно при проектировании городских ландшафтов с искусственным освещением. Амфиподы распространены в морях и пресных водоемах, а также частично на суше. Некоторые представители обитают в полосе прибоя, что привело к развитию у них специфических сенсорных систем, так как воздух иначе пропускает свет и звук, чем вода. Мы изучали цветовое восприятие у беспозвоночных, живущих возле уреза воды. Бокоплавов *Chaetogammarus olivii* H. Milne Edwards, 1830 помещали в длинный узкий канал, часть которого была закрыта от прямых солнечных лучей. Несмотря на активное перемещение по каналу, *C. olivii* предпочитали оставаться в тени, где самцы создавали плотные скопления, а самки с яйцами чаще держались порознь. Эксперименты выявили сходную реакцию амфипод на цветные светодиоды и лазерные источники света. Животные избегали интенсивного белого, синего и фиолетового света, в меньшей степени зеленого, не реагировали на красный, при этом убегали от источников света в полной темноте. Световые импульсы длительностью 1 с и с паузой 1 с не оказывали воздействия на *C. olivii* в отличие от случайных вспышек света, что по частотным характеристикам может соответствовать слабому прибою. Предполагается, что фоторецепция синего и фиолетового света позволяет обитателям прибрежной зоны быстро определять свое местонахождение в воде или на воздухе. Современное световое загрязнение способно дезориентировать животных в темноте, что может негативно сказаться на экологической ситуации в зоне заплеска.

Ключевые слова: Amphipoda, цветовое зрение, опсины, световой смог, поведение

Благодарности: выражаем благодарность М. И. Силакову за привлечение внимания к теме светового загрязнения, А. В. Пирковой, Е. В. Лисицкой и Р. Г. Геворгизу за обсуждение рукописи, а также проф. И. В. Довгалю и Prof. Randy Nelson за полезные советы. Работа выполнена в рамках государственного задания ФИЦ ИнБЮМ

по темам: «Закономерности формирования и антропогенная трансформация биоразнообразия и биоресурсов Азово-Черноморского бассейна и других районов Мирового океана» (№ гос. регистрации 118020890074-2) и «Исследование механизмов управления продукционными процессами в биотехнологических комплексах с целью разработки научных основ получения биологически активных веществ и технических продуктов морского генезиса» (№ гос. регистрации 121030300149-0).

Для цитирования: Цветовое зрение амфипод *Chaetogammarus olivii* H. Milne Edwards, 1830 в условиях острого светового воздействия / В. А. Гринцов [и др.] // Экологическая безопасность прибрежной и шельфовой зон моря. 2022. № 4. С. 104–116. EDN XVLNPZ. doi:10.22449/2413-5577-2022-4-104-116

Light pollution (illumination, light smog) is created by architectural and street lighting, lanterns, billboards and greenhouses, which form light domes over cities and their suburbs. The effect of sky lightening at night is enhanced by dust and aerosol particles floating in the air, which additionally reflect and scatter the incident light. Illumination is typical for densely populated areas of advanced countries. Excessive lighting can cause increased anxiety, fatigue, stress, headache, and other symptoms in a person [1–4]. Therefore, in some countries there are legislative restrictions against light smog. Artificial light sources, the light of which is scattered in the lower layers of the atmosphere, change the biorhythms of living beings [5, 6]. Particularly indicative is environmental light pollution, which disrupts the evolutionary established links between organisms and the environment, which, for example, makes it difficult for animals to navigate, changes the relationships between community members, and can lead to disrupting the endocrine system of the wildlife [7, 8].

Animals' colour vision evolved under the surface of ancient oceans over hundreds of millions of years [9, 10]. The ancestors of Pancrustacea probably already had four genes of visual opsins (LW2 – Long Wavelength, MW1, MW2 – Middle Wavelength, and SW – Short Wavelength), which were later duplicated or lost to varying degrees during evolution process [11]. It is known that many species, such as the sea urchin *Strongylocentrotus purpuratus* [12] and the brittle star *Amphiura filiformis* [13], are sensitive to light due to non-visual types of opsins that function like a huge complicated eye. Such receptors are sensitive to blue-green light and can be involved in signal transduction into the cytoplasm and cell nucleus [14].

Of particular interest is the study of the vision of mass species of animals living near the water's edge, which is due to a number of reasons. The splash zone is one of the most extreme in the World Ocean, since the aquatic organisms living here are under the influence of a number of harmful factors such as light and storm effects, sharp temperature fluctuations, periodic desiccation, etc. An organism needs a quick response to extreme factors to survive in such conditions.

The purpose of this work is to study the effect of light on the amphipod *Chaetogammarus olivii* (H. Milne Edwards, 1830), which lives in the Black Sea in the splash zone.

Materials and methods

Amphipod *C. olivii* was collected in the water edge zone of the pebble-sand beaches of the outer harbour of Sevastopol Bay in August–October 2021 at a water temperature of 17–23°C. Amphipods were placed in plastic containers with water along with a small amount of macrophytes and stones. To analyze the reaction of animals to light, they were separated from macrophytes by shaking, several hundred amphipods were selected and placed on fabric filters, which were immersed in desiccators with sea water. Animals were identified under a microscope with an Olympus C55Z, C5500Z camera.

The experiments were carried out both under sunlight and artificial lighting in a darkened room or in a dark optic box with compartments. Thirty animals were placed into channels 1 × 1 × 50 cm in size. Part of the channel was shaded with a lid 10 cm long in some experiments. In others, an artificial light source was placed on one side of the channel so that approximately half of the channel was illuminated, and the other half was in the shadow. The animals were illuminated for 5 minutes, after which a partition was installed in the middle of the channel to prevent further movement of amphipods from one part of the channel to another, and the number of individuals in both parts of the channel was counted. The light was turned off, the partition was removed, and the animals were left alone for 5 min, allowing them to move freely along the channel. After that, a light source was installed on the opposite side of the channel and the experiment was repeated.

When studying the reactions of amphipods to colour, Light-Emitting Diodes (LEDs) and channels were placed in an optic box with compartments for two LEDs and two channels per compartment for females and males, accordingly, which made it possible to conduct experiments in parallel for white, red, green, and blue colours. Constant lighting was used, as well as light pulses with a 50 % duty cycle and different total durations. The illumination was carried out with lasers of different wavelengths, such as red (630–650 nm, 5 mW), green (532 nm, 10 mW), violet (405 nm, 5 mW), as well as with ultraviolet and white directional light sources (warm LED lamp WOLTA, 6 W, 4 K). To control the light, we used an ATmega328 microcontroller on the Arduino Nano platform with 200 Ohm resistors connected in series to LEDs with the following characteristics: red is 620 nm, green is 529 nm, blue is 470 nm and white is 6000 K. The light flux angle for all LEDs was 20°, and the intensity of the light flux was in the range of 1.5–2.5 lm. In general, ten series of experiments were carried out within two months.

Results

The amphipod *C. olivii* is found in the Atlantic Ocean, as well as in the Mediterranean and Black seas (works [1), 2)] and [15, 16]). Amphipods are distinguished

---

[1)] Borges, P.A.V., ed., 2016. *A List of the Terrestrial and Marine Biota from the Azores*. Princípia, Oeiras, 432 p. doi:10.15468/hyvwxi

[2)] Grintsov, V. and Sezgin, M., 2011. *Manual for Identification of Amphipoda from the Black Sea*. Sevastopol: Digit Print, 2011. 379 p. Available at: http://www.ipdn.ru/periphyton/_private/bibl/Grintsov+manual+12.03.11.pdf [Accessed: 30 November 2022].

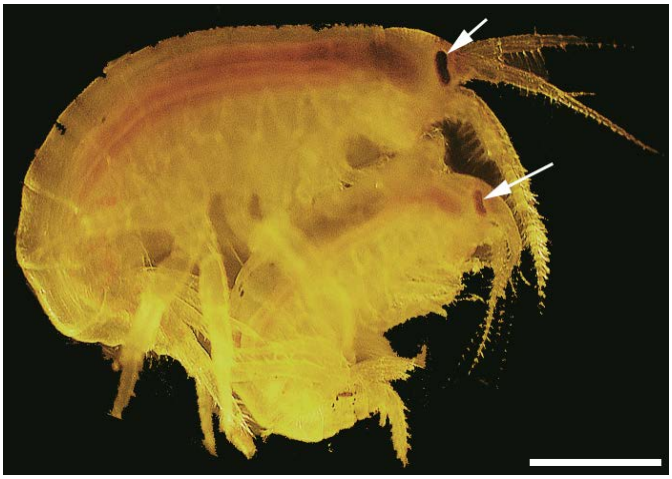

Fig. 1. Light photograph of amphipod *C. olivii* showing a male and female during copulation. The arrows point to their eyes. The scale size is 1 mm

by significant sexual dimorphism: males have larger compound eyes than females. An interesting feature is that their compound eyes are localized under a chitin layer (Fig. 1). These crustaceans were found in the large swarms on pebble beaches directly near the water in the interstitial between stones or, more often, in algae washed ashore.

Experiments using lasers on grids. The amphipods gathered in separate groups in shirs of nylon grid and randomly moved from one group to another in daylight (Fig. 2, *d*). The red light had no noticeable effect on the animals (Fig. 2, *a*); they continued to move in the same way as in the control group. The green light forced some animals to leave the light spot, but they did not move far to the side (Fig. 2, *b*). However, the violet laser provoked a vigorous reaction and the amphipods ran away from the light beam to the opposite edge of the desiccator; in fact, the violet laser beam "cleaned" the surface of the nylon grid from amphipods (Fig. 2, *c*). This reaction, but to a lesser extent, was caused by ultraviolet light. The animals became more sensitive to light in the dark, and even the red laser caused some animals to move away from the light beam. Similar results were also obtained in experiments using a set of directional coloured LEDs (Table 1).

Pool experiments. The reaction of animals to light stimuli in a confined space was evaluated in these experiments. After the transfer of amphipods to round desiccators or Petri dishes, the animals settled mainly along the perimeter near the wall, and when settling in an elongated pool, they created clusters in the corners

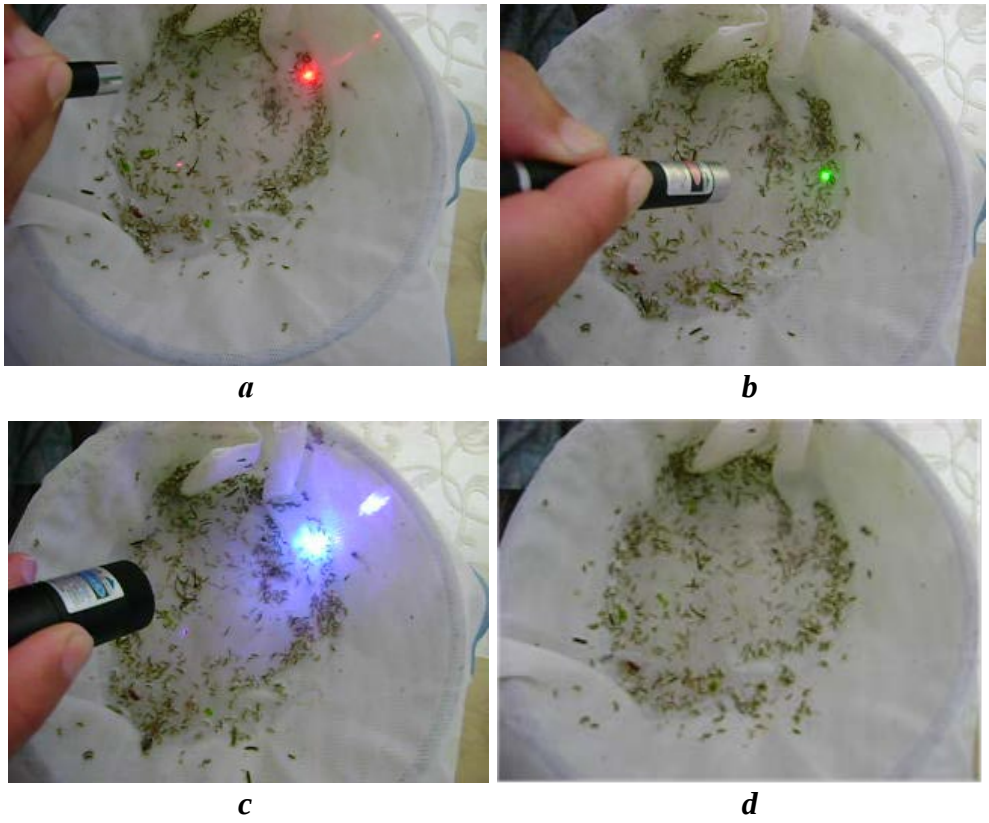

Fig. 2. Experiments with *C. olivii* in the daylight exposed to red (*a*), green (*b*), purple (*c*) lasers; *d* – control

of the end parts of the channels. The animals preferred to gather in groups at the ends of the channel in control experiments without artificial illumination, but often ran from one part of the channel to another. Amphipod males were more mobile than females with eggs; thus, males often gathered in clusters, sometimes fought among themselves and attacked females. The ratio between the sexes in mixed groups in the "houses" was approximately 1:1.

The animals began to move after a second delay and then left the illuminated area, adjoining their neighbors or forming another group in a more shaded section of the channel with white illumination. In general, males ran farther from the light than females (more than 30 cm versus 15 cm). However, both did not demonstrate a simple negative phototaxis, but, on the contrary, often returned to the illuminated zone, exploring the area. Therefore, one can only talk about the preferential stay of zooids in one or another area of the channel.

The results of the experiments revealed differences in daylight avoidance behavior between male and female amphipods. A significant part of the animals hid in the shade, and a large variability in actions is characteristic of females, possibly due to bearing offspring. In the initial experiments, 9 ± 6 % of males

Table 1. *C. olivii* avoidance of illumination with colour light sources in daylight and in the dark

Colour of the source	Response	
	in daylight	in the dark
White	+	+++
Ultraviolet	++	++
Blue	+++	+++
Green	±	±
Red	-	±
Control	-	-

Note: +++ – intensive response; ++ – mild response; + – visible response; ± – weak response; - – no response.

Table. 2. Response of *C. olivii* males and females to light in the dark when using colourful LEDs

LED colour	Number of animals in the dark part of the channel	
	♂♂	♀♀
White	0.92 ± 0.04	0.64 ± 0.16
Blue	0.89 ± 0.05	0.74 ± 0.12
Green	0.91 ± 0.06	0.83 ± 0.06
Red	0.92 ± 0.04	0.74 ± 0.10

Note: ± is the confidence interval for the mean at the significance level p = 0.95.

and 35 ± 18 % of females remained in the illuminated part of the channel. It was shown that almost all males and females accumulated in houses with one entrance, "grottoes", and to a lesser extent in walk-through houses, "tunnels" in experiments with direct sunlight. It follows that amphipods prefer shady places where they gather in groups; males clearly avoid light and form clusters in the shaded ends of the channels, but more often than females leave the houses and migrate farther from them.

The greater sensitivity of males not only to natural daylight, but also to artificial lighting, was revealed by comparing their distribution under the influence of radiation from a directional lamp of warm white light. Thus, amphipod males and females were distributed equally on both sides of the channel under diffused light, but moved to the far shaded end of the channel when illuminated by a lamp from one side, and males accumulated mainly in the dark end of the channel, forming dense compact clusters, while females were distributed more evenly in shadows along the channel. Therefore, it can be concluded that males react more clearly than females.

Application of coloured LEDs in the dark. The amphipods of both sexes showed good light sensitivity and ran away from blue, green, and red LED light, but females were more inert and did not avoid white light as clearly as males in the experiments with coloured LEDs in complete darkness (Table 2).

Experiments with controlled LEDs of different colours in the twilight. Since the animals reacted more strongly to moveable lasers and LEDs in the dark than in the light (see Fig. 2, Table 1), we assumed that the light-sensitive system of amphipods responds to changes in light intensity. To test this assumption, light pulses of different frequencies with a 50% duty cycle, emitted by coloured LEDs under the control of a microcontroller, were used (Table 3). It was found that males are more sensitive to white, blue and green light compared to females under constant illumination in shaded channels, but do not react noticeably, like females, to red light. At the same time, the use of pulses with a duration of 10 ms led to a weakening of the reaction of animals to white, blue, and green pulsating light. This was explicit in a decrease in the number of animals moving to a dark shelter. Reduction of the duration of light flashes and pauses between them to 1 s caused a further weakening of the amphipods' reaction (Table 3).

Thus, all pulsating LEDs are characterized by a common pattern: amphipods almost cease to respond to pulses with a half-cycle of 1 s, which is comparable to the typical sea wave frequency of 0.5 Hz.

Discussion

Multiple losses of opsin genes in the amphipods of Lake Baikal were described previously [17]. They were associated with the lake's ancient glaciation and the immersion of all aquatic organisms in darkness for many years. The loss of some opsins in the genome of the Mexican amphipod *H. azteca* was found, which may be caused by the characteristics of the habitat, the life history of this species, and its survival strategy [18]. Numerous examples of amphipods of different genera and families are well known, which not only lost individual genes encoding light-sensitive receptors (opsins) but also, having inhabited the depths of the oceans

Table 3. Influence of light pulse duration on *C. olivii* escape reaction

Colour	Number of animals in the dark part of the channel					
	Constant illumination		Half-cycle 10 ms		Half-cycle 1 s	
	♂♂	♀♀	♂♂	♀♀	♂♂	♀♀
White	0.85 ± 0.06	0.71 ± 0.11	0.80 ± 0.09	0.73 ± 0.12	0.77 ± 0.13	0.58 ± 0.09
Blue	0.81 ± 0.09	0.70 ± 0.14	0.77 ± 0.09	0.62 ± 0.09	0.62 ± 0.17	0.44 ± 0.11
Green	0.81 ± 0.04	0.70 ± 0.04	0.72 ± 0.08	0.61 ± 0.05	0.69 ± 0.06	0.49 ± 0.09
Red	0.59 ± 0.23	0.54 ± 0.10	0.57 ± 0.12	0.56 ± 0.10	0.48 ± 0.12	0.50 ±0.14

Note: ± is the confidence interval for the mean at the significance level p = 0.95.

(work [3)] and [19, 20]) or caves [21], lost complex organs – eyes. In general, the avoidance by amphipods of the permanent white, blue, and green light, but not of the red light, resembles in our experiments a reaction to coloured LEDs of blue eulimnogammarus *Eulimnogammarus cyaneus* Dybowsky, 1874, found in the littoral zone of Lake Baikal [22].

It should be noted that the water line in the surf zone at the water – air phase boundary is a complex habitat. The animals inhabiting this zone must be adapted not only to rapid changes in the situation during the surf, but also to long-time drifts (daily and seasonal cycles). The colour vision of such species may be the most important functional system that ensures the survival of animals, since, unlike other sensory systems, vision, perhaps, ensures the quick reaction of the inhabitants to a change of scenery during the surf, signaling to the animal where it is at the moment: in the air or the water phase.

The experimental aquatic organisms reacted to violet light by actively avoiding it, since the light of this wavelength can be a signal that the animal was on land. On the one hand, violet light spreads to a depth of up to 100 m and is spectrally close to blue light, which penetrates into the water column up to 300 m and is perceived by many marine animals, including the simplest multicellular organism, *Trichoplax* [23]. On the other hand, violet light spectrally borders on lethal UV radiation, but is not dangerous in itself, and therefore can be a proper indicator of the ultraviolet present in the sun's rays.

It should be added that the experiments were carried out for two months, and during this time, amphipod females managed to partially lay eggs, and the proportion of males in the natural population decreased markedly. Male amphipods have a more signified response to light exposure than females, which is in good agreement with the larger eye size in males compared to females. In addition, females sometimes showed green blindness, while males, on the contrary, gathered near the red colour source, which may correlate with the phase of the animal's reproductive cycle or unknown factors.

The obtained results are consistent with fragmentary data on opsin proteins in invertebrates such as *H. azteca* [18], *P. hawaiensis* [24], *H. americanus* [25], *M. leidyi* [12, 26], and *Trichoplax* sp. H2 [27, 28]. In one part of these animals, opsins are found that are sensitive to red and green light, while in the other part, to green and blue light, which depends both on the taxonomic status of the amphipod and on its habitat. The absence of a noticeable reaction of *C. olivii* to light pulses with a duration of 1 s and a pause of 1 s, which corresponds to a frequency of 0.5 Hz, an approximate frequency of wave impacts on the sea coast, was notable. Instead, the amphipods responded to random pulses of white and blue light.

[3)] Al-Yamani, F.Y., Al-Kandari, M., Polikarpov, I. And Grintsov, V., 2019. *Field Guide of Order Amphipoda (Malacostraca, Crustacea) of Kuwait.* Kuwait: Kuwait Institute for Scientific Research, 390 p. Available at: https://repository.marine-research.org/handle/299011/7092 [Accessed: 30 November 2022].

Consequently, the animals in the channels respond to artificial influences, but do not respond to typical influences that they are accustomed to encountering in their natural habitat and which do not pose a danger to them.

It is important that the eyes of *C. olivii* are localized under a thin layer of chitin, which does not imply a developed vision [24], and colour recognition may not serve to analyze scenes [29], but only to determine the position of an animal on land or in water. Thus, using the example of sharks and rays, it was shown that chromatic vision may be of little use for mobile marine organisms [30]. Our studies demonstrate that amphipods have developed colour vision and may probably have opsin genes that are sensitive to blue and violet light sources in addition to green, as animals clearly avoid the corresponding light spot. It turns out that visual receptors correspond to the habitat and survival strategy of an organism, and illumination can frighten and disorientate animals. The search and sequencing of suitable genes, their subsequent annotation, as well as analysis of products and the network of their interaction can help to answer the questions raised in this study [14, 31]. The proposed experimental approach to the study of behavioral reactions of amphipods using multi-coloured lasers, channels, houses, and controlled coloured LEDs makes it possible to study the colour vision features of invertebrates depending on their adaptation to the environment.

Conclusions

In general, unlike amphipods that live in the dark and are partially or completely blind, the studied *C. olivii*, which live near the water's edge, demonstrated a variety of behavioral responses to light and colour stimuli, namely:

I) sustained avoidance of blue and violet light;

II) insensitivity to red light in daylight, but avoidance of red light in complete darkness;

III) different light and colour perception in females and males;

IV) lack of response to low-frequency periodic light pulses;

V) noticeable response to random flashes of white and blue light.

All this points to the complexity of light perception in the amphipods *Chaetogammarus olivii*, which plays an important role in the life of the animal.

REFERENCES

1. Yasukouchi, A. and Ishibashi, K., 2005. Non-Visual Effects of the Color Temperature of Fluorescent Lamps on Physiological Aspects in Humans. *Journal of Physiological Anthropology and Applied Human Science*, 24(1), pp. 41–43. doi:10.2114/jpa.24.41
2. Chellappa, S.L., Steiner, R., Blattner, P., Oelhafen, P., Götz, T. and Cajochen, C., 2011. Non-Visual Effects of Light on Melatonin, Alertness and Cognitive Performance: Can Blue-Enriched Light Keep us Alert? *PLoS One*, 6(1), e16429. doi:10.1371/journal.pone.0016429
3. Stefani, O., Freyburger, M., Veitz, S., Basishvili, T., Meyer, M., Weibel, J., Kobayashi, K., Shirakawa, Y. and Cajochen, C., 2021. Changing Color and Intensity of LED Lighting across the Day Impacts on Circadian Melatonin Rhythms and Sleep in Healthy Men. *Journal of Pineal Research*, 70(3), e12714. doi:10.1111/jpi.12714
4. Xiao, H., Cai, H. and Li, X., 2021. Non-Visual Effects of Indoor Light Environment on Humans: A Review. *Physiology and Behavior*, 228, 113195. doi:10.1016/j.physbeh.2020.113195

5. Fonken, L.K., Finy, M.S., Walton, J.C., Weil, Z.M., Workman, J.L., Ross, J. and Nelson, R.J., 2009. Influence of Light at Night on Murine Anxiety- and Depressive-Like Responses. *Behavioral Brain Research*, 205(2), pp. 349–354. doi:10.1016/j.bbr.2009.07.001

6. Aulsebrook, A.E., Connelly, F., Johnsson, R.D., Jones, T.M., Mulder, R.A., Hall, M.L., Vyssotski, A.L. and Lesku, J.A., 2020. White and Amber Light at Night Disrupt Sleep Physiology in Birds. *Current Biology*, 30(18), pp. 3657–3663.e5. doi:10.1016/j.cub.2020.06.085

7. Briolat, E.S., Gaston, K.J., Bennie, J., Rosenfeld, E.J. and Troscianko, J., 2021. Artificial Nighttime Lighting Impacts Visual Ecology Links between Flowers, Pollinators and Predators. *Nature Communications*, 12, 4163. doi:10.1038/s41467-021-24394-0

8. Forsburg, Z.R., Guzman, A. and Gabor, C.R., 2021. Artificial Light at Night (ALAN) Affects the Stress Physiology but not the Behavior or Growth of *Rana berlandieri* and *Bufo valliceps*. *Environmental Pollution*, 277, 116775. doi:10.1016/j.envpol.2021.116775

9. Tsujimura, T., 2020. Mechanistic Insights into the Evolution of the Differential Expression of Tandemly Arrayed Cone Opsin Genes in Zebrafish. *Development, Growth, Differentiation*, 62(7–8), pp. 465–475. doi:10.1111/dgd.12690

10. Baden, T., 2021. Circuit Mechanisms for Colour Vision in Zebrafish. *Current Biology*, 31(12), pp. R807–R820. doi:10.1016/j.cub.2021.04.053

11. Henze, M.J. and Oakley, T.H., 2015. The Dynamic Evolutionary History of Pancrustacean Eyes and Opsins. *Integrative and Comparative Biology*, 55(5), pp. 830–842. doi:10.1093/icb/icv100

12. Ullrich-Lüter, E.M., Dupont, S., Arboleda, E., Hausen, H. and Arnone, M.I., 2011. Unique System of Photoreceptors in Sea Urchin Tube Feet. *Proceedings of the National Academy of Sciences of the USA*, 108(20), pp. 8367–8372. doi:10.1073/pnas.1018495108

13. Delroisse, J., Ullrich-Lüter, E., Ortega-Martinez, O., Dupont, S., Arnone, M.-I., Mallefet, J. and Flammang, P., 2014. High Opsin Diversity in a Non-Visual Infaunal Brittle Star. *BMC Genomics*, 15, 1035. doi:10.1186/1471-2164-15-1035

14. Sergeeva, E.V, Fadeeva, M.V., Khavronyuk, I.S., Mamontov, A.A., Ershov, A.B. and Kuznetsov, A.V., 2022. Opsins of the Ctenophore Mnemiopsis leidyi and a Network of Protein-Protein Interactions. *Russian Journal of Biological Physics and Chemistry*, 7(2), pp. 222–229. doi:10.29039/rusjbpc.2022.0506

15. Karaman, G.G., 1982. Genus Echinogammarus Stebbing, 1899. The Amphipoda of the Mediterranean. *Memoires de l'Institut Oceanographique*, 13, pp. 271–282.

16. Makarov, Yu.N., 2004. [*Fauna of Ukraine. Malacostraca. Vol. 26: Malacostraca. Iss. 1–2: Decapods*]. Kiev: Naukova Dumka, 430 p. (in Russian).

17. Drozdova, P., Kizenko, A., Saranchina, A., Gurkov, A., Firulyova, M., Govorukhina, E. and Timofeyev, M., 2021. The Diversity of Opsins in Lake Baikal Amphipods (Amphipoda: Gammaridae). *BMC Ecology and Evolution*, 21(1), 81. doi:10.1186/s12862-021-01806-9

18. Poynton, H.C., Hasenbein, S., Benoit, J.B., Sepulveda, M.S., Poelchau, M.F., Hughes, D.S.T., Murali, S.C., Chen, S., Glastad, K.M. [et al.], 2018. The Toxicogenome of Hyalella azteca: A Model for Sediment Ecotoxicology and Evolutionary Toxicology. *Environmental Science and Technology*, 52(10), pp. 6009–6022. doi:10.1021/acs.est.8b00837

19. Karaman, G.G., 1982. Genus Eriopisa Stebbing, 1890. The Amphipoda of the Mediterranean. *Memoires de l'Institut oceanographique*, 1982, 13, pp. 291–293.
20. Thurston, M.H. and Bett, B.J., 1993. Eyelessness in Marine Gammaridean Amphipoda (Crustacea): Geographical, Bathymetric and Taxonomic Considerations. *Journal of Natural History*, 27(4), pp. 861–881. doi:10.1080/00222939300770531
21. Fong, D.W., 1989. Morphological Evolution of the Amphipod Gammarus minus in Caves: Quantitative Genetic Analysis. *The American Midland Naturalist*, 121(2), pp. 361–378. doi:10.2307/2426041
22. Drozdova, P.B., Saranchina, A.E. and Timofeyev, M.A., 2020. Spectral Sensitivity of the Visual System of Endemic Baikal Amphipods. *Limnology and Freshwater Biology*, (4), pp. 781–782. doi:10.31951/2658-3518-2020-A-4-781
23. Feuda, R., Hamilton, S.C., McInerney, J.O. and Pisani, D., 2012. Metazoan Opsin Evolution Reveals a Simple Route to Animal Vision. *Proceedings of the National Academy of Sciences of the USA*, 109(46), pp. 18868–18872. doi:10.1073/pnas.1204609109
24. Ramos, A.P., Gustafsson, O., Labert, N., Salecker, I., Nilsson, D.E. and Averof, M., 2019. Analysis of the Genetically Tractable Crustacean Parhyale hawaiensis Reveals the Organisation of a Sensory System for Low-Resolution Vision. *BMC Biology*, 17(1), 67. doi:10.1186/s12915-019-0676-y
25. Polinski, J.M., Zimin, A.V., Clark, K.F., Kohn, A.B., Sadowski, N., Timp, W., Ptitsyn, A., Khanna, P., Romanova, D.Y. [et al.], 2021. The American Lobster Genome Reveals Insights on Longevity, Neural, and Immune Adaptations. *Science Advances*, 7(26), eabe8290. doi:10.1126/sciadv.abe8290
26. Schnitzler, C.E., Pang, K., Powers, M.L., Reitzel, A.M., Ryan, J.F., Simmons, D., Tada, T., Park, M., Gupta, J. [et al.], 2012. Genomic Organization, Evolution, and Expression of Photoprotein and Opsin Genes in Mnemiopsis leidyi: a New View of Ctenophore Photocytes. *BMC Biology*, 10, 107. doi:10.1186/1741-7007-10-107
27. Kamm, K., Osigus, H.J., Stadler, P.F., DeSalle, R. and Schierwater, B., 2018. Trichoplax Genomes Reveal Profound Admixture and Suggest Stable Wild Populations without Bisexual Reproduction. *Scientific Reports*, 8(1), 11168. doi:10.1038/s41598-018-29400-y
28. Khavroyuk, I.S., Mamontov, A.A., Bulkov, V.A., Voronin, D.P. and Kuznetsov, A.V., 2021. Assignment of Functions to Opsins of Trichoplax adhaerens and Trichoplax sp. H2. *Russian Journal of Biological Physics and Chemistry*, 6(4), pp. 686–694.
29. Hubel, D.H. and Wiesel, T.N., 1979. Brain Mechanisms of Vision. *Scientific American*, 241, pp. 150–162. doi:10.1038/scientificamerican0979-150
30. Hart, N.S., Lamb, T.D., Patel, H.R., Chuah, A., Natoli, R.C., Hudson, N.J., Cutmore, S.C., Davies, W.I.L., Collin, S.P. [et al.], 2020. Visual Opsin Diversity in Sharks and Rays. *Molecular Biology and Evolution*, 37(3), pp. 811–827. doi:10.1093/molbev/msz269
31. Fernald, R.D., 2006. Casting a Genetic Light on the Evolution of Eyes. *Science*, 313(5795), pp. 1914–1918. doi:10.1126/science.1127889

Submitted 07.07.2022; accepted after review 26.08.2022;
revised 02.11.2022; published 23.12.2022.

About the authors:

Vladimir A. Grintsov, Senoir Research Associate, A.O. Kovalevsky Institute of Biology of the Southern Seas of RAS (2 Nakhimov Av., Sevastopol, 299011, Russian Federation),

Ph.D. (Biol.), **ORCID ID: 0000-0002-9003-3054, Scopus Author ID: 6508301935, ResearcherID: N-5869-2017**, *vgrintsov@gmail.com*

Andrey V. Kuznetsov, Scientific Advisor, A.O. Kovalevsky Institute of Biology of the Southern Seas of RAS (2 Nakhimov Av., Sevastopol, 299011, Russian Federation), Dr.Sci. (Biol.), **ORCID ID: 0000-0002-0015-7994, Scopus Author ID: 57198997858**, *kuznet61@gmail.com*

Svetlana N. Zheleznova, Research Associate, A.O. Kovalevsky Institute of Biology of the Southern Seas of RAS (2 Nakhimov Av., Sevastopol, 299011, Russian Federation), Ph.D. (Biol.), **ORCID ID: 0000-0003-1800-5902, Scopus Author ID: 57191091052, ResearcherID: H-3722-2014**, *zheleznovasveta@yandex.ru*

Vitaly I. Ryabushko, Chief Research Associate, A.O. Kovalevsky Institute of Biology of the Southern Seas of RAS (2 Nakhimov Av., Sevastopol, 299011, Russian Federation), Dr.Sci. (Biol.), **ORCID ID: 0000-0001-5052-2024, Scopus Author ID: 7801673501, Researcher ID: H-4163-2014**, *rabushko2006@yandex.ru*

Contribution of the authors:

Vladimir A. Grintsov – sampling, experimental studies, statistical analysis, analysis of obtained data, preparation of the manuscript

Andrey V. Kuznetsov – study aim and objective statement, sampling, experimental studies, analysis of obtained data, preparation of the manuscript

Svetlana N. Zheleznova – experimental studies, analysis of obtained data

Vitaly I. Ryabushko – scientific consulting, analysis of obtained data, preparation and editing of the manuscript

All the authors have read and approved the final manuscript.